HYBRID POLYETHYLENE GLYCOL HYDROGELS FOR TISSUE ENGINEERING APPLICATIONS

A Dissertation

by

DANY JAIR MUNOZ PINTO

Submitted to the Office of Graduate Studies of
Texas A&M University
in partial fulfillment of the requirements for the degree of

DOCTOR OF PHILOSOPHY

May 2011

Major Subject: Chemical Engineering

Hybrid Polyethylene Glycol Hydrogels for Tissue Engineering Applications

HYBRID POLYETHYLENE GLYCOL HYDROGELS FOR TISSUE ENGINEERING APPLICATIONS

A Dissertation

by

DANY JAIR MUNOZ PINTO

Submitted to the Office of Graduate Studies of
Texas A&M University
in partial fulfillment of the requirements for the degree of

DOCTOR OF PHILOSOPHY

Approved by:

Chair of Committee,	Mariah Hahn
Committee Members,	Melissa Grunlan
	Michael Pishko
	Victor Ugaz
Head of Department,	Michael Pishko

May 2011

Major Subject: Chemical Engineering

ABSTRACT

Hybrid Polyethylene Glycol Hydrogels for Tissue Engineering Applications. (May 2011)

Dany Jair Munoz Pinto, B.S, Universidad Industrial de Santander

Chair of Advisory Committee: Dr. Mariah Hahn

Currently, organ transplant procedures are insufficient to address the needs of the number of patients that suffer of organ failure related disease. In the United States alone, only around 19% of the patients are able to get an organ transplant surgery and 25% die while waiting for a suitable donor. Tissue engineering (TE) has emerged as an alternative to organ transplant; thus, the aim of the present study was to validate a poly(ethylene glycol) diacrylate (PEG-DA) hydrogel system as a model for material scaffolding in TE applications.

This work explores the influence of scaffold material properties on cell behavior. Specifically, scaffold modulus, mesh size, and biochemical stimuli were characterized and their influence on cell response was analyzed at the biochemical, histological and microenvironmental levels. Three different TE targets were evaluated: vocal fold restoration, vascular grafts and osteochondral applications.

Vocal fold fibroblast (VFF) phenotype and extracellular matrix (ECM) production were impacted by initial scaffold mesh size and modulus. The results showed increasing levels of SM-α-actin and collagen production with decreasing initial mesh size/increasing initial modulus, which indicated that VFFs were induced to take an undesirable myofibroblast-like phenotype. In addition, it was possible to preserve VFF phenotype in long-term cultured hydrogels containing high molecular weight hyaluronan (HA_{HMW}). On the other hand, regarding vascular graft applications, smooth muscle cell (SMC) phenotype was enhanced by increasing scaffold mesh size and modulus. Finally, the effect of scaffold inorganic content (siloxane) on rat osteoblasts and mouse mesenchymal stem cells was evaluated. Interestingly, the impact of inorganic content on

cell differentiation seemed to be highly dependent on the initial cell state. Specifically, mature osteoblasts underwent transdifferentiation into chondrocyte-like cells with increasing inorganic content. However, Mesenchymal stem cells appeared to be preferentially driven toward osteoblast-like cells with an associated increase in osteocalcin and collagen type I production.

The use of PEG-DA based hydrogels as scaffold model showed the relative effect of scaffold material properties on cell behavior. Therefore, desired cell phenotype as well as specific profile of ECM production could be potentially modulated with the appropriate tuning of material properties.

DEDICATION

To parents, Luz Mila and Orlando Munoz Granados and to my brother Diego.

To my wife Andre Carolina.

To the memory of my grandfather Matias Pinto Leon.

ACKNOWLEDGEMENTS

I would like to express my gratitude to my advisor and committee chair, Dr. Mariah Hahn, for her support, patience and guidance during the course of my research. I would also like to thank my committee members, Dr. Grunlan, Dr. Pishko and Dr. Ugaz, for their guidance and support.

Thanks also go to my friends and colleagues, and the department faculty and staff, for making my time at Texas A&M University a great experience. I also want to extend my gratitude to Dr. Aristobulo Centeno, Dr. Sonia Giraldo, and Dr. Alvaro Ramirez, at Universidad Industrial de Santander who encouraged me to start my graduate studies at Texas A&M University.

TABLE OF CONTENTS

CHAPTER Page

CHAPTER Page

CHAPTER Page

LIST OF FIGURES

FIGURE Page

LIST OF TABLES

CHAPTER I
INTRODUCTION

1.1 Problem statement

Each year millions of people around the world die of organ failure related diseases such as stroke, arteriosclerosis, kidney and liver failure. In the United States alone, around 100,000 people are enrolled in the organ transplant waiting list from which approximately a quarter of the patients die while waiting for a suitable donor, and only around 19,000 patients are able to get an organ transplant surgery [1]. Given the needs for organ replacement, the study of alternative treatments to organ donation constitutes a major challenge. A possible alternative is tissue engineering (TE), which combines synthetic, natural or hybrid scaffolds with or without the incorporation of patients own living cells. However, the success of these engineered tissues depends on the appropriate design of the scaffolds properties and their interaction with living cells.

This work focuses on the understanding of cell material interactions with the systematic and controlled design of material properties and their isolated effect on cell response for 3D tissue engineering applications: vocal fold restoration, small diameter vascular graft, and bone regeneration.

Cell responses were analyzed at the biochemical, histological and microstructural levels. The specific aims for this work were:

- Quantitatively characterize cell density, collagen type I and III in the human midmembranous vocal fold lamina propria.
- Investigate the effects of the initial scaffold elastic modulus and mesh size on encapsulated vocal fold fibroblast and smooth muscle cells responses.
- Validate a 3D model system for probing the effects of hyaluronan molecular weight on vocal fold fibroblast behavior.

This dissertation follows the style of *Tissue Engineering: Part A*.

- Analyze the effect of scaffold inorganic content on mesenchymal cell fate and differentiation.

The achievement of these goals attempts to highlight the relevance of scaffold properties on cell behavior and tissue regeneration. This work represents a novel strategy for the tuning and optimization of scaffold properties for tissue engineering applications in a 3D context, which was accomplished by the use of polyethylene glycol hybrid hydrogels as a material platform. The implementation of this innovative approach can bring to light the relative influence of different material properties on cell response, which in turn allows for the analysis of the individual impact of each property in order to reduce the number of variables and range of stimuli applied. This understanding will contribute to the creation of more efficient scaffolds capable of sustaining cell function based on a desired application.

1.2 Background

Tissue regeneration is a natural process that involves a very complex collection of interactions between cells, soluble factors and the micro-environment surrounding the cells. These surrounding materials are known as extracellular matrix (ECM), which is mostly composed of proteins and polysaccharides such as collagens, hyaluronic acid, and glycosaminoglycans that reside outside the cells (Figure 1.1). From a structural standpoint, ECM is not randomly arranged; instead, it is highly organized at the nano and microstructural levels, being such spatial orientation distinct from tissue to tissue. Initially, it was believed that ECM played a passive role, which was limited to serving as a structural support for tissues. However, early studies performed by Hauschka, Konigsberg and Hay [2] showed that ECM components were actively involved in differentiation, morphogenesis and cell function. The ECM started to be seen as a dynamic structure not only responsible for offering mechanical support to the cell, but also able to regulate water content, select and retain different growth factors as well as interact with the cells through cell receptors.

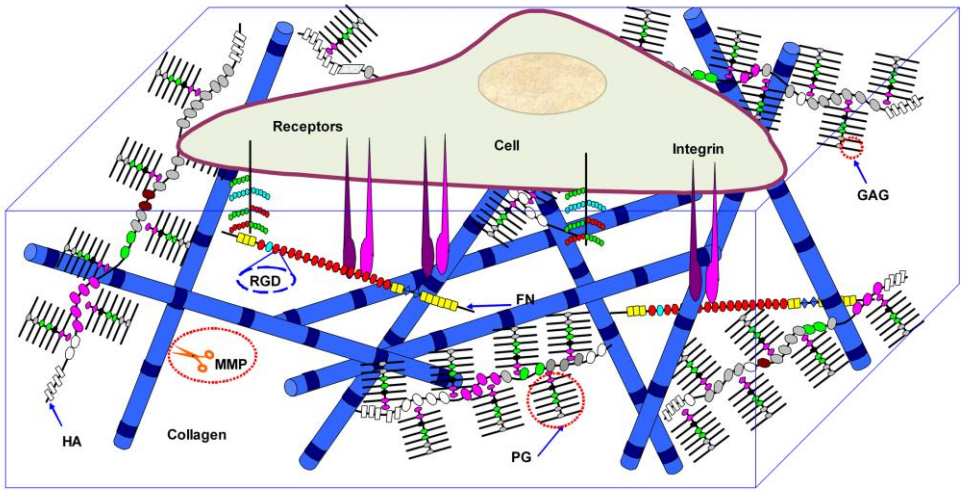

Figure 1.1 Model of extracellular matrix (ECM) and cell-ECM interactions* [3].

Tissue engineering applications require the adequate selection and design of materials that closely mimic the natural cell environment provided in vivo by the ECM. The active role of materials in tissue regeneration motivates the need for a better understanding of the relative influence of material properties on cell response. This has become an area of increasing interest, which is reflected on the multiple contributions from scientists worldwide: for instance, Benoit et al. [4] demonstrated that human mesenchymal stem cell (hMSC) differentiation was guided towards multiple lineages by small synthetic functional groups that were covalently tethered to the scaffold. On the other hand, Engler et al [5]. showed the relevance of matrix stiffness on cell differentiation in 2D systems. However, these results cannot be directly extrapolated to 3D contexts due to the increased complexity associated with the interplay between variables such as mesh structure, modulus, and bioactivity.

*Adapted with permission from "Bioactive modification of poly(ethylene glycol) hydrogels for tissue engineering" by Junmin Zhu, 2010, *Biomaterials 31*(17):4639-4656, Copyright 2010, Elsevier Limited.

Poly (ethylene glycol) (PEG) hydrogels can be used as a platform in 3D environments in order to study the isolated influence of material properties on cell behavior in a systematic manner. Poly(ethylene glycol) is an aliphatic polyether [6] that can be chemically modified by the addition of terminal vinyl groups so as to create a three-dimensional cross-linked hydrophilic polymer network (Figure1.2).

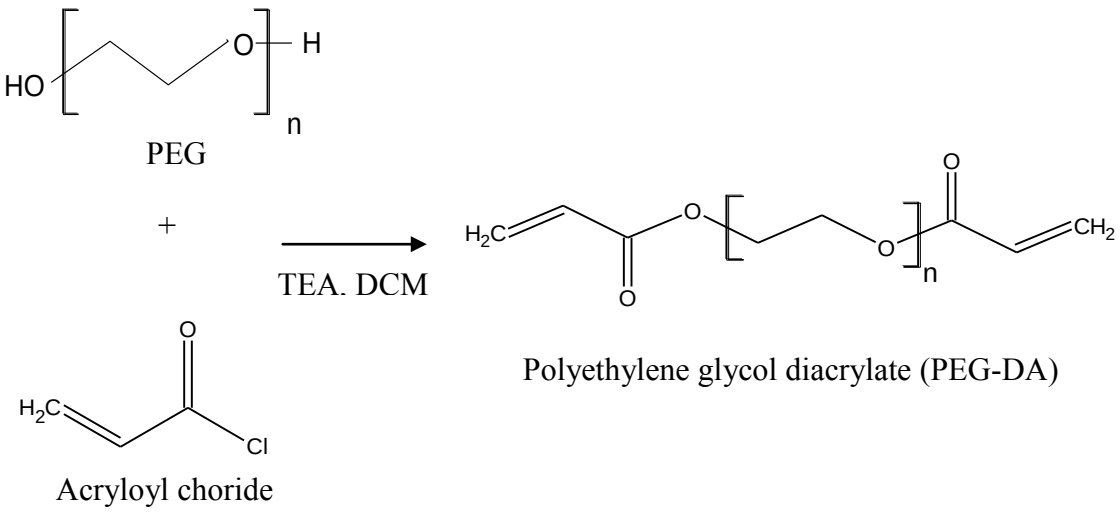

Figure 1.2 Schematic representation of PEG-DA synthesis.

PEG-DA in aqueous solutions can be rapidly photopolymerized in direct contact with cells and tissues without deleterious effects in the presence of the adequate photo-initiator [7]. The physical properties of PEG-DA hydrogels are highly versatile and they vary depending on the concentration, molecular chain length, and crosslinking density [8]. PEG-DA is hydrophilic, biocompatible and intrinsically resistant to protein adsorption and cell adhesion [7]. Thus, PEG-DA hydrogels provide a “blank slate” devoid of biological interactions. Figure 1.3 shows the ideal representation of a PEG-DA crosslinked network.

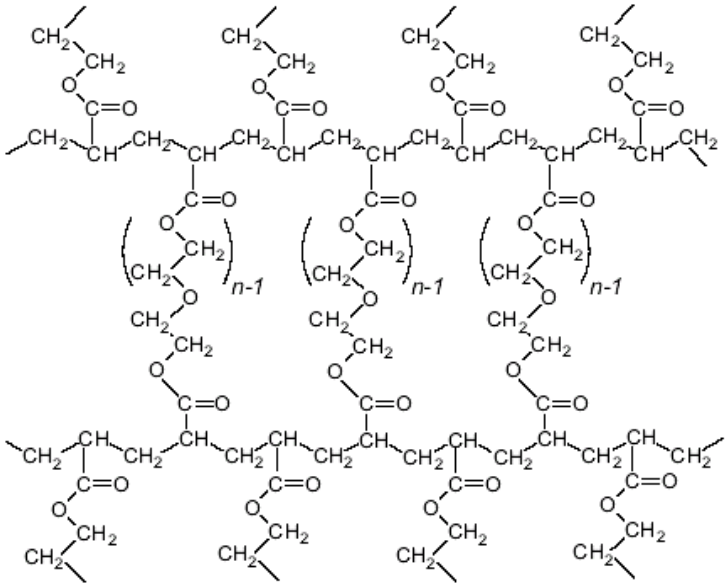

Figure 1.3 Idealized network for crosslinked PEG-DA** [9].

The "blank slate" condition of PEG-DA can be modified by the addition of biomolecules (amino acid, peptides, proteins, glycosaminoglycans GAGs) that are covalently bound to PEG-DA chains either directly [10] or by the use of acryloyl-PEG-N hydroxysuccinimide [11, 12]. This exceptional ability of PEG-DA hydrogels makes them desirable materials for further studying the function of biomolecules and their role in cell behavior.

Figures 1.4 and 1.5 present examples in which biomolecules can be chemically modified in order to be covalently linked onto the PEG-DA hydrogel network. Heparin, a highly sulfated glycosaminoglycan is conjugated with methacrylic anhydride, and Arginine-Glycine-Aspartic Acid-Serine, an adhesion peptide, is conjugated to acryloyl-PEG-N hydroxysuccinimide.

**Reprinted with permission from "Molecular relaxation in cross-linked poly(ethylene glycol) and poly(propylene glycol) diacrylate networks by dielectric spectroscopy" by Sumod Kalakkunnath; Douglass S. Kalika; Haiqing Lin; Roy D. Raharjo; Benny D. Freeman", 2006, *Polymer 48*(2):579-589, Copyright 2006, Elsevier Limited.

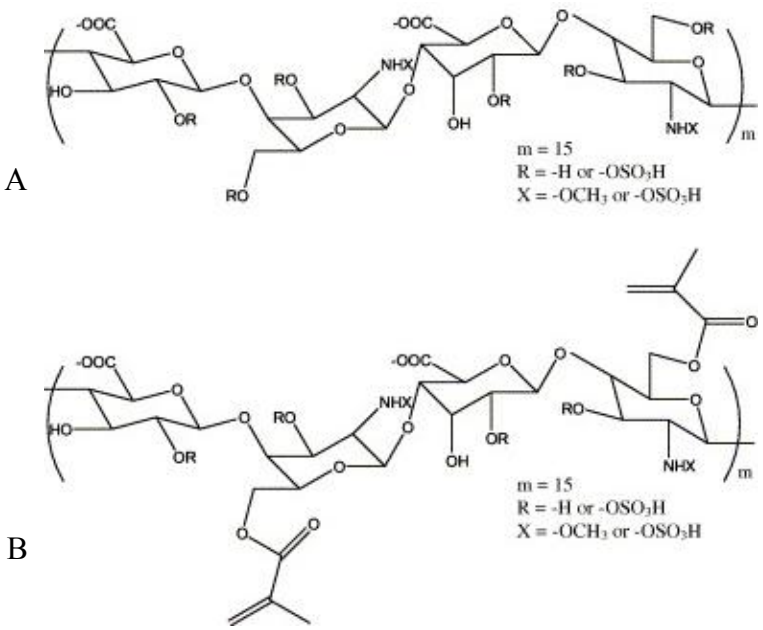

Figure 1.4 Chemical Structure of (A) heparin and (B) methacrylated heparin*** [13].

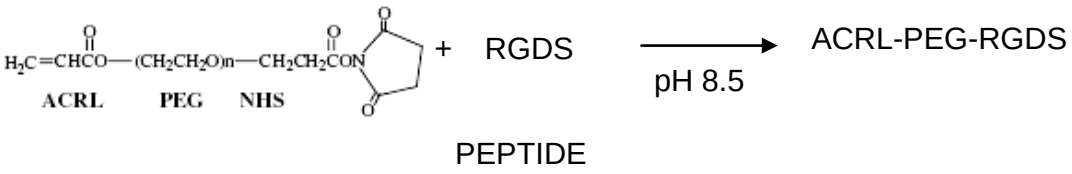

Figure 1.5 Peptide conjugation with ACRL- PEG-NHS.

Although PEG is considered a non degradable polymer, its degradation can be systematically tailored. Pure PEG-DA hydrogels degrade by hydrolytic cleavage of the ester bonds between the aliphatic PEG polymer backbone and the crosslinking units [14, 15]. Variations in this degradation rate can be achieved by conjugating α-hydroxy acids or enzymatically cleavable peptides to the PEG macromer backbone [14, 16].

***Adapted with permission from "Heparin functionalized PEG gels that modulate protein adsorption for hMSC adhesion and differentiation" by Danielle S.W. Benoid; Kristi S. Anseth, 2005, *Acta Biomaterialia 1*(4): 461-470, Copyright 2005, Elsevier Limited.

CHAPTER II
LAMINA PROPRIA CELLULARITY AND COLLAGEN COMPOSITION: AN INTEGRATED ASSESSMENT OF STRUCTURE IN HUMANS*

2.1 Overview

Objectives: In this study, we quantitatively examined cell density, collagen types I and III, in the human midmembranous vocal fold lamina propria (LP).

Methods: Lamina propria samples were solubilized with proteinase K or with cyanogen bromide. Cell density was assessed in proteinase K digests by measuring DNA and normalizing it to tissue total protein. Collagen types I and III were quantified by enzyme-linked immunosorbent assaySbased detection of collagen typeSspecific peptides generated by cyanogen bromide digestion. In addition, LP total collagen was determined by measuring sample hydroxyproline levels.

Results: The mean (±SEM) cell density in the LP and associated epithelium was approximately 0.57 ± 0.09 million cells per milligram of tissue total protein. Collagen type III composed an average of 34% to 40% of LP total collagen.

Conclusions: The total cell density of the LP and associated epithelium was intermediate between that of hyaline cartilage and dermis. The ratio of collagen type III to total collagen in the LP was similar to that of highly elastic lung parenchyma and roughly twice that of the comparatively less-elastic dermis.

*Reprinted with permission from "Lamina propria cellularity and collagen composition: an integrated assessment of structure in humans" by Dany Muñoz-Pinto; Peter Whittaker, PhD; Mariah S. Hahn, PhD, 2009, *Annals of Ototogy. Rhinology & Laryngology* 118(4):299-306, Copyright 2009, Annals Publishing Company.

2.2 Introduction

Characterizing the cellularity and collagen composition of the normal vocal fold lamina propria (LP) is important for understanding LP disease processes and for designing LP repair strategies. For instance, the cellular composition and density within tissues are frequently altered in growth, aging, disease, and repair [17]. Several studies have histologically evaluated the relative abundance of the various cell types (fibroblasts, myofibroblasts, macrophages) composing the midmembranous LP [18]. Although these studies indicate that fibroblasts constitute approximately 80% of the cells within the normal adult human LP, the cell density (cells by tissue weight or volume) characteristic of normal LP has not yet been quantified. A primary aim of the present study was therefore to measure the total cell density in the human LP and associated epithelium.

As with cell density, the relative abundance of the various collagen types is altered in a number of physiological and pathological processes [19]. These changes in collagen type composition can have a profound impact on tissue mechanical properties [20]. Although at least 27 different collagen types have been identified, [20] the fibrillar collagen types I, II, and III constitute 80% to 90% of total collagen in most tissues [21]. A number of studies have investigated collagen types in the LP. These qualitative histology studies indicate that collagen types I and III are the dominant collagens in the midmembranous LP, [22-25] collagen types IV and V also present in localized regions [23-25]. However, the relative levels of these collagen types have not yet been quantitatively evaluated. An additional aim of the current work was therefore to quantify the collagen composition of the vocal fold LP, with a focus on collagen types I and III.

2.3 Material and methods

2.3.1 Tissue procurement and preparation

Fifteen human larynges were obtained from Massachusetts General Hospital (MGH; Boston, Massachusetts), Clinomics Biosciences (Pittsfield, Massachusetts), and the National Disease Research Interchange (Philadelphia, Pennsylvania). The human

donors had no known medical history of vocal fold surgery or chronic voice disorders. All larynges were placed in neutral buffered formalin within 24 hours of death and remained in formalin for 1 day to 6 months, depending on the source of the specimen. One specimen of human lung parenchyma (MGH) and 3 specimens of porcine hyaline cartilage (Research 87, Inc, Cambridge, Massachusetts) were processed as controls for the collagen type and cellularity assays, respectively. All tissues were procured with the approval of and in accordance with institution committees on human and animal experimentation, respectively. For the specimens reserved for the cellularity or collagen type assays, the midmembranous vocal folds were retrieved and transferred to 70% ethanol. The underlying muscle and glandular tissues that border the LP ventricular and subglottic regions were then removed with the aid of a dissecting microscope. The remaining LP was lyophilized and stored at -80°C until the time of analysis. Further information on each specimen is provided in the Table 2.1.

Table 2.1 Vocal fold specimen information.

SPECIMEN INFORMATION			
		Assay	
Age (y)	**Sex**	**Cellularity**	**Collagen Typing**
16	F		+
40	F	+	
40	F		+
47	F	+	+
57	F	+	
81	F		+
82	F		+
94	F		+
48	M	+	
49	M	+	+
61	M		+
61	M	+	
79	M		+
Child*	Unknown		+
Child*	Unknown		+

*Define age unknown. Estimated ages based on laryngeal size are approximately 2 years and 6 to 10 years.

2.3.2 Sample preparation and DNA and total protein quantitation

Tissue DNA content is a standard indirect measure of tissue cellularity, since normal diploid cells from a given species each contain characteristic levels of DNA [17]. Therefore, tissue DNA assessments can be translated to cell numbers by dividing by the DNA levels characteristic of a diploid cell. To release DNA from the 6 selected vocal fold samples and the hyaline cartilage controls, we added approximately 200 μL of a solution containing 50 μg/mL DNase-free proteinase K (Worthington Biochemical, Lakewood, New Jersey) in 100 mmol/L sodium acetate buffer, pH 7.0, per 1 mg of tissue dry weight. Digestion proceeded for 24 hours at approximately 58 °C. The DNA content of each digest was measured in triplicate with the PicoGreen DNA assay kit (Invitrogen, Carlsbad, California) according to the manufacturer instructions [17]. The human LP and porcine cartilage DNA levels were converted to cell numbers by dividing by 6.9 pg DNA per cell or by 6.6 pg DNA per cell, respectively [26]. As a normalization measure for the DNA assessments, sample total protein was quantitated in triplicate by AAA Service Laboratory, Inc (Boring, Oregon).

2.3.3 Collagen type assessments

As collagen becomes increasingly cross-linked, it becomes more difficult to fully extract from tissue while simultaneously preserving information required distinguishing individual collagen types [27, 28]. One approach that enables this type of extraction is cyanogen bromide (CNBr)-based digestion [27, 29]. In the presence of 70% formic acid, CNBr cleaves collagen molecules at methionine residues, yielding peptide fragments that are characteristic of each collagen type [27, 29]. In addition, CNBr digestion can solubilize approximately 90% of total collagen from highly cross-linked tissues. We therefore used CNBr-based digestion in the present study, and resultant collagen type I and type III peptides were quantified by enzyme-linked immunoabsorbent assay (ELISA).

Sample digestion. We conducted CNBr digestion according to a modification of the method of Light [27]. In brief, 11 LP samples (9 from adults and 2 from children) were transferred to 2-mL screw-cap tubes containing 1 mL of stainless steel beads (3.2-mm diameter, Biospec Products, Inc, Bartlesville, Oklahoma) and 1 mL of 70% formic acid. The tubes were then inserted into a Bead-beater homogenizer (Biospec Products, Inc) and were shaken at the highest speed setting in two 10-second bursts with an intervening 1-minute period on ice. A 100-mg/mL stock solution of CNBr (MP Biomédicals, Solon, Ohio) in 70% formic acid was prepared, and argon was bubbled into the solution for 1 minute. One hundred microliters of this solution was added to each sample tube. Digestion was allowed to proceed at room temperature for 24 hours, after which samples were dried (and formic acid and CNBr evaporated) in a Centrivap (Labconco, Kansas City, Missouri). Fresh 70% formic acid and CNBr were added to the dried samples, and a second 24-hour digestion cycle was conducted. The samples were then dried as described above. To remove residual formic acid and CNBr, we resuspended the dried samples in 1 mL deionized water and dried them again. This cycle of rehydration and drying was repeated twice, after which 600 µL of deionized water was added to each dried sample. The samples were then vortexed and centrifuged at 8,000g for 10 minutes. Aliquots of the supernatant were used in collagen type I and III immunoassays and for total collagen quantification. Collagen Type I and III Immunoassays. Aliquots of CNBr-solubilized samples were diluted in phosphate-buffered saline solution (PBS) and passed through a charcoal-packed centrifugal microcolumn (Nunc, Rochester, New York). One hundred microliters of each filtered sample was applied to a high-binding 96-well enzyme immunoassay plate (Corning, Lowell, Massachusetts) for 3 hours at room temperature. Each well was then blocked for 3 hours with 300 µL of a 3 weight percent (wt%) solution of bovine serum albumin (BSA) in PBS (3 wt% BSA). For detection of collagen type III, an antibody specific for a collagen type III peptide released by CNBr digestion (Calbiochem, San Diego, California) was diluted 1:100 in 3 wt% BSA, and 100 µL of the resultant solution was applied to each sample well for 1 hour at room temperature. After application of donkey

anti-rabbit horseradish peroxidase (HRP) secondary antibody (1:1,000 in 3 wt% BSA, Jackson ImmunoResearch, West Grove, Pennsylvania), 100 μL of 2,2'-azino-bis(3-ethylbenzotbiazoline-6-sulfonic acid) (Sigma-Aldrich, St Louis, Missouri) was added to each well. After 20 minutes of incubation, color development was quenched with an equal volume of a 1% sodium dodecyl sulfate solution and well absorbance was read at 410 nm. To quantify collagen type I, we repeated the above procedure, except that we applied an antibody specific for a collagen type I peptide preserved in CNBr digestion (Clone H-197, Santa Cruz Biotechnology, Santa Cruz, California), followed by a bovine antigoat HRP secondary antibody (Jackson ImmunoResearch). Purified human collagen type I and collagen type III (Rockland Immunochemicals, Gilbertsville, Pennsylvania) that had been subjected to the same CNBr digestion conditions as the samples served as standards and as negative controls (for the antibody of the opposite collagen type). Each sample was measured in duplicate for collagen type I and in triplicate for collagen type III.

Hydroxyproline analyses. The total collagen levels in all CNBr-solubilized samples were assessed in duplicate by a standard colorimetric assay for hydroxyproline (OHPr), an amino acid found almostexclusively in collagen [30]. Aliquots of the CNBr solubilized fraction of each specimen were digested with 6 mol/L hydrochloric acid for 24 hours at 100°C to convert proteins into free amino acids. Each sample was then dried on a Labconco Centrivap to remove hydrochloric acid, resuspended in deionized water, and passed through a charcoalpacked centrifugal microcolumn (Nunc). The resultant samples were reacted with chloramine T and p-dimethylbenzaldehyde reagents, and sample color development was read at 550 nm [31]. L-4-OHPr (Sigma-Aldrich) was used as a standard. The conversion factors for relating measured grams of OHPr to grams of collagen type I or collagen type III are 0.125 and 0.15, respectively [30]. Similarly, the corresponding conversion factor for collagen type IV is 0.135. Therefore, the appropriate conversion factor relating OHPr to total collagen depends on the collagen type composition of the tissue.

Calculation of fraction of collagen type III. For each adult human LP sample, the ratio of collagen type III to total collagen was calculated according to two methods, each involving a different set of assumptions: Fraction 1 = [mg type IIIELISA]/[(mgtotal OHPr)/0.135], and Fraction 2 = [mg type IIIELISA]/[mg type IELISA + mg type IIIELISA]. Fraction 1 assumes, via use of an OHPr conversion factor of 0.135, that collagen types I and III are present in roughly equal proportion. However, this conversion factor also leaves room for other collagen types (ie, the 0.135 conversion factor holds for a tissue containing 50% collagen type I, 33% collagen type III, and 17% collagen type IV, as well as for a tissue containing 40% collagen type I, 27% collagen type III, and 33% collagen type IV). In contrast, fraction 2 assumes collagen types aside from I and III to be negligible contributors to LP total collagen. The degree of agreement between these two fractions gives insight into the dominance of collagen types I and III in the LP. For the lung parenchymal controls, an OHPr conversion factor of 0.130 [29] was used in calculating fraction 1.

2.4 Results

Based on DNA assessments, the LP and associated epithelium contained approximately 0.57 ± 0.09 million cells per milligram of tissue total protein (Figure 2.1A). This translates to approximately 57 ± 9 million cells per gram of tissue wet weight (per g ww), assuming the LP contains similar protein levels by wet weight (approximately 10%) as other loose connective tissues. By the same assumption, hyaline cartilage contains approximately 17 million cells per g ww (Figure 2.1A), in line with previous literature [17]. Approximately 33.6% ± 6.5% of total collagen in the adult LP specimens was collagen type III, according to the combined OHPr and collagen type III ELISA results (fraction 1; Figure2.1B). In contrast, the combined collagen type I and collagen type III ELISA results indicated that collagen type III constituted approximately 40.4% ± 2.7% of adult LP total collagen (fraction 2; Figure 2.1B). The collagen in the child LP samples contained 5.5% ± 2.8% to 8.4% ± 1.5% collagen type III (fraction 1 and fraction 2, respectively). For the human lung parehchyma control,

fraction 1 was determined to be 0.170 and fraction 2 to be 0.320, in agreement with the most recent literature values for these quantities of approximately 0.22 ± 0.08 and approximately 0.24 ± 0.08, respectively [29].

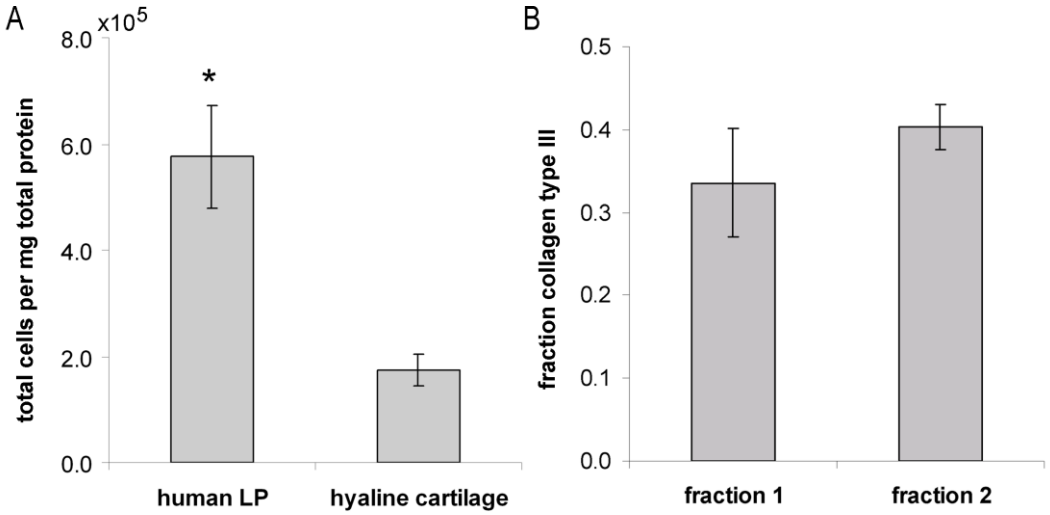

Figure 2.1. Cellularity and collagen type. (**A**) Total cells per mg tissue total protein in human LP and in hyaline cartilage. * indicates significant difference, $p < 0.05$. (**B**) The average fraction LP total collagen comprised by collagen type III as calculated by two separate methods.

2.5 Discussion

This study quantitatively examined cell density, collagen types I and III, in the humanmidmembranous vocal fold LP. Based on DNA assessments, the total cell density in the human LP and associated epithelium was ~57 ± 9 million cells per g ww, ~3.3 times greater than that of the hyaline cartilage control. This value should be regarded as an upper bound on LP fibroblast density, since vocal fold epithelial cells contributed to themeasured cell density in addition to LP fibroblasts, myofibroblasts and macrophages.

We can estimate LP fibroblast density from the measured total cell density using information regarding average vocal fold epithelial thickness and LP geometry provided in literature. Assuming the vocal fold epithelium consists of a 4 layer thick sheet [32] of continuous ~10 μm x 10 μm squamous cells and that the underlying LP is ~1.1 mm thick, [33] epithelial cells comprise ~60% of the measured total cell number. According

to the results of Catten et al., [34] ~80% of the remaining ~23 million cells per g ww are fibroblasts. Thus, the human LP can be estimated to contain ~18 million fibroblasts per g ww. This fibroblast cell density is similar cell density of hyaline cartilage, a relatively low cell density connective tissue. As an additional comparison, human papillary dermis contains ~$100x10^6$ fibroblasts per g ww [35]. Thus, the present results support the view of the vocal fold LP as a relatively low cell density connective tissue. Furthermore, the above estimate of LP fibroblast cell density is in good agreement with that predicted by the results of Catten et al. [34]. Although the latter reported cell count data relative to "imaged field" (IF) rather than relative to tissue wet weight, we can use incidental information included in the manuscript to approximate cells per g ww from measured cells per IF. These calculations indicate average LP fibroblast cell density to be ~21 ± 4 million cells per g ww [34].

Based on combined OHPr and collagen type III ELISA assessments, collagen type III constitutes ~34% of total adult LP collagen (fraction 1). These results are further underscored by the combined collagen type I and collagen type III ELISA measures, which indicate that collagen type III composes ~40% of total adult LP collagen (fraction 2). The degree of agreement between these two calculations for the fractional presence of collagen type III suggests that collagen types I and III are the dominant collagen types within the adult LP. Interestingly, the child LP appears to have significantly lower collagen type III content than the adult LP, with child LP collagen containing less than 10% collagen type III. To place these results in context, the percent that collagen type III comprises of total collagen types I and III is ~15% in the dermis [36] but is 24-33% in the relatively more elastic lung parenchyma [28, 29]. Since collagen type III tends to be more highly concentrated in dynamic/elastic tissues, [19] alterations in collagen type III presence in disease, repair, or aging [19, 27] may impair the elasticity critical to normal LP function.

Due to limited sample number (n = 9 adult LP samples, n = 2 child LP samples), care should be taken in making generalizations based on the present collagen type data. In addition, the average donor age of the adult tissues used for collagen typing was 61

years, and thus the degree to which the present results are representative of normal healthy adult LP awaits confirmation. The same caveats regarding limited sample size and age apply to the cellularity (n = 6).

In summary, our study provides the first quantitative measures of cell density and collagen type in human midmembranous LP.

CHAPTER III
INFLUENCE OF HYDROGEL MECHANICAL PROPERTIES AND MESH SIZE ON VOCAL FOLD FIBROBLAST EXTRACELLULAR MATRIX PRODUCTION AND PHENOTYPE*

3.1 Overview

Current clinical management of vocal fold (VF) scarring produces inconsistent and often suboptimal results. Researchers are investigating a number of alternative treatments for VF lamina propria (LP) scarring, including designer implant materials for functional LP regeneration. In the present study, we investigate the effects of the initial scaffold elastic modulus and mesh size on encapsulated VF fibroblast (VFF) extracellular matrix (ECM) production toward rational scaffold design. Poly(ethylene glycol) diacrylate (PEG-DA) hydrogels were selected for this study since their material properties, including mechanical properties, mesh size, degradation rate and bioactivity, can be tightly controlled and systematically modified. Porcine VFF were encapsulated in four PEG-DA hydrogels with degradation half lives of ~25 days, but with initial elastic compressive moduli and mesh sizes ranging from ~30 to 100 kPa and from ~9 to 27 nm, respectively. After 30 days of static culture, VFF ECM production and phenotype in each formulation was assessed biochemically and histologically. Sulfated glycosaminoglycan synthesis increased in similar degree with both increasing initial modulus and decreasing initial mesh size.

---

*Reprinted with permission from "Influence of hydrogel mechanical properties and mesh size on vocal fold fibroblast extracellular matrix production and phenotype" by Huimin Liao a, Dany Munoz-Pinto, Xin Qu, Yaping Hou , Melissa A. Grunlan, Mariah S. Hahn, 2008, *Acta Biomaterialia 4 (2008) 1161–1171*, Copyright 2008, Acta Materialia Inc. Published by Elsevier Ltd.

In contrast, elastin production decreased with increasing initial modulus but increased with decreasing initial mesh size. Both collagen deposition and the induction of a myofibroblastic phenotype depended strongly on initial mesh size but appeared largely unaffected by variations in initial modulus. The present results indicate that scaffold mesh size warrants further investigation as a critical regulator of VFF ECM synthesis. Furthermore, this study validates a systematic and controlled approach for analyzing VFF response to scaffold properties, which should aid in rational scaffold selection/design.

3.2 Introduction

Although no firm statistics exist, voice disorders, including scarring of the vocal fold (VF) lamina propria (LP), are estimated to affect 3-9% of the population to various degrees [37]. The VFs are paired, multi-layered structures (Figure 3.1), each consisting of underlying muscle, followed by the LP and overlying epithelium [38]. When the VFs are brought together by the intrinsic laryngeal muscles, they can be set into vibratory motion by airflow from the lungs. Ordered oscillation yields efficient cycle-to-cycle closure of the VFs and high quality voice [39]. The human LP is generally subdivided into superficial (SLP), intermediate (ILP), and deep (DLP) layers (Figure 3.1) [40, 41]. At normal pitch and loudness, the SLP is believed to "slide" over the ILP, undergoing the high frequency and strain excursions required for cyclic VF closure [40, 41]. When the pliability and physical volume of the VF SLP are reduced by scarring, voice changes ranging from hoarseness to complete voice loss result, depending on the severity of scar [39, 42-44].

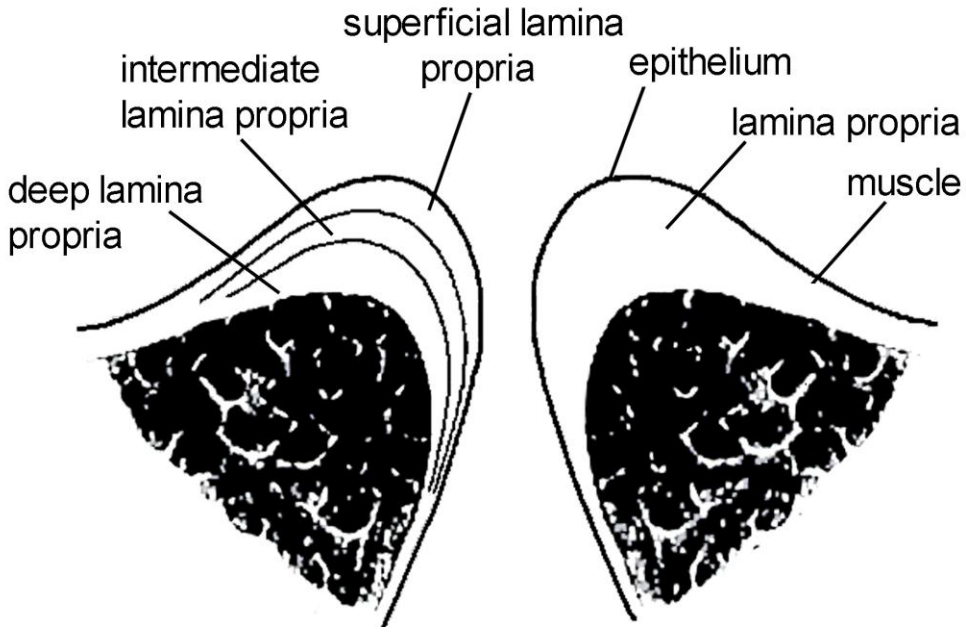

Figure 3.1. Schematic of a coronal section through the human vocal folds.

VF scar has proven difficult to treat with current surgical techniques and standard augmentation substances (e.g., collagen and fat) [39, 42, 45]. As such, researchers are actively exploring alternative treatment routes, including the development of designer implants for functional LP regeneration [46-51]. Although it is understood that scaffold properties, such as bioactivity, [52] mesh size, [53] mechanical properties, [54-56] and degradation rate [57] critically impact cell behavior, it has proven difficult to directly attribute alterations in VF fibroblast (VFF) response to specific changes in scaffold parameters. This situation has hampered rational selection/design of implant materials for LP regeneration. The aim of the present study is validate an approach for the systematic and quantitative assessment of the influence of scaffold properties on VFF behavior. Specifically, the current work focuses on the impact of initial scaffold mesh size and mechanical properties on VFF extracellular (ECM) production and phenotype. Ultimately, these data will be applied toward the rational design of LP regeneration matrices.

Central to these studies is the selected scaffold material: poly(ethylene glycol) diacrylate (PEG-DA). PEG-DA hydrogels have several properties which make them appropriate for systematic exploration of cell response to specific alterations in scaffold material properties. Pure PEG-DA hydrogels function as biological "blank slates," meaning that they do not significantly adsorb bioactive plasma proteins. Thus, these hydrogels do not promote cell interaction without the specific conjugation of biochemical stimuli to the scaffold [58]. This is significant since most synthetic and natural scaffolds adsorb a range of bioactive proteins from serum (in the in vitro setting) or from plasma (in the in vivo setting). These adsorbed proteins are often major determinants of cell behavior, in addition to any bioactive moiety deliberately conjugated or adsorbed to the scaffold [59, 60]. In contrast, the biological "blank slate" nature of PEG-DA hydrogels permits the controlled and defined investigation of bioactivity on cell behavior. In the present study, we explored the effects of initial PEG-DA scaffold modulus and mesh size in the presence of constant initial levels of cell adhesion peptide, RGDS, thus removing initial scaffold bioactivity as a design variable [61].

An additional benefit of PEG-DA hydrogels is the ability to tune their initial mesh size and mechanical properties over a broad range simply by varying the molecular weight (M_W) and/or concentration of PEG-DA [62]. Moreover, the degradation rate of PEG-based hydrogels can be systematically tailored. Pure PEG-DA hydrogels degrade by hydrolytic cleavage of the ester bonds between the aliphatic PEG polymer backbone and the crosslinking units [14, 15]. Variations in this degradation rate can be achieved by conjugating α-hydroxy acids or enzymatically cleavable peptides to the PEG macromer backbone [14, 16]. Thus, PEG-based hydrogels have the property that their bioactivity, mesh size, modulus, and degradation rate can each be systematically tuned, [53, 57, 62] a critical property for the proposed studies.

In the present work, porcine VFF were encapsulated in four PEG-DA hydrogel formulations with initial elastic compressive moduli ranging from ~30 to 100 kPa and with initial mesh sizes ranging from ~9-27 nm. To simplify the investigation of the

dependence of VFF ECM synthesis and phenotype on scaffold properties, PEG-DA hydrogel formulations with similar degradation rates were selected [15]. After 30 days of static culture, VFF collagen, elastin, and sulfated glycosaminoglycan (sGAG) production as well as VFF phenotype in each hydrogel formulation were analyzed using biochemical and histological techniques.

3.3 Materials and methods

3.3.1 Polymer synthesis

PEG-DA was prepared as previously described [63] by combining 0.1 mmol/ml dry PEG (8 kDa or 10 kDa, Fluka), 0.4 mmol/ml acryloyl chloride, and 0.2 mmol/ml triethylamine in anhydrous dichloromethane (DCM) and stirring under argon overnight. The resulting solution was washed with 2 M K_2CO_3 and separated into aqueous and DCM phases to remove HCl. The DCM phase was subsequently dried with anhydrous MgSO4, and PEG-DA was precipitated in diethyl ether, filtered, and dried under vacuum.

3.3.2 Synthesis of acrylate-derivatized peptides

Cell adhesion peptide RGDS (American Peptide) was conjugated to an acrylated PEG derivative (3.4 kDa) by reaction with acryloyl-PEG-Nhydroxysuccinimide (ACRL-PEG-NHS, Nektar) at a 1:1 molar ratio for 2 h in 50 mM sodium bicarbonate buffer, pH 8.5 [63]. The product (ACRL-PEG-RGDS) was purified by dialysis, lyophilized, and stored at -20 ºC until use.

3.3.3Hydrogel characterization

Hydrogel preparation. The following four hydrogel formulations were examined: (1) 10wt % of 10 kDa PEG-DA (10% 10 kDa), (2) 10 wt % of 8 kDa PEG-DA (10% 8 kDa), (3)20 wt % of 10 kDa PEG-DA (20% 10 kDa), and (4) 30 wt % of 10 kDa PEG-DA (30% 10 kDa). Precursor solutions were prepared by dissolving PEG-DA macromers and ACRLPEG-RGDS in HEPES buffered saline (HBS; 10 mM HEPES,

150 mM NaCl, pH 7.4). The solutions were then sterilized using 0.22 μm PVDF filters, and 10 μl of a 300 mg/ml solution of 2,2-dimethoxy-2-phenyl-acetophenone dissolved in N vinylpyrrolidone was added per ml precursor solution. Each solution was poured into molds composed of two glass plates separated by 1.1 mm polycarbonate spacers and then polymerized by 2 min exposure to longwave UV light (Spectroline, ~ 6 mW/cm^2, 365 nm) [64, 65].

Hydrogel swelling. To isolate the effects of scaffold modulus and mesh size on VFF ECM production and phenotype, it was important that the cell density and bioactivity presented to the cells remain constant among formulations. Since PEG-DA hydrogels swell significantly post-polymerization, the amount of ACRL-PEG-RGDS and cellsadded to each hydrogel precursor solution had to account for the change in hydrogel volume with swelling. To characterize the equilibrium swelling of each hydrogel, PEG-DA hydrogels were prepared as described above. One cm diameter samples were cored from each PEG-DA hydrogel immediately following polymerization and weighed. The samples were then transferred to HBS supplemented with 0.05 wt % sodium azide (HBS-azide) and incubated at 37 ºC. After 24 h, samples were blotted and weighed. Since swollen PEG-DA hydrogels are primarily water, the increase in weight with swelling can be directly related to the increase in gel volume (V) with swelling, i.e., $\left(\frac{V_{swollen}}{V_{Initial}}\right) = \left(\frac{swollen\_weight}{Initial\_weight}\right)$ [66]

Hydrogel mesh size. PEG-DA hydrogel mesh size cannot be visualized using standard techniques such as scanning electron microscopy (SEM) [67]. Thus, a variety of methods to estimate PEG-DA hydrogel mesh size have been developed, including correlations linking measurable quantities, such as equilibrium hydrogel swelling, to mesh size [66, 68]. Although these correlations appear to yield reasonable mesh size estimates for relatively high weight percent PEG-DA hydrogels, [66, 68] the predictions for lower weight percent hydrogels have been called into question. Thus, in this study,

hydrogel mesh size was characterized via a series of dextran diffusion experiments based on an adaptation of the methodology of Watkins et al. [69].

In brief, PEG-DA hydrogels containing 2 μmol/mL ACRL-PEG-RGDS postswelling were prepared and allowed to swell overnight at 37 ºC in HBS-azide. One cm diameter discs were cored from each hydrogel formulation. Fluorescently-labeled dextrans (10 kDa, 20 kDa, 40 kDa, 70 kDa, or 150 kDa, Sigma) were dissolved at 0.01 mg/mL in HBS-azide and added at 1 mL per hydrogel disc (3 discs per dextran M_W). Dextran solutions were allowed to diffuse into the hydrogels for 24 h at 37 ºC. Each gel disc was gently blotted and transferred to 1 mL fresh HBS-azide. Dextran that had penetrated into the hydrogels was then permitted to diffuse out into the surrounding solution at 37 ºC. After 24 h, the fluorescence of the HBS-azide solution surrounding each disc was measured at ex/em 488/532. Dextran standard curves were used to convert each fluorescence signal to a concentration.

For the 30% 10 kDa hydrogel formulation, the dextran readings fell to background levels for dextran M_ws exceeding 20 kDa (data not shown). The 20 kDa dextran had a mean hydrodynamic radius of ~3.2 nm, whereas the next largest dextran investigated (40 kDa) had a mean hydrodynamic radius of ~4.5 nm. Thus, the mesh size of the 30% 10 kDa hydrogel was taken to be ~(2 x 4.5) = 9 nm. The mesh sizes of the remaining formulations were calculated relative to that of the 30% 10 kDa hydrogel as follows. For each hydrogel formulation, the measured concentration readings for each dextran M_w were divided by gel thickness and then plotted versus dextran hydrodynamic radius [70]. The area (A) under the resulting curve served a quantitative indicator of hydrogel permissivity over the hydrodynamic radii range assayed. For a given hydrogel (x), the mesh size (ξ) could then be calculated according to the following equation: $\xi_x \approx \left(\frac{A_x}{A_{30\%10kDa}} \right)(9nm)$.

Hydrogel mechanical properties. To assess the mechanical properties of the selected PEG-DA formulations, hydrogels containing 2 μmol/mL ACRL-PEG-RGDS postswelling were prepared and allowed to swell at 37 ºC. After 48 h swelling, three

samples, each 1.25 cm in diameter, were cored from each hydrogel and mechanically tested under unconstrained compression at room temperature using a DMA 800 (TA Instruments). During mechanical testing, samples were immersed in silicone oil to prevent hydrogel dehydration. Following application of a 0.01 N preload, each hydrogel was subjected to 10 μm cyclic compression (~1% cyclic strain) at frequencies of 0.01-100 Hz (100 Hz being the system maximum) The higher frequency testing conditions were selected to approach the frequencies of cyclic LP loading experienced during phonation [71]. The elastic and viscous compressive moduli of each hydrogel formulation were extracted from the resulting stress-strain data. In assessing the impact of initial scaffold properties on VFF ECM production and phenotype, the elastic compressive modulus of each hydrogel formulation at 0.01 Hz (approximately static conditions) was utilized since static culture conditions were employed. In evaluating the initial mechanical properties of each PEG-DA hydrogel relative to those of the VF LP, hydrogel elastic compressive moduli data at 40 Hz (mechanical measures above 40 Hz being neglected due to data quality limitations) were compared to literature values of LP elastic shear moduli at similar frequencies [71]. The fact that PEG-DA hydrogels can be considered homogenous and isotropic was used in these comparisons [15, 72]. For homogenous, isotropic materials, the elastic compressive modulus (E) is related to the elastic shear modulus (G) by the following relationship: $G = E/(2+2\upsilon)$, where υ is the hydrogel Poisson ratio. For polymeric hydrogels, $\upsilon \sim 0.5$, and thus, $G = E/3$ [15].

Hydrogel degradation rate. A PEG-DA hydrogel is a 3D network of inter-crosslinked PEG-DA macromers. The modulus and mesh size of this hydrogel is intimately related to the organization and density of these crosslinks. As PEG-DA hydrogels degrade hydrolytically, the crosslinks among PEG-DA chains are broken, resulting in a decrease in hydrogel modulus and a corresponding increase in hydrogel mesh size [73]. At the low cell densities used in the present study (~0.5x106 cells/mL), change in hydrogel modulus with time can be assumed to be dominated by the hydrolytic degradation of the hydrogel network rather than by ECM deposited by

encapsulated cells. Thus, by monitoring the change in construct mechanical properties with time, the degradation rate of each hydrogel network can be assessed.

To confirm that our initial assumption that selected hydrogels had similar degradation rates, the compressive elastic modulus of each hydrogel formulation at day 30 was assessed according to the methodology described above. The resulting modulus data were compared to the corresponding measures at day 0 to determine a degradation half-life for each hydrogel formulation assuming first-order degradation kinetics [73].

3.3.4 Cell culture

Frozen VFF at passage 3 (provided by Robert Langer, ScD)[31] were thawed and cultured at 37 ºC/5% CO2 in DMEM supplemented with 10% FBS, 1 mg/L bFGF, 100 U/mL penicillin, and 100 mg/L streptomycin (Hyclone). These VFF were isolated via primary explantation from the mid-membranous LP of 6-12 month old pigs, a common animal model for the human VF LP [74]. The discarded animal tissue was obtained via the MIT Division of Comparative Medicine with the approval and according to the guidelines of the MIT animal care committee.

3.3.5 Cell encapsulation and hydrogel maintenance

VFF at passage 8-9 were harvested and resuspended in each precursor solution such that the post-swelling cell density would be ~0.5x106 cells/mL. A low cell density was selected so that the evolution in each hydrogel modulus with time could be attributed primarily to scaffold degradation. ACRL-PEG-RGDS was added to each precursor solution so that the concentration of RGDS in the swollen hydrogel would be 2 μmol/mL. The cell-precursor solution mixtures were photopolymerized into hydrogels as described above. The hydrogel slabs were transferred to Omnitrays (Nunc) fitted with 4 sterile polycarbonate bars to simultaneously prevent gel flotation and prevent gel contact with the tray bottom. Gels were immersed in DMEM supplemented with 10% FBS, 100 U/mL penicillin, and 100 mg/L streptomycin and maintained at 37 ºC/5% CO2. Media was changed every two days. At day 30 of culture, a series of 1.25 cm diameter samples

were collected from each hydrogel formulation for biochemical, histological and mechanical analyses. Mechanical analyses were conducted as described above.

3.3.6 Biochemical analyses

Samples harvested for biochemical analyses were transferred to screw-cap vials, weighed, flash-frozen in liquid nitrogen, and stored at -80 ºC. At time of analysis, hydrogel samples were digested for 24 h at 37 ºC in 1 ml of 0.1 M NaOH per 0.2 g hydrogel wet weight [75]. The samples were then centrifuged (10,000xg for 10 min), and aliquots were taken for DNA and sGAG quantification. Any material pelleted during centrifugation was resuspended by vortexing, and additional hydrolysis was carried out by transferring the samples to a 100 ºC oven for 90 min to solubilize collagen but not elastin [75]. These samples were then centrifuged (10,000xg for 10 min), and the supernatant was retrieved for collagen quantification. The pellets (containing elastin) were washed with dIH_2O at least four times and stored at -80 ˚C until use.

DNA analysis. Aliquots of the hydrolyzed samples (n = 6 per formulation) were neutralized and their DNA content determined using the PicoGreen assay (Invitrogen) [75]. DNA measures were translated to cell number using a conversion factor of 6.6 pg DNA per cell [76]. Calf thymus DNA (Sigma) served as a standard.

Sulfated GAG analysis. sGAG production was measured using a modification of the Blyscan assay (Biocolor). In brief, 80 µL of each sample digest (n = 4 per formulation) was neutralized, mixed with 120 µL Blyscan dye reagent, and the absorbance at 525 nm immediately measured relative to chondroitin sulfate B (Sigma).

Collagen analysis. Levels of hydroxyproline were quantified as an indirect measure of total collagen. In brief, supernatants (n = 3-4 per formulation) collected for collagen quantitation were hydrolyzed for 18 h at 110 ºC in 6 M HCl. Hydrolyzed samples were then dried (Centrivap, Labconco) followed by resuspension in dIH_2O and

reaction with chloramine T and p-dimethylbenzaldehyde reagents [31]. Sample absorbance was read at 550 nm relative to that of L-4-hydroxyproline (Sigma) [31]. Total collagen content was estimated from measured grams of hydroxyproline by dividing by 0.13 [77].

Elastin analysis. Elastin levels were determined according to the procedure detailed in Long et al.48 Briefly, material pelleted following 100 °C NaOH exposure was further digested in 6 M HCl at 110 ºC for 18 h. Samples (n = 3 per formulation) were then dried (Centrivap, Labconco), and the resulting free amino acids were dissolved in 100 µl of 0.1M sodium citrate buffer (pH 5.0). Following addition of an equal volume of ninhydrin reagent (Sigma), samples were boiled for 15 min, cooled, and their absorbance read at 570 nm. Hydrolyzed α-elastin (MP Biochemicals) was used as the standard.

The ninhydrin-based elastin readings were verified for a subset of samples (n = 2 per formulation) using direct ELISA [78] according to the following protocol. Undigested samples were hydrolyzed with 0.1 M NaOH for 24 h at 37 ºC, neutralized, and further digested with 0.25 M oxalic acid at 100 ºC overnight. Oxalic acid was then removed and exchanged for PBS using Microcon YM-3 centrifugal filters (Millipore). 100 µL of the resulting samples were applied to a high binding EIA 96 well plate (Nunc) for 3 h at room temperature. After blocking the plate with bovine serum albumin, adsorbed elastin fragments were detected by applying elastin antibody (clone B4, Santa Cruz Biotechnology, SCBT) followed by donkey anti-mouse HRP secondary antibody (SCBT) and 2,2'-azino-bis(3-ethylbenzthiazoline-6-sulphonic acid). Absorbance was read at 410 nm, with bovine aortic elastin (Sigma) serving as a standard.

For the DNA, sGAG, hydroxyproline and direct ELISA assays, the standards used were subjected to the same association with PEG-DA, hydrolysis, and processing conditions as the samples. Resulting collagen, elastin, and sGAG levels were normalized to cell number.

3.3.7 Histological analysis

Samples collected for histological analyses were fixed with 10% formalin for 30 min, embedded in Tissue-Tek media, and cut into 35 μm sections. ECM deposition was analyzed in duplicate sections for each formulation using standard immunohistochemical technique. In brief, sections were exposed to Terminator (Biocare Medical) for 30 min followed by 1 h exposure to primary antibody for elastin (B4, Sigma), fibrillin-1 (12A.5, LabVision), or collagen type I (Rockland) diluted in HBS. After 30 min treatment with Peroxidase (Biocare Medical), bound primary antibody was detected using the AEC Histostain-SP kit (Invitrogen). To detect GAG, sections were stained with toluidine blue solution (0.0714% toluidine blue, 0.0714% pyronin Y, and 0.143% borax) for 6 min and rinsed with distilled water [31]. Stained sections were imaged using an Axiovert A200 microscope (Zeiss).

To identify VFF displaying a myofibroblast-like phenotype and cells undergoing proliferation, immunohistochemical staining for SM-α-actin (1A4, LabVision) was conducted as described above. For each stained section, the number of cells which stained positively for SM-α-actin was counted by two separate observers relative to total cells in each section. To assess cell proliferation, immunostaining for PCNA (Zymed) was carried out.

3.3.8 Statistical analyses

All data is reported as mean ± standard deviation. Comparison of sample means was performed using ANOVA and Tukey`s post-hoc test (SPSS software), $p < 0.05$.

3.4 Results

The aim of the present study was to analyze the effects of initial scaffold mesh size and elastic modulus on VFF ECM production and phenotype. To isolate these scaffold parameters, 4 PEG-DA hydrogel formulations with similar degradation rates but differing moduli and mesh sizes were examined: (1) 10% 10 kDa, (2) 10% 8 kDa, (3) 20% 10 kDa, and (4) 30% 10 kDa. Furthermore, cell adhesion peptide RGDS was

conjugated into each hydrogel so that scaffold bioactivity could be considered a design constant.

3.4.1 Hydrogel mesh size, mechanical properties, and degradation rate

To evaluate initial scaffold material properties, average mesh size was evaluated for each hydrogel formulation at day 0. As previously mentioned, the mesh size of PEG-DA hydrogels cannot be visualized using conventional SEM. Thus, hydrogel resistance to the diffusion of dextrans of various M_ws was used as a quantitative indicator of scaffold mesh size. The resulting mesh sizes are displayed in Figure 3.2A. As expected, initial mesh size increased as the weight percent of PEG-DA decreased [66, 68].

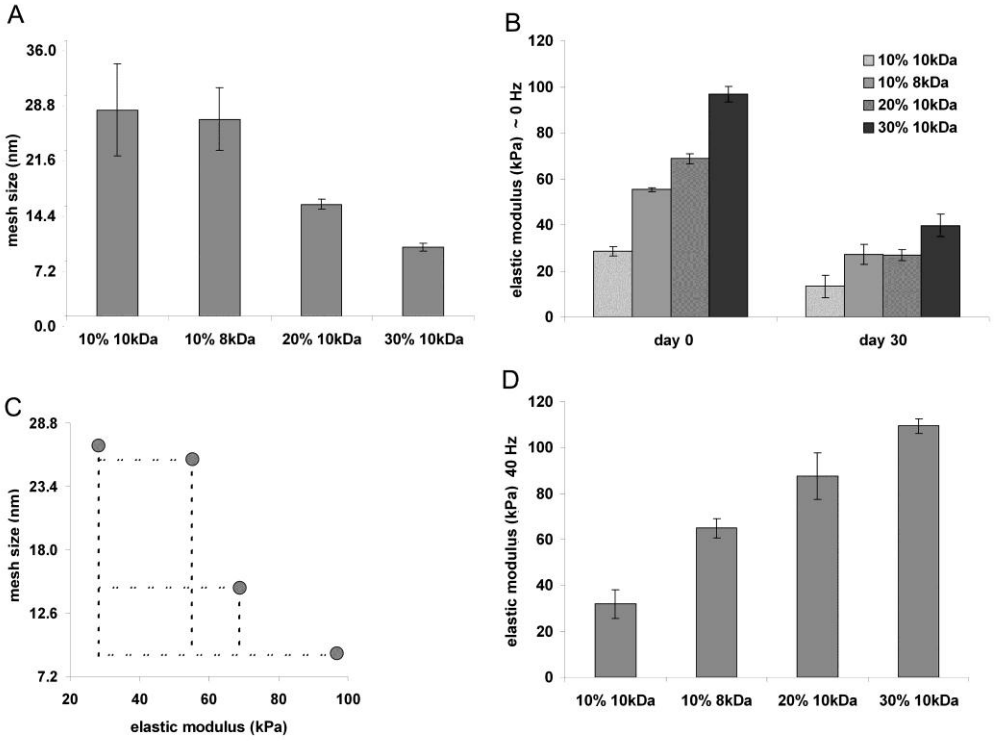

Figure 3.2 Scaffold material properties. (**A**) Hydrogel mesh size at day 0, (**B**) elastic compressive modulus at approximately static (0.01 Hz) conditions at days 0 and 30, and (**C**) time-zero mesh size-elastic modulus sample-space. Gray dots correspond to initial mesh size-modulus combinations explored. Dashed lines are intended to highlight alterations in initial mesh size and modulus among the formulations. (**D**) Hydrogel elastic compressive modulus at 40 Hz at day 0.

To assess the initial mechanical environment experienced by encapsulated VFF and to confirm that the degradation rate of each hydrogel formulation was similar, the elastic compressive modulus of each hydrogel at ~1% cyclic strain was measured over a range of frequencies at day 0 and day 30. To represent the scaffold stiffness experienced by cells under the selected culture conditions, static (0.01 Hz) mechanical property data are presented in Figure 3.2B. Concordant with existing literature, hydrogel elastic compressive modulus at a given time-point increased significantly as PEG-DA M_w decreased and/or concentration increased (Figure 3.2B) [75]. Furthermore, the elastic moduli of all hydrogel formulations decreased significantly from day 0 to day 30 (Figure 3.2B).

Since the cell density in each hydrogel was low, the evolution in the elastic modulus of each hydrogel could be assumed to be dominated by the material degradation kinetics rather than by cell ECM deposition. Based on the modulus data at day 0 versus day 30, the mean degradation half-life of all hydrogel formulations was determined to be 25.4 ± 3.3 days, assuming first order degradation kinetics [73]. Thus, since each hydrogel formulation displayed a similar degradation rate, the rate of change in hydrogel elastic modulus (and, hence, hydrogel mesh size) [73] could be treated as a design "constant". This allowed variations in VFF ECM deposition and phenotype with scaffold formulation to be evaluated relative to initial scaffold material properties without loss of information. VFF ECM production and phenotype will therefore be discussed referencing time-zero hydrogel mesh size and elastic modulus. To aid in this discussion, Figure 3.2C shows a map of the time-zero mesh size - modulus sample space probed in the present study.

Note that the maximum initial mesh size explored was ~3 times that of the minimum and that the maximum initial elastic modulus was ~3.4 times the minimum. Thus, similar ranges of initial mesh size and of initial elastic modulus were explored in the present study, enhancing our ability to compare the relative impact of these two scaffold variables on VFF behavior. As demonstrated in Figures 3.2A, B, the initial mesh size and elastic modulus of hydrogels formed from PEG-DA macromers of a

single M_w cannot be independently modified (i.e., as the concentration of PEG-DA is increased from 10% to 30% for the 10 kDa PEG-DA hydrogels, the mesh size decreases and modulus increases). However, we can explore the effects of mesh size and elastic modulus in an uncoupled manner by appropriately varying both PEG-DA concentration and M_w. For instance, the 10% 10 kDa and the 10% 8 kDa hydrogels have similar initial mesh sizes but significantly different initial elastic moduli. Similarly, the 10% 8 kDa hydrogel and the 20% 10 kDa hydrogels have mesh sizes that differ by ~55% but elastic moduli which differ by only ~19%. To demonstrate that the initial mechanical properties of the selected hydrogels are within a stiffness range appropriate for VF LP tissue engineering, 40 the time-zero elastic compressive modulus of each hydrogel at 40 Hz (nearer adult phonatory threshold) is presented in Figure 3.2D.

3.4.2 Biochemical and histological analyses

PEG-DA constructs were harvested at day 30 for biochemical and histological analyses. Cell density in each formulation at day 30 was > 60% of the initial seeding density based upon DNA assessments, consistent with results from previous PEG-DA tissue engineering studies [55]. Measured collagen, elastin, and sGAG levels for each hydrogel formulation are given on a per cell basis in Figure 3.3 sGAG production increased smoothly and ~16 fold from the 10% 10 kDa to the 30% 10 kDa hydrogels ($p < 0.032$). A significant increase in collagen ($p < 0.001$) was observed at the transition between 10% 8 kDa and 20% 10 kDa hydrogels, although no further significant change was observed progressing from the 20% 10 kDa to the 30% 10 kDa hydrogels. Elastin levels increased between the 10% 8 kDa and 20% 10 kDa hydrogels ($p < 0.001$) but then decreased proceeding to the 30% 10 kDa formulation ($p = 0.003$). A significant increase in the fraction of cells expressing SM-α-actin ($p = 0.019$) was observed from the 10% 8 kDa to the 20% 10 kDa hydrogels, although no further change was observed between the 20% 10 kDa and 30% 10 kDa hydrogels (Figure 3.3).

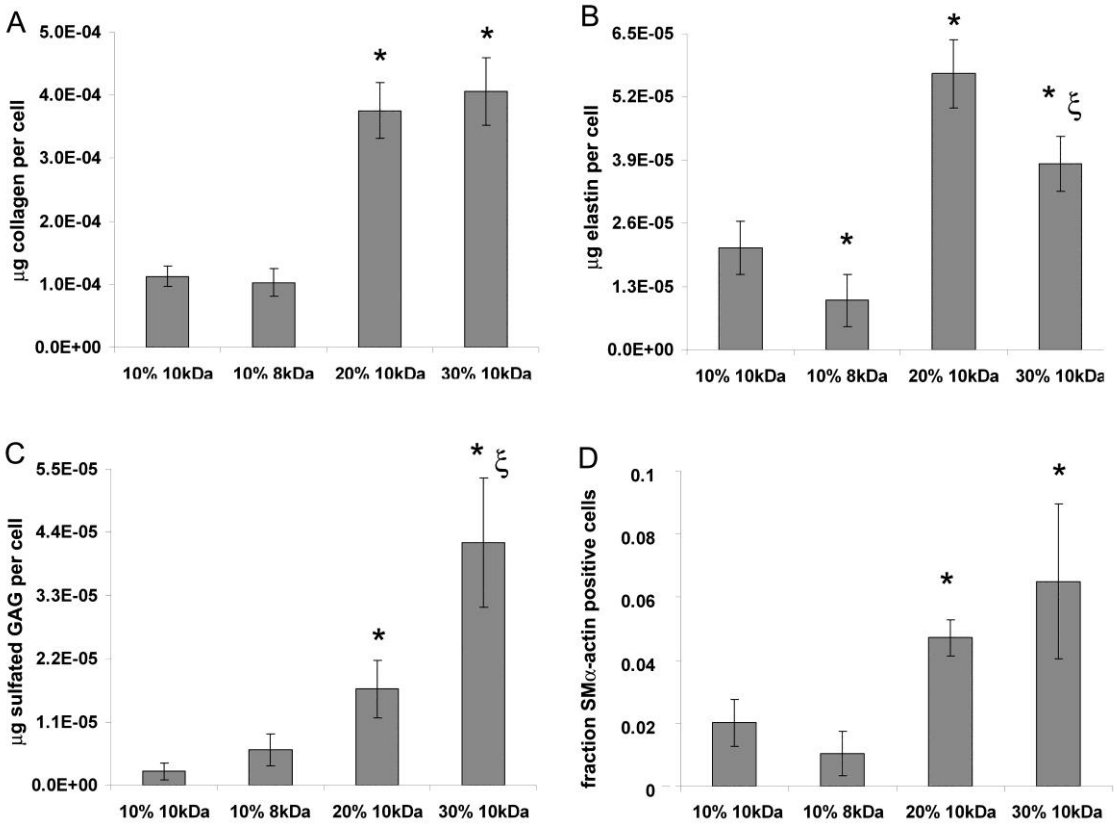

Figure 3.3 Vocal fold fibroblast ECM deposition and phenotype. (**A**) collagen, (**B**) elastin, (**C**) sulfated glycosaminoglycan (sGAG), and (**D**) relative SM-α-actin expression at day 30 in each hydrogel formulation. *indicates a significant difference with the 10% 10 kDa formulation. ξ indicates a significant difference with the 20% 10 kDa formulation.

Histological analyses of collagen, elastin, and GAG supported the biochemical results (Figure 3.4). To gain insight into the quality of elastic fiber formation, staining was also conducted for the elastin organizing microfibril, fibrillin-1. The relative intensity of fibrillin-1 staining among formulations corresponded closely with that of elastin staining, suggesting that the deposited elastin may be organizing into functional fibers, in contrast to elastin deposition in many tissue engineered situations [79]. Immunostaining for PCNA indicated heightened rates of VFF proliferation with increasing scaffold mesh size and/ordecreasing modulus (data not shown).

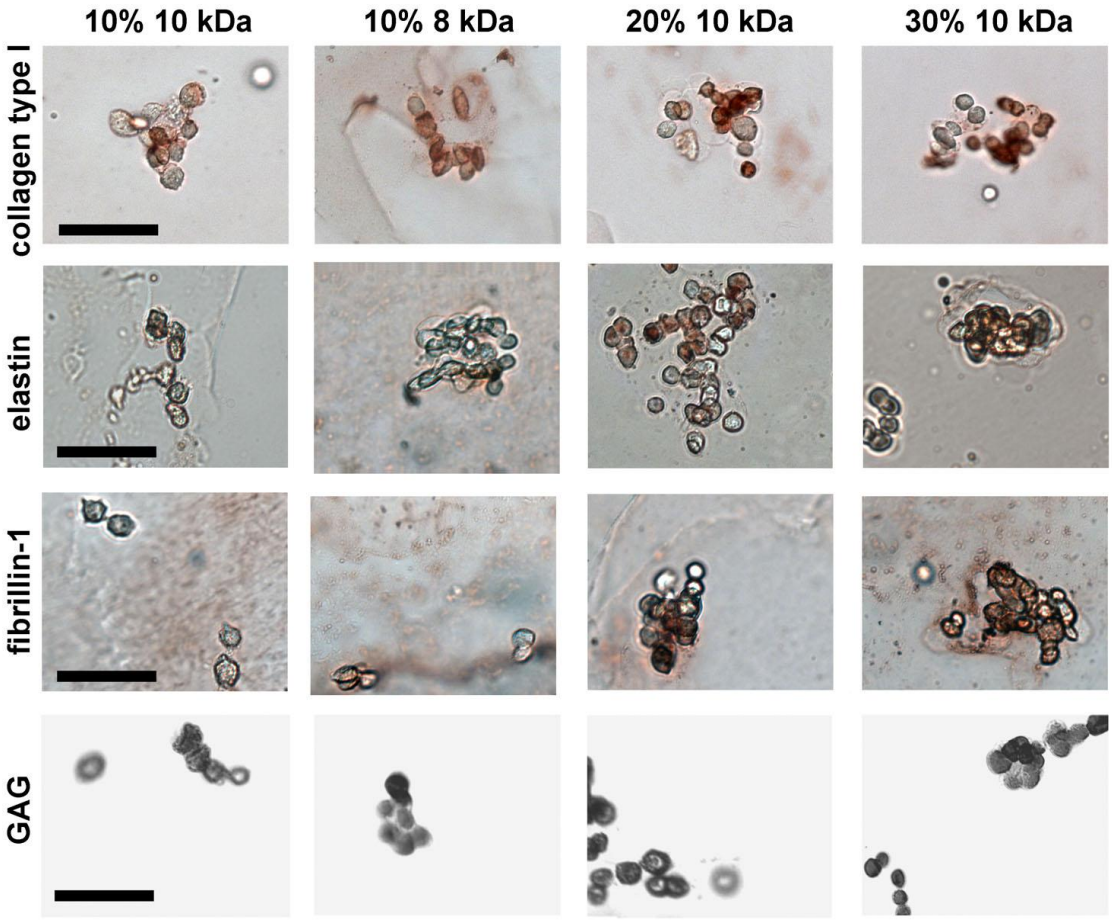

Figure 3.4 Representative images of staining for collagen type I, elastin, fibrillin-1, and GAG. GAG images are shown in grayscale to enhance contrast. Scale bars = 50μm.

3.5 Discussion

A range of scaffold properties are known to influence cell behavior, including bioactivity, mesh size, mechanical properties, and degradation rate [30, 53-57]. For controlled examination of the effects of various scaffold properties on cell behavior, we selected the scaffold material PEG-DA. Like many scaffolds formed from synthetic materials, the mechanical properties, mesh size, and degradation rate of PEG-DA hydrogels can be tuned over a relatively broad range [62, 80]. However, unlike most synthetic material scaffolds, PEG-DA hydrogels do not significantly adsorb bioactive plasma proteins [58]. Thus, scaffold presentation of bioactive stimuli can be tightly controlled in addition to mesh size, modulus, and degradation rate. For the PEG-DA

hydrogels investigated (with degradation half lives of ~25 days), both VFF ECM deposition and phenotype demonstrated a strong dependence on initial hydrogel mesh size and elastic modulus. sGAG synthesis increased both with increasing initial elastic modulus (e.g., 10% 10 kDa vs 10% 8 kDa) and with decreasing initial mesh size (e.g.,, 10% 8 kDa vs 20% 10 kDa).

The relative expression of SM-α-actin, a marker indicative of fibroblast differentiation into a myofibroblast phenotype, demonstrated a similar trend as collagen (Figure 3.3D). VFF are believed to transform into myofibroblasts in response to LP injury, and higher myofibroblast levels have been linked with increased collagen deposition [18]. Studies of lung and arterial tissue indicate that cell elastin [81] and GAG secretion [82] are also elevated with increasing myofibroblast phenotype. Furthermore, elevated VFF proliferation rates (fraction of cells expressing PCNA) were observed with increasing mesh size and decreasing modulus. Increased cell proliferation has frequently been correlated with decreased matrix synthesis. Thus, the increased induction of a myofibroblast-like phenotype and decreased proliferation rates observed with decreasing initial mesh size may contribute to the observed dependence of collagen, elastin, and GAG levels on initial scaffold mesh size. Given the mesh sizes of the selected hydrogel formulations relative to the diameters of collagen (~4-25 nm), elastin (~2-10 nm), and moderately sized proteoglycans (~9 nm), the heightened potential of these molecules to diffuse out of the hydrogel network as mesh size increased may also contribute to the observed dependence of ECM deposition on mesh size.

A limitation of the present study is the range of mesh-size and mechanical properties probed. Future experiments will explore a broader range of initial moduli and mesh sizes as well as investigate the impact of degradation rate. A drawback of the current approach can be seen in examining Figure 3.4. Despite the presence of adhesion peptide RGDS, encapsulated VFF took on rounded or stellate morphologies within the PEG-DA hydrogels, in agreement with previous 3D PEG-DA studies. These morphologies are non-native for VFF in the midmembranous VF LP, in which fibroblasts generally take on spindle-shaped morphologies. The cell morphologies and

pericellular localization of deposited ECM localization observed herein arise from the basic character of PEG-DA hydrogels that have not been modified with additional hydrolytically or enzymatically degradable segments [55, 57, 58, 75, 83]. This particular characteristic of the selected PEG-DA formulations is not optimal for fibroblasts. However, as indicated in the Introduction, PEG-DA hydrogels were selected for the present study not because they are necessarily the optimal materials for vocal fold restoration, but for our ability to systematically tune their material properties. This characteristic of PEG-DA hydrogels permits more controlled examination of the dependence of cell ECM production and phenotype on specific scaffold material properties, enhancing our ability to rationally design scaffolds to achieve desired cell responses.

Interestingly, the trends in collagen and elastin production with respect to alterations in initial scaffold modulus/mesh size appear to mimic those observed in native LP [25, 31, 84]. Specifically, the SLP is a relatively loose, low modulus, connective tissue, containing low levels of collagen and elastin relative to deeper regions of the LP [31, 84]. The ILP and DLP are traditionally demarcated from the SLP by a marked increase in tissue density, stiffness, and elastin and collagen levels [25, 31, 84]. Thus, the initial 10% 10 kDa hydrogel material properties and stimulated ECM production correspond to those of the SLP, whereas the initial 20% 10 kDa and 30% 10 kDa hydrogel material properties and resultant ECM synthesis are more similar to those of the ILP and DLP. The correspondence between the dependence of ECM deposition with varying scaffold mesh size/modulus observed in the current work and the dependence of ECM composition with regional LP mesh size/modulus lends further strength to the present data. While it is perhaps natural that many LP bioimplant studies have focused on implant modulus rather than on microstructure [46-51] due to the LP's key biomechanical function, the present results suggest that implant mesh size may be as critical as its mechanical properties in modulating observed ECM levels.

CHAPTER IV
PROBING VOCAL FOLD FIBROBLAST RESPONSE TO HYALURONAN USING PEG-BASED HYDROGELS*

4.1 Overview

A number of treatments are being investigated for vocal fold (VF) scar, including designer implants. The aim of the present study was to validate a 3D model system for probing the effects of various bioactive moieties on VF fibroblast (VFF) responses toward rational implant design. We selected poly(ethylene glycol) diacrylate (PEG-DA) hydrogels as our base-scaffold due to their broadly tunable material properties. However, since cells encapsulated in PEG-DA hydrogels are forced to take on rounded/stellate morphologies, validation of PEG-DA gels as a 3D VFF model system required that the present work directly parallel previous studies involving more permissive scaffolds. We therefore chose to focus on hyaluronan (HA), a polysaccharide that has been a particular focus of the vocal fold community.

Toward this end, porcine VFFs were encapsulated in PEG-DA hydrogels containing consistent levels of high M_w HA (HA_{HMW}), intermediate M_w HA (HA_{IMW}), or the control polysaccharide, alginate, and cultured for 7 and 21 days. HA_{HMW} promoted sustained increases in active ERK1/2 and collagen type III relative to HA_{IMW} and alginate. In contrast, VFFs in HA_{IMW} gels displayed a more myofibroblast-like phenotype, higher elastin production, and greater protein kinase C (PkC) levels at day 21 than VFFs in HA_{HMW} gels.

The present results are in agreement with a previous 3D study of VFF responses to HA_{IMW} relative to alginate in collagen-based scaffolds permissive of cell elongation, indicating that PEG-DA hydrogels may serve as an effective 3D model system for probing at least certain aspects of VFF behavior.

4.2 Introduction

Voice disorders resulting from scarring of the vocal fold (VF) lamina propria (LP) affect millions in the US alone and can significantly impact quality of life [37]. VF scar has proven difficult to treat with current surgical techniques and standard augmentation substances, such as collagen and fat [39, 42, 45]. Researchers are actively exploring alternative treatment routes, including the development of designer implants for functional LP regeneration [46-51].

Hyaluronan (HA) has been a particular focus as a component of these designer implants due to its role in wound healing and in VF mechanical properties[46-48, 50, 51]. Although several in vivo studies suggest HA to be a promising material for VF regeneration, [50, 85, 86] to rationally improve the design and formulation of these HA-based implants requires a deeper understanding of the impact of HA on VFF extracellular matrix (ECM) production and phenotype.

A number of tissue engineering studies have examined cellular response to HA in 2D scenarios [87-90]. However, evaluating the specific influence of HA in more physiologically-relevant 3D contexts has proven challenging due to the additional, often interdependent, matrix variables introduced in 3D. To understand this, examine a recent study in which mesenchymal stem cells encapsulated within collagen beads displayed an increased tendency to differentiate into chondrocytes as collagen density increased [91]. Whether this increased chondrocytic potential was due primarily to the increased spatial density of bioactivity (collagen) or to the increased matrix stiffness associated with heightened collagen concentration is unclear. Being able to make such distinctions is particularly important since both scaffold modulus [92] and bioactivity [93] have been shown to exert profound effects on cell behavior in 2D.

To begin to uncouple the effects of various stimuli on VFF behavior in 3D requires a scaffold whose material properties can be more tightly controlled. Hydrogels prepared from poly(ethylene glycol) diacrylate (PEG-DA) are intrinsically resistant to cell attachment and spreading [58]. This biological "blank slate" character of PEG-DA hydrogels permits the controlled introduction of desired bioactivity and examination of its effects on cell behavior [94]. Furthermore, the initial bulk average mesh size and modulus of PEG-DA hydrogels can be tuned in an uncoupled manner by simultaneously varying both the molecular weight (M_w) and/or concentration of PEG-DA [95]. PEG-DA gels have been widely employed incartilage tissue engineering due to their tailorable material properties [52, 62, 96]. However, they are rarely used for encapsulation of natively elongated cells, such as fibroblasts, due to the fact that encapsulated cells are forced to take on rounded/stellate morphologies. Thus, validation of PEG-DA gels as a 3D VFF model system requires that the present study be performed so as to permit direct comparison with previous studies involving scaffolds permissive of cell elongation.

We therefore designed the current work to be a direct analog of a previous 3D study of the influence of HA on VFF behavior by Hahn et al. [31]. In that work, porcine VFF responses to intermediate M_w HA (HA_{IMW}, ~490 kDa) relative to the control polysaccharide alginate (~300-350 kDa, 65–75% guluronate) were investigated in basehydrogels of collagen type I. In the present work, porcine VFFs from the same explant population employed in Hahn et al. [31] were encapsulated in 100 mg/mL (10 wt%) PEG-DA hydrogels containing 0.5 wt% of high M_w HA (HA_{HMW}, ~$1.65x10^3$ kDa), HA_{IMW} (~600 kDa), or alginate (~300-350 kDa, 65–75% guluronate). The promiscuous integrin adhesion peptide RGDS [97] was used in place of integrin adhesion ligand collagen type I. Following 7 and 21 days of culture, VFF ECM production and phenotype in each formulation was assessed biochemically and histologically. Furthermore, the modulation of two primary signaling pathways (protein kinase C (PkC) and ERK) triggered by HA interactions with cell receptors, RHAMM (receptor for hyaluronan-mediated motility) and CD44, [98-100] were semi-quantitatively evaluated.

4.3 Materials and methods

4.3.1 Polymer synthesis and characterization

PEG-diacrylate synthesis .PEG-DA was prepared as previously described by Hahn et al. [94] by combining 0.1mmol/mL dry PEG (10 kDa, Sigma, St. Louis, MO), 0.4 mmol/mL acryloyl chloride, and 0.2 mmol/mL triethylamine in anhydrous dichloromethane (DCM) and stirring under argon overnight. The resulting solution was washed with 2M K_2CO_3 and separated into aqueous and DCM phases to remove HCl. The DCM phase was subsequently dried with anhydrous $MgSO_4$, and PEG-DA was precipitated in diethyl ether, filtered, and dried under vacuum. The degree of acrylate functionalization was determined by ^{1}H-NMR to be ~70%.

Synthesis of acrylate-derivatized. Cell Adhesion Peptide Cell adhesion peptide RGDS (American Peptide, Sunnyvale, CA) was reacted with acryloyl-PEG-N hydroxysuccinimide (ACRL-PEG-NHS, 3.4 kDa, Nektar, San Carlos, CA) at a 1:1 molar ratio for 2 h in 50mM sodium bicarbonate buffer, pH 8.5 [94]. The product (ACRLPEG- RGDS) was purified by dialysis, lyophilized, and stored at -20 ºC until use.

Synthesis of methacrylate-derivatized high molecular weight HA and alginate. Methacrylate-derivatized high M_w HA (HA_{HMW}-MA) and methacrylate-derivatized alginate (alginate-MA) were prepared according to standard methodologies (Masters et al., 2005). HA (Streptococcus equi, M_w ~$1.65x10^3$ kDa, Fluka) or alginate (Laminaria hyperborea, 300–350 kDa, 65–75% guluronate, FMC BioPolymer Philadelphia, PA) was dissolved at 1-wt% in dIH_2O and the pH of the resulting solution was adjusted to 8.0 using NaOH. A 10-fold molar excess of methacrylic anhydride (Polysciences, Warrington, PA) was added per disaccharide unit. Each reaction was allowed to proceed under constant stirring at 4 ºC, with the solution pH being maintained at ~8.0 by periodic addition of 5M NaOH. The product of each reaction was precipitated twice into chilled ethanol 95%, dialyzed against dIH_2O for 48 h, and lyophilized. The extent of

methacrylatederivatization of both HA and alginate was characterized by ^{1}H-NMR to be ~3.2%.

Synthesis of methacrylate-derivatized Intermediate molecular weight HA. HA_{HMW}-MA was dissolved at 1 mg/mL in PBS containing 0.05% sodium azide and 5 U/mL hyaluronidase IV-S (H3884, Sigma). Following incubation at 37 ºC for 12 h, the enzyme was heat-inactivated. The digestion time and conditions were selected to yield a mean HA product size consistent with the HA M_w used in Hahn et al. [31] The resulting digestion product (HA_{IMW}-MA) was dialyzed against dIH_2O for 48 h and lyophilized. The M_w of the isolated HA_{IMW}-MA was determined to be ~600 kDa using gel permeation chromatography (Viscotek, Houston, TX).

Assessment of alginate as a control and of HA-MA activity The ability of alginate and HA_{HMW}-MA to interact with HA link protein (HABP) was evaluated relative to HA_{HMW} using an HA competitive ELISA assay (Echelon Biosciences, Salt Lake City, UT).

4.3.2 Cell culture

Cryopreserved porcine VFFs at passage 3 from the same VFF explant culture employed in Hahn et al. [31] were obtained from Robert Langer, ScD (Massachusetts Institute of Technology (MIT), Cambridge, MA). These cells had been isolated from the mid-membranous LP of 6- to 12-month-old pigs, a common animal model for the human VF LP [74]. The discarded animal tissue was obtained via the MIT Division of Comparative Medicine and with the approval and according to the guidelines of the MIT animal care committee. The cryopreserved VFFs were thawed and expanded at 37 ºC/5% CO_2 in Dulbecco's Modified Eagle's Media (DMEM, Hyclone, Logan, UT) supplemented with 10% fetal bovine serum (FBS), 2 ng/mL bFGF, 100 mU/mL penicillin, and 100 mg/L streptomycin (Hyclone).

4.3.3 Cell encapsulation and hydrogel maintenance

Hydrogels were fabricated by preparing precursor solutions containing 100 mg/mL (10 wt%) PEG-DA, 5 mg/mL of methacrylate-derivatized polysaccharide (HA_{HMW}-MA, HA_{IMW}-MA, or alginate-MA), and 1 mmol/mL ACRLPEG- RGDS in HEPES buffered saline (HBS; 10mM HEPES, 150mM NaCl, pH 7.4). The concentrations of HA and alginate were selected to be consistent with Hahn et al. [31]. A 10-wt% 10 kDa PEG-DA hydrogel was chosen for the base-scaffold due to a previous study of VFF responses to PEG-DA gels [101]. In addition, the 100:5 weight ratio of PEG-DA to polysaccharide was selected so that the degradation rate, modulus, and initial mesh structure of each hydrogel network would be dominated by PEG-DA.

A 300 mg/mL solution of UV photoinitiator 2,2- dimethoxy-2-phenyl-acetophenone in N-vinylpyrrolidone was added at 1% (v/v) to each precursor solution. VFFs at passages 8–9 were harvested and resuspended in the filtersterilized precursor solutions at ~$1x10^6$ cells/mL (the seeding density employed in Hahn et al. [31]. The cell suspensions were then poured into molds composed of two glass plates separated by 1.1mm polycarbonate spacers and polymerized by 2 min exposure to longwave UV light (Spectroline, Westbury NY, ~6mW/cm^2, 365 nm). The hydrogel slabs were transferred to Omnitrays (Nunc, Rochester, NY) fitted with four sterile polycarbonate bars to simultaneously prevent gel flotation and prevent gel contact with the tray bottom. Hydrogels were immersed in DMEM supplemented with 10% FBS, 100 U/mL penicillin, and 100 mg/L streptomycin, and maintained at 37 ºC/5% CO_2. Media was changed every 2 days.

4.3.4 Hydrogel characterization

Initial water uptake. To compare the extent of initial water uptake by the various hydrogel formulations following polymerization, the initial weight (W_i) of each hydrogel was determined immediately following polymerization, after which the gelswere

submerged in media. Following 3 days of culture, the swollen weight (W_s) of each gel was determined. The equilibrium water uptake (S) was calculated as: $S = \frac{W_s}{W_i}$.

Hydrogel mechanical properties and contraction After 72 h swelling, three 8 mm diameter samples were cored from each hydrogel. The thickness of each disc was measured using a digital caliper. These thickness measuresserved both as gauge lengths for mechanical testing and as indicators of hydrogel degradation and/or VFF-mediated gel compaction. Following application of a 0.01N preload, each hydrogel was subjected to cyclic unconstrained compression (~1% cyclic strain) at 2.5 Hz using an Instron 3342 (Instron, Norwood, MA). During mechanical testing, samples were immersed in silicone oil to prevent hydrogel dehydration. The dynamic compressive modulus of each hydrogel formulation was extracted from the resulting stress–strain data.

4.3.5 Biochemical analyses

At days 7 and 21 of culture, a series of 8 mm diameter samples were collected from each hydrogel formulation for mechanical, biochemical, and histological analyses. Mechanical samples were tested as described above. Samples harvested for biochemical analyses were transferred to screw-cap vials, weighed, flash-frozen in liquid nitrogen, and stored at -80 ºC until time of analysis. The weight of each 8 mm disc was used as a second indicator of gel degradation and/or compaction, since associated reductions in gel volume would be reflected in a mass loss. Hydrogel samples were digested for 72 h at 37 ºC in 1 mL of 0.12M NaOH per 0.2 g hydrogel wet weight [75, 102]. Digest aliquots were then analyzed for DNA, total collagen, elastin, and sulfated glycosaminoglycan (sGAG) content per established protocols.

DNA analysis. Aliquots of the hydrolyzed samples (n=3–6 per formulation) were neutralized and their DNA content determined using the Invitrogen (Carlsbad, CA) PicoGreen assay [75]. DNA measures were translated to cell number using a conversion

factor of 6.6 pg DNA per cell (Gregory, 2000). Calf thymus DNA (Sigma) served as a standard.

Sulfated GAG analysis. sGAG production was measured using a modification of the Biocolor Blyscan assay (Accurate Chemical and Scientific Corp., Westbury, NY) [95]. In brief, 40 µL of each sample digest (n=3–4 per formulation) was neutralized, mixed with 60 µL Blyscan dye reagent, and the absorbance at 525nm immediately measured relative to chondroitin sulfate B (Sigma).

Collagen analysis. The amino acid hydroxyproline was quantified as an indirect measure of total collagen. In brief, aliquots (n=3–7 per formulation) collected for collagen quantitation were hydrolyzed for 18 h at 110 ºC in 6M HCl. Each sample was then dried on a Labconco Centrivap to remove HCl, resuspended in deionized water, and passed through a charcoal-packed centrifugal microcolumn (Nunc). The resultant samples were reacted with chloramine T and p-dimethylbenzaldehyde reagents. [75, 102] Sample absorbance was read at 550 nm relative to that of L-4-hydroxyproline (Sigma). Total collagen content was estimated from measured grams of hydroxyprolineby dividing by 0.13.

Elastin analysis. Elastin production was measured using direct ELISA [78]. NaOH digested samples (n=4–11 per formulation) were neutralized and further digested with 0.25M oxalic acid at 100 ºC overnight. Oxalic acid was removed from the samples and exchanged for PBS using Microcon YM-3 centrifugal filters (Millipore, Billerica, MA). One hundred microliters of the resulting samples were applied to a high binding multiwell plate for 3 h at room temperature. After blocking the plate with bovine serum albumin, adsorbed elastin fragments were detected by applying elastin antibody (BA-4, Santa Cruz Biotechnology, [SCBT], Santa Cruz, CA) followed by donkey anti-mouse HRP secondary antibody (SCBT) and 2,2'-azino-bis(3- ethylbenzthiazoline-6-sulphonic

acid). Absorbance was read at 410 nm, with bovine aortic elastin (Sigma) serving as a standard.

For each assay, the standards used were subjected to the same association with PEG-DA and polysaccharide and to the same digestion conditions as the samples. Resulting collagen, elastin, and sGAG levels were normalized to cell number.

4.3.6 Histological analyses

Days 7 and 21 samples harvested for histological analyses were fixed in 10% formalin for 30 min, embedded in Tissue-Tek freezing media, and frozen at -80 ºC. Thirty-five micrometer-thick sections were cut using a cryomicrotome. All immunostaining steps took place at room temperature unless otherwise noted.

ECM and cell phenotype analyses. ECM deposition was analyzed in duplicate sections for each formulation using standard immunohistochemical technique. Rehydrated sections were blocked with peroxidase for 10 min followed by 10 min exposure to Terminator (Biocare Medical, Concord, CA). Primary antibodies for elastin (BA-4, SCBT), collagen type I (Rockland Immunochemicals, Gilbertsville, PA), or collagen type III (Rockland Immunochemicals) diluted in HBS were then applied for 1 h. To identify VFFs displaying a myofibroblast-like phenotype, primary antibody for SM-α-actin (1A4, LabVision, Fremont, CA) was applied. HA cell surface receptors were also examined using antibodies to RHAMM (H-90, SCBT) and CD44 (F-4 SCBT). Bound primary antibody was detected by using AP-conjugated secondary antibody followed by application of the chromogen Ferangi Blue (Biocare Medical) or by using HRP-conjugated secondary antibody followed by application of the chromogen AEC (LabVision).

Cell proliferation and apoptosis and signaling. To identify VFFs undergoing proliferation, sections were stained for Proliferating Cell Nuclear Antigen (PCNA; PC10, Invitrogen) per the above staining procedure, except that rehydrated sections were

permeabilized (10mM HEPES, pH 6.8, 100mM NaCl, 3mM $MgCl_2$, 300mM sucrose, 0.5% Triton X-100) for 30 min prior to Terminator application. Apoptotic cells were identified using a Terminal deoxynucleotidyl transferase dUTP nick end-labeling (TUNEL) assay (Roche, Indianapolis, IN) per manufacturer's protocol. Cell signaling was evaluated by staining permeabilized sections for PkC (C-15, SCBT) and active ERK1/2 (pERK1/2(Thr202/Tyr 204), SCBT).

Semi-quantitative assessments. For intracellular markers of cell behavior (SM-α-actin, pERK1/2, PkC, PCNA, TUNEL), cell counts were carried out to semi-quantitatively evaluate immunostaining results. These assessments were conducted per established protocols [73, 83, 103, 104]. For each cell, i, in a given section, a staining intensity, d_i, was recorded on a scale of 0–3, 0''no staining'' and 3''highest intensity among all treatment groups for that antibody.'' The cumulative staining intensity, d, for a given antibody in a particular section was calculated using the following equation:

$$d = \frac{\Sigma d_i}{Totalcel\,\ln umber}.$$

Since deposited ECM remained localized around the parent cells in each hydrogel formulation, as is characteristic for PEG-DA gels, [57, 62] the relative levels of collagen and elastin among hydrogel formulations were also evaluated by cell counts per the above procedure. Each HA_{HMW} and HA_{IMW} cumulative staining intensity assessment was normalized to the corresponding intensity assessment for alginate hydrogels.

4.3.7 Statistical analyses

Data are reported as mean ± standard error of the mean. Comparison of sample means was performed by one-way ANOVA and Tukey's post hoc test (SPSS software, Chicago, IL), $P<0.05$.

4.4 Results

The present study was designed to examine the impact of HA_{HMW} and HA_{IMW} relative to alginate on VFF ECM production and phenotype. Following 7 and 21 days of

total culture, constructs were harvested and subjected to mechanical, histological, and biochemical analyses.

4.4.1 Alginate as a control and HA-MA activity

We first verified that alginate was an effective control for HA and that HA-MA retained similar biological function as pure HA. Alginate was intended to serve as a ‘‘scrambled’’ polysaccharide sequence which would impart similar viscoelasticity to the hydrogel network as HA but which would not have the associated cell-interactions. This is similar in concept to the use of the ‘‘scrambled’’ peptide sequence RGES as a control for the cell adhesion peptide RGDS [93]. Competitive ELISA results indicated that alginate was unable to effectively interact with HABP (Figure 4.1B), despite the physiochemical similarities between alginate and HA (Figure 4.1A). In contrast, HA-MA appeared to retain a similar level of affinity for HABP as unmodified HA (Figure 4.1B). This was consistent the work of Masters et al., which demonstrated that HA-MA and unmodified HA each resulted in similar valvular interstitial cell (VIC) ECM production at the HA methacrylation level used herein.

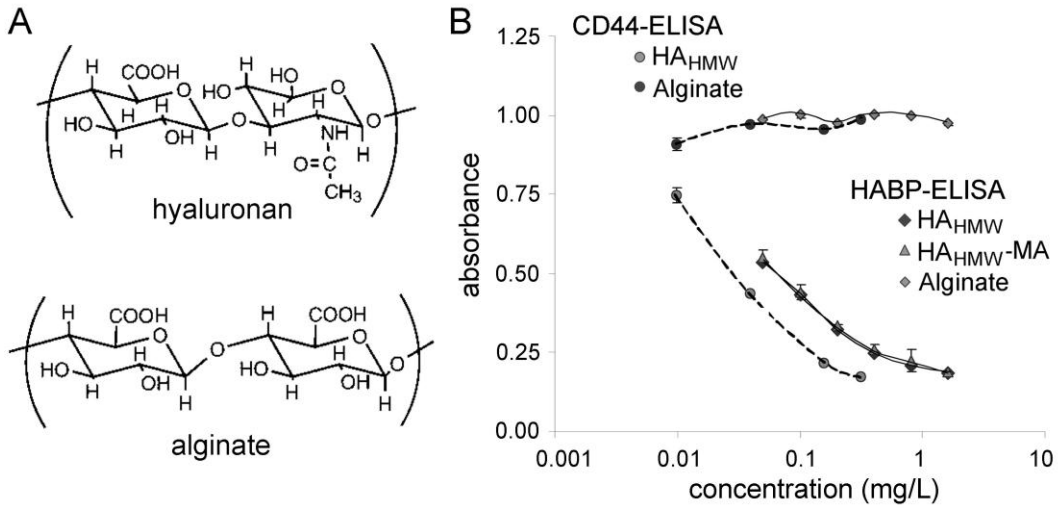

Figure 4.1 A: Structure of hyaluronan (HA) versus alginate disaccharide units. **B**: Competitive ELISA results in which an increased absorbance signal corresponds to a decreased concentration of the test molecule and/or lower affinity of the test molecule for HA link protein (HABP). The ELISA results demonstrate that alginate does not effectively interact with HABP but that methacrylate-derivatized HA (HA-MA) has a similar affinity for HABP as unmodified HA.

4.4.2 Hydrogel material properties

The dense covalent crosslinking and chemical composition of pure PEG-DA hydrogels result in gels that are essentially non-degradable and which permit limited cell-mediated remodeling [55, 57, 75]. These features, although non-physiological, are desirable for studies focused on controlled evaluation of the impact of specific material properties (in the present work, bioactivity) on cell responses. To assess the degree to which the selected polysaccharide hydrogels retained the character of pure PEG-DA hydrogels, the ‘‘bulk’’ material properties of each gel formulation were characterized.

The initial water uptake, S, of each gel following polymerization was similar to that of a pure PEG-DA gel (HA_{HMW}: 1.37 ± 0.06, HA_{IMW}: 1.43 ± 0.04, alginate: 1.43 ± 0.04, pure PEG-DA: 1.40 ± 0.05). Furthermore, the initial (day 3) moduli of the HA_{HMW}, HA_{IMW}, and alginate cells were statistically indistinguishable, as were the day 2 moduli (Table 4.1). Comparison of the day 7 and day 21 moduli reveals indicated that the reduction in modulus for each gel with time in culture was similar to that of pure PEG-DA hydrogels (also containing encapsulated VFFs). To evaluate the potential contribution of gel degradation and VFF-mediated compaction on the observed temporal changes in gel modulus, the thickness and mass of harvested gel discs were measured with time in culture (Table 4.1). These data correspond to a negligible reduction in gel volume with time. Collectively, the bulk modulus, thickness, water uptake, and gel mass assessments indicate that the material properties of the polysaccharide-containing gels were dominated by the presence of PEG-DA rather than by the associated polysaccharides.

Table 4.1. Hydrogel modulus, thickness, and mass assessments.

	Modulus (kPa)		Thickness (mm)		Mass of 8 mm Discs (mg)		
	Day 3	Day 21	Day 3	Day 21	Day 3	Day 7	Day 21
HA_{HWM}	58.1 ± 0.9	54.2 ± 6.5	1.12 ± 0.03	1.08 ± 0.03	58.3 ± 1.1	59.9 ± 1.2	57.7 ± 1.1
HA_{IMW}	55.0 ± 5.3	49.1 ± 2.7	1.12 ± 0.03	1.13 ± 0.03	59.7 ± 1.0	60.6 ± 0.9	59.7 ± 0.9
Alginate	60.5 ± 7.6	57.0 ± 6.1	1.12 ± 0.02	1.11 ± 0.02	58.1 ± 1.2	59.6 ± 0.8	59.1 ± 0.6
PEG-DA	51.9 ± 2.6	46.1 ± 3.3	1.12 ± 0.03	1.13 ± 0.02	58.7 ± 1.0	61.6 ±0.5	59.5 ± 0.9

4.4.3 Cell density, proliferation, and apoptosis

The influence of scaffold composition on VFF proliferation and apoptosis was assessed via PCNA and TUNEL-based immunostaining, respectively. At day 7, no differences in cell proliferation or apoptosis across hydrogel formulations were noted (Figure 4.2. B and C). These day 7 PCNA and TUNEL results are reflected in the day 21 DNA measures, which indicate that net VFF proliferation and loss was similar across hydrogel formulations from day 7 to day 21 (Figure 4.2 A). Similar levels of cell apoptosis across hydrogel formulations continued to be observed through day 21 (Figure 4.2 C). However, PCNA expression was significantly elevated in HA_{IMW} hydrogels relative to HA_{HMW} ($P=0.013$) and alginate gels ($P=0.016$, Fig. 2B). These day-21 proliferation and apoptosis results suggest that, if cell densities had continued to be monitored past 21 days of culture, differences in cell densities across formulations would have begun to be detected.

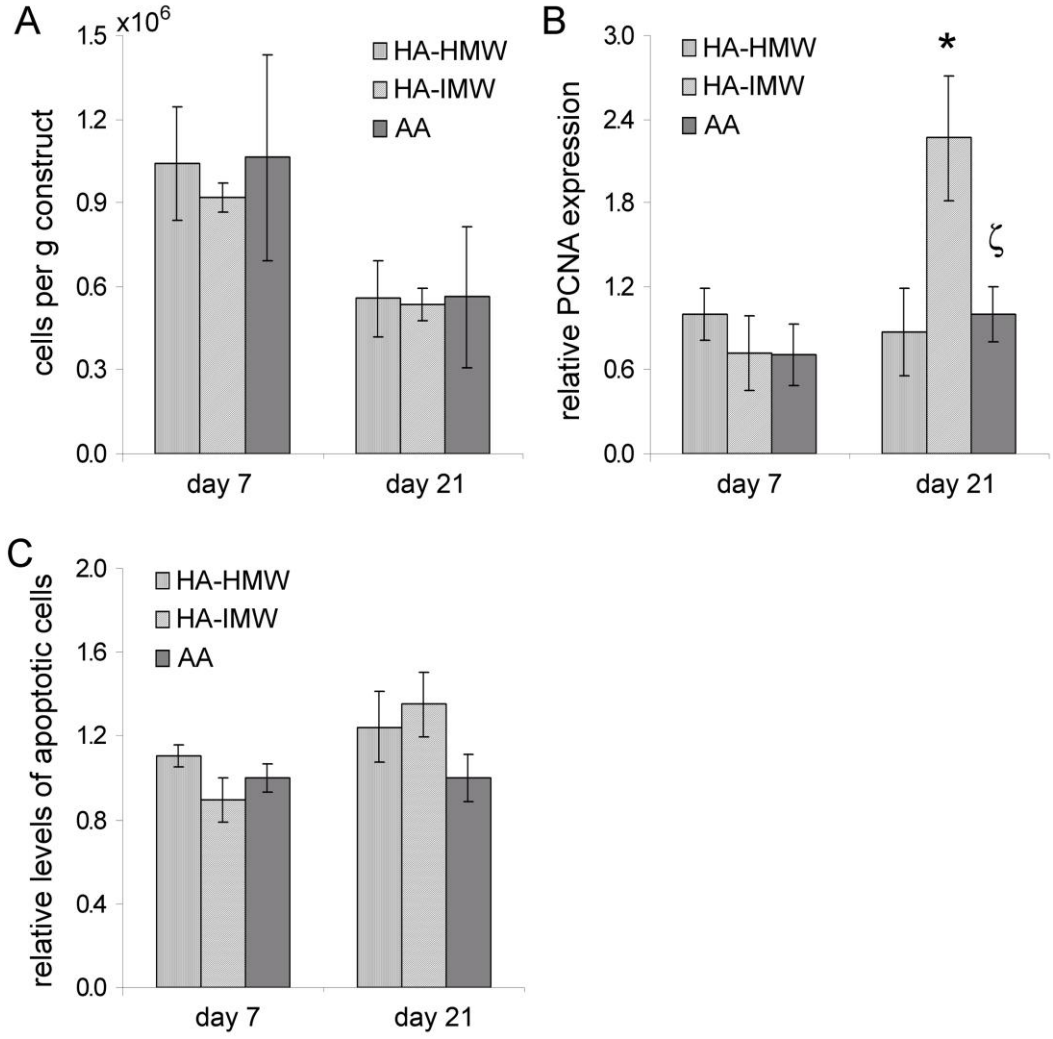

Figure 4.2 Cell density, proliferation, and apoptosis. **A**: The cell density within each hydrogel at days 7 and 21. **B**: Relative levels of proliferation at days 7 and 21 based on PCNA immunostaining. **C**: Relative levels of apoptotic cells at days 7 and 21 based on TUNEL assay results. *Significantly different from HA_{HMW} hydrogels, $P<0.05$. $^{\xi}$Significantly different from HA_{IMW} hydrogels, $P<0.05$.

4.4.4 VFF ECM deposition and phenotype

VFF ECM production showed marked variations with hydrogel bioactivity (Figure 4.3). The trends in elastin production at both days 7 and 21 indicated that elastin synthesis was greater in HA_{IMW} gels than in HA_{HMW} and alginate gels, with the differences at day 21 being statistically significant (HA_{HMW}, $P=0.050$; alginate, $P<0.001$). Although both days 7 and 21 data suggested an increasing trend for sGAG levels in alginate gels relative to both HA_{IMW} and HA_{HMW} hydrogels, these differences

fell below statistical significance (Figure 4.3B). Total collagen levels were significantly higher at day 7 in HA_{HMW} hydrogels than in HA_{IMW} ($P<0.001$) and alginate ($P=0.03$) gels. By day 21, this trend had shifted, with collagen levels in the alginate controls exceeding those in the HA_{HMW} hydrogels ($P=0.025$, Figure 4.3C). In contrast, the trend of lower total collagen production in HA_{IMW} hydrogels relative to alginate controls was stable from day 7 ($P=0.015$) to day 21.

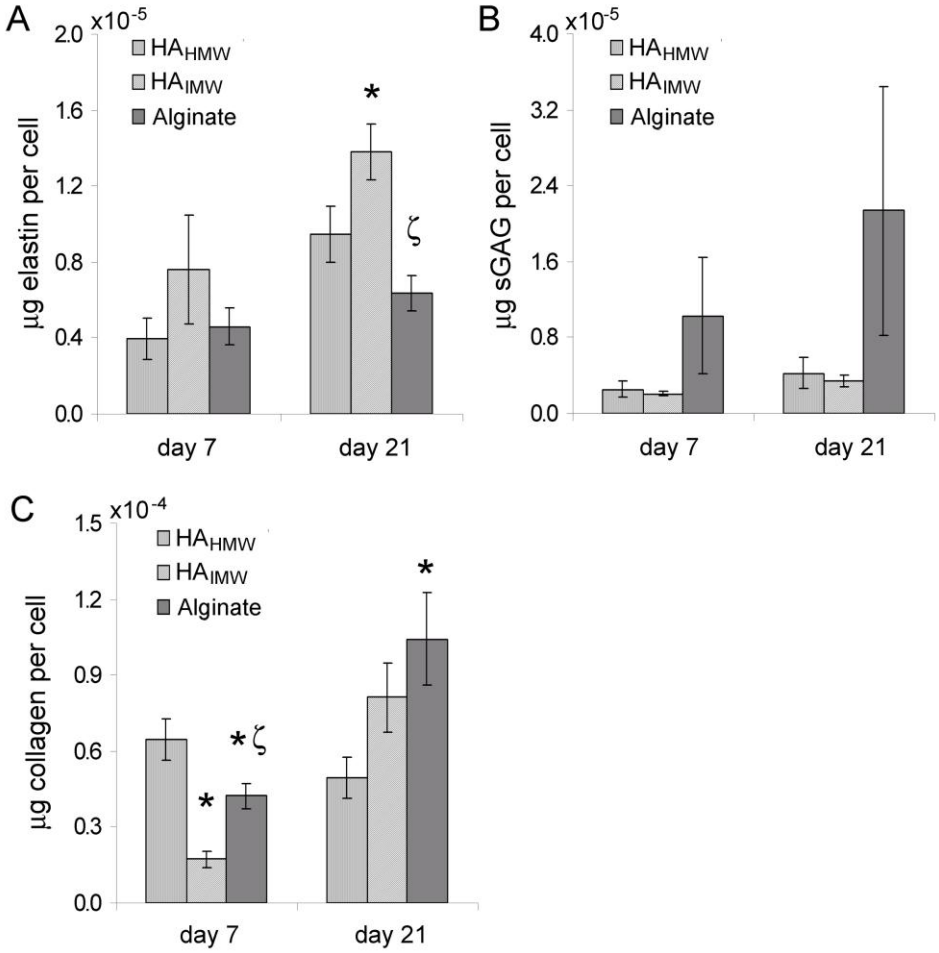

Figure 4.3 Evaluation of VFF ECM deposition. A: Elastin, (**B**) sGAG, and (**C**) total collagen production on a per cell basis at days 7 and 21. *Significantly different from HA_{HMW} hydrogels, $P<0.05$. $^{\xi}$Significantly different from HA_{IMW} hydrogels, $P<0.05$.

To gain further insight into effects of HA_{HMW} and HA_{IMW} on VFF ECM deposition, immunostaining for the two primary VF LP collagen types (collagen types I and III) [105] was conducted (Figure 4.4A and B). Expression of both collagen type I and collagen type III displayed similar trends with hydrogel formulation at day 7, with collagen type I deposition being significantly higher in the HA_{HMW} gel relative to HA_{IMW} ($P<0.001$) and alginate ($P=0.001$) gels. By day 21, differences in collagen type I expression across hydrogels had flattened. However, collagen type III production was significantly higher in HA_{HMW} hydrogels relative to alginate controls ($P=0.003$). As expected for PEG-DA gels, [62] staining for collagen types I and III (Figure 4.5) and elastin (data not shown) was confined to the immediate pericellular space in each formulation. To identify VFFs displaying a myofibroblast-like phenotype, expression of SM-α-actin was evaluated. The results for SM-α-actin were analogous to those for PCNA in that SM-α-actin levels were statistically indistinguishable across hydrogel formulations at day 7 (Figure 4.4C). However, by day 21, VFFs in HA_{IMW} gels expressed higher levels of SM-α-actin relative to HA_{HMW} ($P=0.004$) and alginate ($P<0.001$) gels (Figure 4.4D).

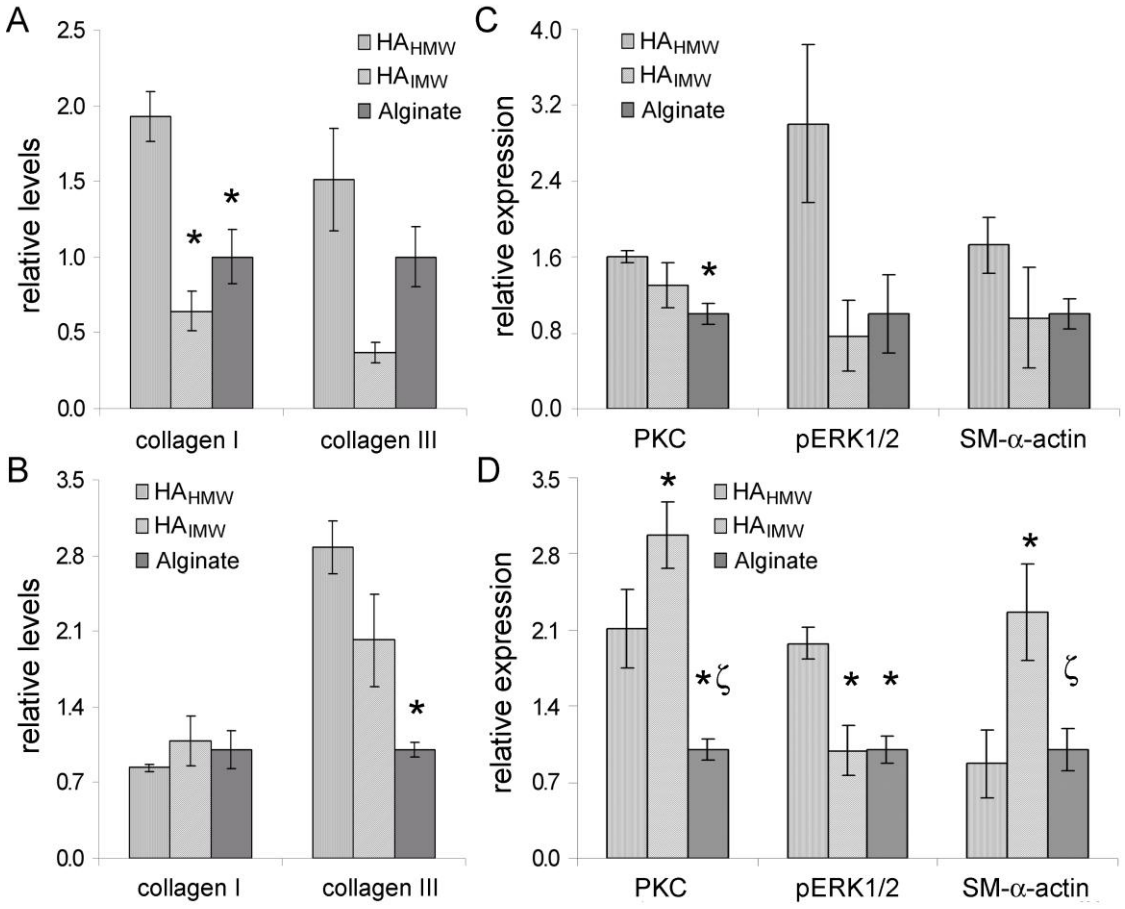

Figure 4.4 Assessment of VFF collagen type production, phenotype, and signaling. Relative collagen type I and collagen type III expression across hydrogels at (**A**) day 7 and (**B**) day 21. Relative expression of PkC, pERK1/2, and SM-α-actin at (**C**) day 7 and (**D**) day 21. *Significantly different from HA_{HMW} hydrogels, $P<0.05$. $^{\xi}$Significantly different from HA_{IMW} hydrogels, $P<0.05$.

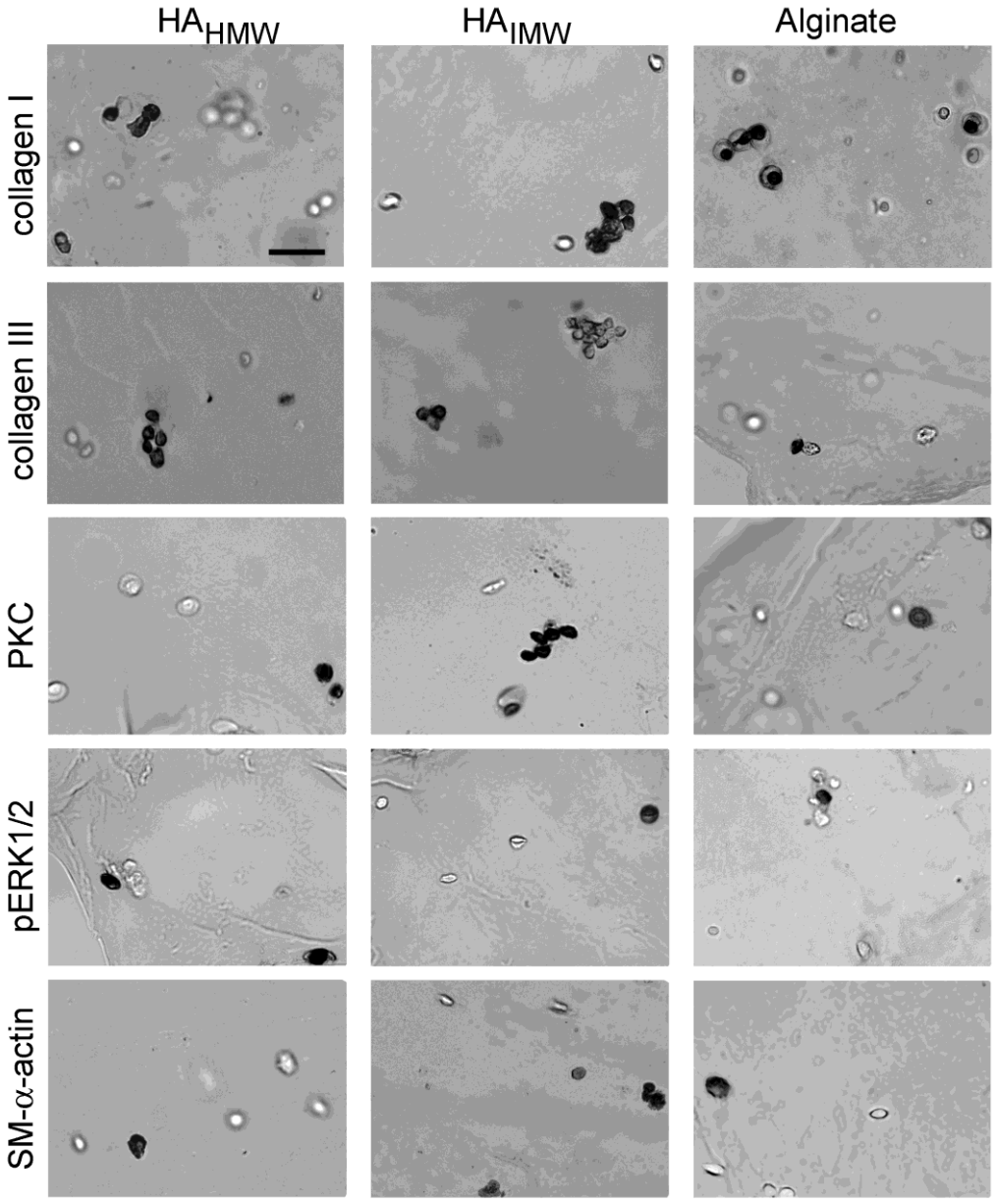

Figure 4.5 Representative images of day 21 HA_{HMW}, HA_{IMW}, and alginate hydrogel sections immunostained for collagen type I, collagen type III, PkC, pERK1/2, or SM-α-actin. The scale bar in the upper-left image equals 40 mm and applies to all images.

4.4.5 Cellular signaling

HA interactions with cell receptors, RHAMM and CD44, [99, 100] trigger two primary signaling pathways, PkC and ERK, which then modulate cell gene expression. Therefore, the relative levels of RHAMM, CD44, PkC, and active ERK1/2 (pERK1/2)

were semi-quantitatively assessed across hydrogel formulations. CD44 staining at both day 7 and day 21 was weak (<4 % of cells positively stained despite several antibody dilutions being assayed). In contrast, RHAMM staining was prominent at both time points and was significantly greater in HA_{HMW} and HA_{IMW} gels than in alginate gels ($P<0.03$). Specifically, VFF expression of RHAMM at day 7 in HA_{HMW} and HA_{IMW} gels was 1.94 ± 0.05 and 2.89 ± 0.32 times greater, respectively, than in alginate gels. Relative RHAMM levels at day 21 followed a similar trend (data not shown). PkC expression was consistently higher in HA_{HMW} than in alginate gels ($P<0.006$) at both days 7 and 21 (Figure 4.4C and D). In addition, day 21 PkC levels were greater in HA_{IMW} hydrogels than in HA_{HMW} gels ($P=0.038$) and alginate gels ($P<0.001$). Relative pERK1/2 levels maintained a similar trend across formulations from day 7 to day 21, with day 21 pERK1/2 content being significantly higher in HA_{HMW} hydrogels relative to HA_{IMW} ($P=0.029$) and alginate ($P=0.013$) gels.

4.5 Discussion

The aim of the present study was to validate PEG-DA hydrogels as a model system to probe the effects of various bioactive moieties on VFF responses in 3D toward rational VF LP implant design. To accomplish this objective required that the current study be conducted so as to permit direct comparison with previous studies involving more permissive scaffolds. Therefore, we chose to focus on HA, a polysaccharide that has been a particular focus in VF regeneration community.

In the current work, porcine VFFs were encapsulated in PEG-DA hydrogels containing consistent levels of HA_{HMW} (~1.65×10^3 kDa), HA_{IMW} (~600 kDa), or the control polysaccharide alginate. Modulus, water uptake, and gel mass assessments indicate that the bulk average microstructure, modulus, and degradation rate of the polysaccharide- containing gels were dominated by PEG-DA. This enabled focus on the identity of the polysaccharide as the main source of variation in net cell responses. Although there were certainly local differences in gel properties at the microscale, our

ECM and cell phenotypic measures represent averages over the bulk, as do our material property measures. Thus, since both the material property and cell response measures were made at the same length scales, the data represent an internally consistent set from which meaningful deductions can be made.

Regarding ECM production, VFF elastin deposition demonstrated an increasing trend with decreasing HA M_w by day 21 of culture. In comparing these results to literature, we are limited by the fact that most HA studies which permit the impact of HA M_w to be isolated from other experimental variables have been conducted in 2D with soluble, rather than matrix-bound, HA. Thus, the comparisons to follow must be interpreted with caution. That being said, the present results are in agreement with a recent 2D study of VICs by Masters et al. In that study, elastin synthesis at 20 days of culture was significantly higher in VICs exposed to ~400 kDa HA relative to ~800 kDa HA. However, a separate 2D study by Joddar and Ramamurthi, [89] showed a decrease in vascular smooth muscle cell (SMC) elastin deposition at 21 days of culture with a decrease in HA M_w from 2 x 10^3 kDa to ~200 kDa. Combined, these studies suggest that the influence of HA M_w on elastin synthesis may be cell-type dependent.

Examination of VFF sGAG deposition indicated no significant alteration in sGAG synthesis with increasing HA M_w, consistent with the results of Masters et al. [106]. Although, VFF total collagen production in HA_{IMW} hydrogels was significantly lower than that in HA_{HMW} gels at day 7, their day 21 total collagen content could not be statistically distinguished. As with elastin, literature shows conflicting results for the dependence of collagen deposition on HA M_w. Masters et al. found no significant difference in VIC total collagen production with increasing HA M_w at 20 days of culture. Joddar and Ramamurthi, [89] however, observed an increase in vascular SMC collagen synthesis with decreasing HA M_w as HA dosages approached those used herein. Regarding the synthesis of individual collagen types, VFF collagen type III deposition displayed an increasing trend with increasing HA M_w at both days 7 and 21. In contrast, although collagen type I expression at day 7 decreased with decreasing HA M_w, day 21 collagen type I levels did not vary significantly across formulations. This temporal

alteration in collagen type I production may be linked to the corresponding shifts in PkC signaling with time in culture. The present collagen type III results agree with the effects of HA M_w on human dermal fibroblast collagen type III synthesis observed by David-Raoudi et al. Further comparison of the trends in collagen types I and IIIacross hydrogels with that of total collagen suggests that collagen type I was the dominant collagen produced by the encapsulated VFFs, in each hydrogel formulation, at least by day 21. The ratios of the various collagen types secreted by VFFs are significant because collagen type III tends to more abundant in highly elastic tissues, such as the VF LP [19]. Furthermore, the ratios of the various collagen types are frequently altered in aging and disease [19, 27].

Cell phenotype also appeared to be modulated by HA M_w. VFFs in HA_{IMW} hydrogels displayed a more proliferative phenotype at day 21 than cells in alginate or HA_{HMW} gel, as indicated by PCNA staining. A similar dependence of cell proliferation on HA M_w has been previously observed for VICs [106] and for vascular SMCs [89]. In addition, VFFs in HA_{IMW} hydrogels demonstrated increased SM-α-actin expression by day 21 relative to HA_{HMW} and alginate hydrogels. The increased levels of SM-α-actin and PCNA at day 21 in HA_{IMW} gels may be associated with the increased levels of PkC in the HA_{IMW} gels relative to alginate gels. Indeed, PkC signaling has previously been shown to increase the expression of SM-α-actin in lung fibroblasts [107]. Furthermore, the increased myofibroblastic phenotype of cells in the HA_{IMW} hydrogels at day 21 was associated with increased elastin deposition, consistent with the literature [81, 108-111].

Cumulatively, the present results suggest that HA M_w must be carefully selected to achieve desired VFF responses. However, based on the current data, the HA_{HMW} gels would be the most appropriate for VF regeneration of the formulations examined. Specifically, the HA_{HMW} gel resulted in an elastin and collagen type composition most mimetic of normal superficial LP, which contains ~40% collagen type III [105] and a relatively low elastin to collagen ratio [31]. Furthermore, the lower induction of a myofibroblastic phenotype observed in the HA_{HMW} gels relative to HA_{IMW} gels with prolonged culture is desirable for inhibition of LP scar formation [18].

As previously mentioned, the effects of HA_{IMW} on VFF behavior relative to the control alginate have been examined in 3D using base-hydrogels of collagen type I [31]. However, it is difficult to extend upon that study to probe a broader HA concentration or M_w range due the interdependences among collagen gel bioactivity, modulus, and microstructure. In addition, collagen gels are prone to fibroblast-mediated contraction, making gel material properties difficult to control over time [31]. Although the material properties of PEG-DA hydrogels are tunable and more readily controlled, cells encapsulated within PEG-DA hydrogels take on rounded/stellate morphologies even in the presence of cell adhesion ligands such as RGDS (Fig. 4.4). This particular characteristic of PEG-DA hydrogels, which results from their dense crosslinking and relatively slow degradation rates, [55, 57, 75] is not optimal for cells such as VFFs, which natively take on spindle-shaped morphologies. However, due to several of their unique properties, PEG-DA hydrogels have been employed as a model scaffold by number of researchers focusing on fibroblast-like cells, in spite of this limitation [75, 106, 112-114]. To validate PEG-DA hydrogels for the investigation of VFF responses to defined bioactivity in 3D, the day 21 setup for the present study was designed to be a direct analog of the previous collagen-based 3D study in which encapsulated VFFs were able to assume spindle-shaped morphologies [31].

Interestingly, each of the aspects of VFF behavior measured for HA_{IMW}-collagen relative to alginate-collagen control gels displayed similar trends in the HA_{IMW}-PEG-DA gels relative to alginate-PEG-DA gels (Table 4.2). Although elastin deposition was not measured in the alginate-collagen and HA_{IMW}-collagen study, the relative trends in day 21 total collagen synthesis, sGAG production, cell proliferation, and myofibroblastic phenotype between hydrogel formulations were maintained across the two studies [31]. This similarity in relative VFF response occurred despite the significant difference in cell morphologies in the PEG-based gels relative to the collagen gels. The good agreement between these two studies indicates that PEG-DA hydrogels can serve as an effective model system for probing at least certain aspects of fibroblast-like cell

responses to scaffold material properties despite the enforced non-native cell morphologies.

Table 4.2. Comparison of HA and alginate impact in PEG-DA-versus collagen-based hydrogels.

	PEG-DA hydrogels with RGDS functioning as the integrin adhesion ligand at day 21		**Collagen hydrogels with collagen type I functioning as the integrin adhesion ligand [31]**	
	HA_{HMW} relative to HA_{IMW}	HA_{IMW} relative to Alginate	HA_{HMW} relative to HA_{IMW}	HA_{IMW} relative to Alginate
Total collagen	↔	↓	—	↓
Collagen type I: type III	↓	↓	—	—
Elastin	↓	↑	—	—
sGAG	↔	↓*	—	↓
Proliferative cells	↓	↑	—	↑
Myofibroblast-like cells	↓	↑	—	↑

↔, indicates indeterminate, ↓ decrease, ↑ increase, — not measured. In Hahn et al. [31], the levels of proliferative cells were assessed via BrdU incorporation and the levels of myofibroblast-like cells were assessed by evaluating the degree of hydrogel compaction with time in culture. Collagen synthesis and sGAG production were evaluated histologically by reticular collagen stain and toluidine blue stain, respectively.
***** indicates that the result was not statistically significant.

A limitation of the present study is the relatively restricted HA concentration and M_w range interrogated. Future experiments will explore a broader range of initial concentration and M_w. Furthermore, the present 3D model system can be readily extended to examining the influence of other biochemical moieties on VFF cell responses.

CHAPTER V
UNCOUPLED INVESTIGATION OF SCAFFOLD MODULUS AND MESH SIZE ON SMOOTH MUSCLE CELL BEHAVIOR*

5.1 Overview

Although scaffold material properties are known to critically impact cell behavior, it has proven difficult to correlate specific cell responses to isolated scaffold parameters, inhibiting rational design of scaffold material properties. The aim of this study was to validate a systematic approach for evaluating the influence of initial scaffold modulus and mesh size on cell extracellular matrix (ECM) deposition and phenotype. Poly(ethylene glycol) diacrylate (PEG-DA) hydrogels were selected for this study because of their tunable material properties. Following screening of six distinct PEG-DA hydrogels, three formulations were identified which permitted uncoupled investigation of scaffold mesh size and modulus within the target incremental modulus range of ~100–300 kPa. Smooth muscle cells (SMCs) were encapsulated within these three formulations, and cell ECM deposition and phenotype were evaluated following days of culture.

Although elastin content appeared to be correlated with scaffold mesh size and modulus to a similar degree, levels of collagen and serum response factor (SRF), a key regulator of SMC phenotype, were more strongly correlated with mesh size. To gain insight into the cell signaling underlying these observed correlations, variations in cell metabolic state and in RhoA signaling were semi-quantitatively evaluated. Both RhoA activity, which is largely modulated by scaffold mechanics in 2D, and cell metabolic activity were highly correlated with hydrogel mesh size.

These results indicate that the effects of scaffold mechanics on RhoA activity in 3D may be distinct from those in 2D and underscore the need for uncoupled investigation of scaffold parameters on cell behavior. Furthermore, the present data suggest that RhoA signaling and cell metabolic regulation may be closely linked.

5.2 Introduction

The material properties of tissue engineering scaffolds are understood to critically influence cell behavior. However, it has proven difficult to attribute alterations in cell response to specific changes in scaffold parameters, such as bioactivity, [52] mesh size, [53] mechanical properties, [55, 115, 116] and degradation rate [117] due to the complexity and/or interdependence of these variables. For instance, an important recent study observed that mesenchymal stem cells encapsulated within collagen beads displayed an increased tendency to differentiate into chondrocytes as collagen density increased [91]. However, whether this alteration in cell behavior resulted primarily from the increase in the spatial density of bioactivity (collagen) or from the associated increase in bead stiffness (or decrease in gel mesh size) cannot be readily determined with this model system. This is because the concentration of collagen cannot be uncoupled from changes in modulus and mesh size using standard collagen hydrogel formulation strategies. This interdependence of scaffold variables has hampered our ability to correlate specific cell responses to isolated scaffold material properties, inhibiting the rational selection of scaffold parameters to achieve desired cell behaviors. The aim of this study was to validate a systematic approach for evaluating the influence of isolated scaffold material properties on cell phenotype and ECM deposition, with a focus on initial scaffold modulus and mesh size. Ultimately, these data will be applied toward rational scaffold design.

Central to this work is the selected scaffold material: poly(ethylene glycol) diacrylate (PEG-DA). PEG-DA hydrogels have several properties that make them appropriate for controlled exploration of cell response to specific alterations in scaffold material properties. Specifically, their bioactivity, mesh size, modulus, and degradation

rate can be systematically tuned [53, 57, 62, 117]. Regarding bioactivity, pure PEG-DA hydrogels function as biological ‘‘blank slates,’’ meaning that they do not significantly adsorb bioactive plasma proteins. Thus, these hydrogels do not promote cell interaction without the specific conjugation of biochemical stimuli to the scaffold [58]. This is significant because most synthetic and natural scaffolds adsorb a range of bioactive proteins from serum (in the in vitro setting) or from plasma (in the in vivo setting). These adsorbed proteins, the levels of which are variable and difficult to quantify, are often major determinants of cell behavior, in addition to any bioactive moiety deliberately conjugated or adsorbed to the scaffold. This situation complicates the study of cell response to defined biochemical stimuli. In contrast, the biological ‘‘blank slate’’ nature of PEG-DA hydrogels permits the controlled introduction of desired bioactivity and examination of its effects on cell behavior [61]. In this study, we explored the impact of initial PEG-DA scaffold modulus and mesh size in the presence of constant initial levels of cell adhesion peptide, RGDS, thereby removing initial scaffold bioactivity as a design variable.

An additional benefit of PEG-DA hydrogels is the ability to tune their initial mesh size and mechanical properties over a broad range simply by varying the molecular weight (M_w) and/or concentration of PEG-DA [62]. This particular characteristic of PEG-DA hydrogels, although widely recognized, has not been fully exploited in terms of analyzing cell responses to specific scaffold properties. This is due, in part, to the interdependence of PEG-DA hydrogel modulus and mesh size. Namely, as the concentration of PEG-DA of a specific M_w is increased, the mesh size of the resulting hydrogel decreases while the modulus increases. Thus, cell responses to hydrogel modulus have proven difficult to investigate separated from mesh size. In this study, we circumvent this limitation in a unique manner, which permits uncoupled examination of the effects of scaffold modulus and mesh size.

The degradation rate of PEG-DA hydrogels can also be systematically tuned. Pure PEG-DA hydrogels degrade by hydrolytic cleavage of the ester bonds between the aliphatic polymer backbone and the crosslinking units [60, 73]. Variations in degradation

rate can be achieved by conjugating enzymatically-cleavable peptides or a-hydroxy acids, such as lactic acid, to the macromer backbone [14, 16]. The PEG-DA formulations investigated herein were selected to display similar degradation rates, significantly simplifying the systematic interrogation of modulus and mesh size impact on cell behavior. In validating this approach, we have employed tissue engineered vascular grafts (TEVGs) as a model system. Annually, ~100,000 patients require vascular bypass of small-caliber arteries (<6 mm ID) but lack autologous arteries or veins suitable for grafting [118]. Tissue engineering represents a potential means to construct vascular grafts in situations where autologous tissue is unavailable and current synthetic materials fail [119, 120]. Because of its key role in vessel physiology, the smooth muscle cell (SMC)-rich medial layer of blood vessels has been a focus of much of TEVG research [121, 122]. We therefore concentrated on evaluating the responses of vascular SMC to scaffold mesh size and modulus. In assessing SMC response, we examined the production of key determinants of mediallayer mechanical properties, including collagen, elastin, and sulfated glycosaminoglycans (sGAG). Expression of SMC marker calponin h1, as well as two of its regulators, namely, the transcription factors myocardin and serum response factor (SRF), [123-125] was employed in evaluating SMC phenotype.

To gain insight into the signaling pathways underlying observed variations in SMC ECM production and phenotype with hydrogel mesh size and modulus, alterations in RhoA activity and cell metabolic state were semi-quantitatively evaluated. RhoA signaling was selected for examination due to its known role in modulating cell response to scaffold mechanics in 2D [126, 127]. Cell metabolic state was investigated as gel mesh size frequently imposes constraints on nutrient diffusion and gas exchange, both of which impact cell metabolism.

5.3 Materials and methods

5.3.1 Polymer synthesis

PEG-DA was prepared as previously described by combining 0.1 mmol/mL dry PEG (10 kDa or 20 kDa, Fluka), 0.4 mmol/mL acryloyl chloride, and 0.2 mmol/mL triethylamine in anhydrous dichloromethane (DCM) and stirring under argon overnight. The resulting solution was washed with 2M K_2CO_3 and separated into aqueous and DCM phases to remove HCl. The DCM phase was subsequently dried with anhydrous $MgSO_4$, and PEG-DA was precipitated in diethyl ether, filtered, and dried under vacuum. The extent of acrylation of both products was characterized by ^{1}H NMR to be ~65%.

Cell adhesion peptide RGDS (American Peptide) was reacted with acrylate-derivatized PEG-N-hydroxysuccinimide (ACRL-PEG-NHS, 3.4 kDa, Nektar) at a 1:1 molar ratio for 2 h in 50 mM sodium bicarbonate buffer, pH 8.5 [128]. The product (ACRL-PEG-RGDS) was purified by dialysis, lyophilized, and stored at -20 °C until use.

5.3.2 Hydrogel formulation selection

Human coronary arteries experience mean circumferential stresses of 20–50 kPa under normal physiological loading [129]. The slope of the tangent to the stress–strain curve at this mean stress point is referred to as the incremental modulus of the vessel [129]. The incremental modulus for a normal human coronary artery ranges from ~100–300 kPa [129]. To identify a set of hydrogels that would permit uncoupled examination of scaffold mesh size and mechanical properties within this incremental modulus range, the following series of PEG-DA hydrogels were prepared and characterized: (1) 10 wt % of 10 kDa PEG-DA (10% 10 kDa), (2) 20 wt % of 10 kDa PEG-DA (20% 10 kDa), (3) 30 wt % of 10 kDa PEG-DA (30% 10 kDa), (4) 10 wt % of 20 kDa PEG-DA (10% 20 kDa), (5) 20 wt % of 20 kDa PEG-DA (20% 20 kDa), and (6) 30 wt % of 20 kDa PEG-DA (30% 20 kDa).

Hydrogel preparation. Hydrogel precursor solutions were prepared by dissolving PEG-DA macromers in HEPES buffered saline (HBS;10 mM HEPES, 150 mM NaCl, pH 7.4). Each precursor solution was sterilized using a 0.22 μm PVDF filter. Ten microliters of a 300 mg/mL solution of photoinitiator 2, 2-dimethoxy-2-phenyl-acetophenone dissolved in N-vinylpyrrolidone was then added per mL precursor solution. Each solution was poured into molds composed of two glass plates separated by thin polycarbonate spacers and then polymerized by 2 min exposure to longwave UV light(Spectroline, ~6 mW/cm^2, 365 nm) [62, 65].

Hydrogel swelling. To isolate the effects of scaffold modulus and mesh size on SMC ECM production and phenotype, it was necessary that the initial cell density and scaffold bioactivity be consistent across formulations. Because PEG-DA hydrogels swell significantly postpolymerization, [130] the amount of ACRL-PEG-RGDS and cells added to each hydrogel precursor solution had to account for the change in hydrogel volume with swelling. To characterize equilibrium swelling, each PEG-DA gel was prepared as described above. Samples of 1 cm diameter were cored from each PEG-DA hydrogel immediately following polymerization and weighed. The samples were then transferred to HBS supplemented with 0.05 wt % sodium azide (HBS-azide) at 37 °C. After 24 h, samples were blotted and weighed. Because PEG-DA hydrogels are primarily water, the increase in weight with swelling can be directly related to the increase in gel volume (V) with swelling, that is, $\left(\frac{V_{swollen}}{V_{initial}}\right) \approx \left(\frac{swollenweight}{Initialweight}\right)$. This ratio was used to calculate the amount of cells and ACRL-PEG-RGDS to be added to each hydrogel precursor solution so as to ensure the desired cell density and RGDS concentration in the swollen hydrogels.

The desired postswelling RGDS concentration was 2 μmol/g. To confirm that the levels of added ACRL-PEGRGDS did not significantly alter the relative swelling ratios of the selected PEG-DA formulations, the swelling ratios of RGDS-containing hydrogels were characterized, as described above. These swelling ratios were compared with those

of the non-RGDS containing gels. No significant differences were found, indicating that the incorporated ACRL-PEG-RGDS had minimal impact on the relative hydrogel swelling ratios at the selected RGDS concentration (data not shown).

Hydrogel mesh size. PEG-DA hydrogel mesh size cannot be visualized using techniques such as conventional scanning electron microscopy (SEM) [131]. Thus, a variety of methods to estimate PEG-DA hydrogel mesh size have been developed, including correlations linking measurable quantities, such as equilibrium hydrogel swelling and PEG-DA M_w, to mesh size [68, 130]. Although these correlations appear to yield reasonable mesh size estimates for relatively high-weight percent PEG-DA hydrogels [68, 130] the predictions for lower-weight percent hydrogels have been called into question. Thus, in this study, hydrogel mesh size was characterized via a series of dextran diffusion experiments based on an adaptation of the methodology of Watkins and Anseth [69].

In brief, PEG-DA hydrogels containing 2 μmol/g ACRLPEG- RGDS postswelling were prepared and allowed to swell overnight at 37 °C in HBS-azide. Discs of 1 cm diameter were cored from each hydrogel formulation. FITClabeled dextrans (10, 20, 40, 70, or 150 kDa, Sigma) were dissolved at 0.01 mg/mL in HBS-azide and added at 1 mL per hydrogel disc (three discs per dextran M_w). Dextran solutions were allowed to diffuse into the hydrogels for 24 h at 37 °C. Each gel disc was then gently blotted and transferred to 1 mL fresh HBS-azide. Dextran that had penetrated into the hydrogels was permitted to diffuse out into the surrounding solution at 37 °C. After 24 h, the fluorescence of the HBS-azide solution surrounding each disc was measured at ex/em 488/532. Dextran standard curves were used to convert each fluorescence signal to a corresponding concentration.

The mesh size of each gel formulation was calculated relative to that of the 10% 10 kDa hydrogel as follows. For each hydrogel formulation, the measured concentration readings for each dextran M_w were divided by gel thickness and then plotted versus dextran hydrodynamic radius. The area (A) under the resulting curve served as a

quantitative indicator of hydrogel permissivity over the hydrodynamic radii range assayed. The relative mesh size, μ, of hydrogel x, to that of the 10% 10 kDa gels could therefore be calculated as the ratio of A_x to $A_{10\%\ 10\ kDa}$. To give insight into the absolute mesh sizes represented by these relative mesh size assessments, the 30% 10 kDa hydrogel served as a basis. For this gel formulation, the dextran readings fell to background levels for dextran M_ws exceeding 20 kDa (data not shown). The 20 kDa dextran had a mean hydrodynamic radius of ~3.2 nm, whereas the next largest dextran investigated (40 kDa) had a mean hydrodynamic radius of ~4.5 nm [132]. Thus, the mesh size of the 30% 10 kDa hydrogel was taken to be ~(2 x 4.5) = 9 nm. For a given hydrogel (x), the absolute mesh size (n) can be estimated as: $\xi_x \approx \left(\frac{\mu_x}{\mu_{30\%10kDa}}\right)(9nm)$.

Furthermore, cryoSEM was conducted on the 30% 20 kDa gel formulation. Although, as previously noted, conventional SEM does not enable visualization of PEG-DA hydrogel mesh structure, we reasoned that cryoSEM may prevent the collapse of the hydrogel network that appears to accompany conventional and environmental SEM. Following high pressure freezing, a 30% 20 kDa sample was split under liquid nitrogen using a pre-chilled scapel blade. One sublimation cycle was then conducted in a Balzer MED-010 cryo prep vacuum chamber followed by sputter coating with 8–10 nm of platinum. The coated sample was then imaged at 5kV and -170 °C. The average mesh size observed for the 30% 20 kDa gel using cryoSEM (Figure 5.1) agrees well with ~13 nm estimated using the above equation.

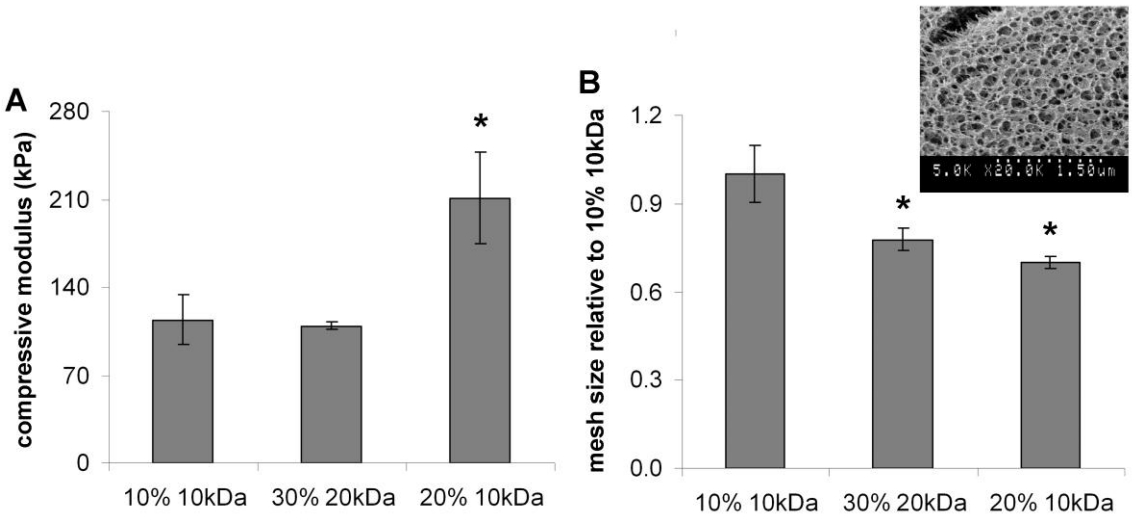

Figure 5.1 Initial (day 3) hydrogel material properties. (A) compressive modulus and (B) relative mesh size. *, indicates significant difference, $p < 0.05$. These dextran diffusion assessments were supplemented by cryoSEM imaging of the 30% 20 kDa hydrogel (inset). The mesh structure revealed in this cryoSEM image is in good agreement with the absolute mesh size predicted by dextran diffusion for this hydrogel formulation (the Table on p.76, footnote a).

Hydrogel mechanical properties. Hydrogels containing 2 μmol/g ACRL-PEG-RGDS postswelling were prepared and allowed to swell at 37 °C in HBS-azide. To compare PEG-DA hydrogel mechanical properties to literature values for the incremental tensile modulus of the normal human coronary artery media, hydrogel samples were measured under tension after 48 h swelling. Rectangular strips 5 mm in width and 2 cm in length were cut from each formulation, mounted onto an Instron 3342 using rubber-coated grips, and pulled at 6 mm/min until failure. The incremental modulus was defined as the slope of the linear region of the stress–strain curve at a reference stress of 20 kPa.

To assess the mechanical properties of the selected PEG-DA formulations as experienced by the encapsulated SMC, three additional 1.25 cm discs were cored from each hydrogel and mechanically tested under unconstrained compression at room temperature using an Instron 3342. Following application of a 0.05N preload, each hydrogel was subjected to compression at 1 mm/min up to 10% strain. Hydrogel compressive moduli were extracted from the resulting stress–strain data.

For both testing methods, samples remained immersed in PBS until immediately prior to mechanical testing, and testing was completed for each sample within 60 s. This rapid handling avoided sample dehydration during testing.

5.3.3 Cell culture studies

Based on the mesh size and incremental moduli measured in the above characterization studies, the following three hydrogel formulations were selected for further examination in cell encapsulation studies: (1) 10% 10 kDa, (2) 30% 20 kDa, and (3) 20% 10 kDa.

Cell culture. Cyropreserved aortic SMCs (Cell Applications) isolated from pigs, a common animal model for vascular SMC physiology, [133, 134] were thawed and expanded in monolayer culture between passages [55, 57, 62, 91, 116, 117]. Prior to encapsulation, cells were maintained at 37°C/5% CO_2 in Dulbecco's Modified Eagles' Media (DMEM, Hyclone) supplemented with 10% fetal bovine serum (FBS, Hyclone), 1 mg/L bFGF (BD Biosciences), 100 U/mL penicillin, and 100 mg/L streptomycin (Hyclone).

Cell encapsulation and hydrogel maintenance. SMCs at passage [57, 62] were harvested and resuspended in each hydrogel precursor solution such that the postswelling cell density would be ~0.5 x 10^6 cells/mL. ACRL-PEG-RGDS was added to each precursor solution so that the concentration of RGDS in the swollen hydrogels would be 2 μmol/g. The cell-precursor solution mixtures were photopolymerized into hydrogels as described above. The hydrogel slabs were transferred to Omnitrays (Nunc) fitted with four sterile polycarbonate bars to simultaneously prevent gel flotation and prevent gel contact with the tray bottom. Gels were immersed in DMEM supplemented with 10% FBS, 100 U/mL penicillin, and 100 mg/L streptomycin and maintained at 37°C/5% CO_2. Media was changed every 2 days. After 48 h of culture (day 3), three 1.25 mm diameter samples were collected from each gel and subjected to the mechanical

compression and dextran diffusion studies detailed above. At day 21 of culture, a series of 1.25 cm diameter samples were collected from each hydrogel formulation for subsequent mechanical, biochemical, and histological analyses.

Hydrogel degradation rate. A PEG-DA hydrogel is a 3D network of inter-crosslinked PEG-DA macromers. Both the modulus and mesh size of the hydrogel are intimately related to the organization and density of these crosslinks. As PEG-DA scaffolds degrade by hydrolytic cleavage of the ester bonds between the aliphatic polymer backbone and the crosslinking units, [73, 135] the linkages among PEG-DA chains are broken. This process results in a decrease in hydrogel modulus and a corresponding increase in hydrogel mesh size [73]. At the relatively low cell densities employed in this study, changes in hydrogel modulus with time could be assumed to be dominated by the hydrolytic degradation of the hydrogel network rather than by ECM deposited by encapsulated cells. Hence, by monitoring the change in construct modulus with time, the degradation rate of each hydrogel network could be assessed [73].

To confirm our initial assumption that the selected hydrogels had similar degradation rates, the compressive modulus of each hydrogel formulation at day 21 was evaluated according to the methodology described above. The day 21 modulus data were compared to the initial (day 3) measures to determine a degradation half-life for each hydrogel formulation, assuming pseudo first-order degradation kinetics for the ester linkages [73, 135].

Biochemical analyses. Samples harvested for biochemical analyses were transferred to screw-cap vials, weighed, flash-frozen in liquid nitrogen, and stored at -80°C. At the time of analysis, hydrogel samples were digested for 24 h at 37°C in 1 mL of 0.1M NaOH per 0.2 g hydrogel wet weight [75]. The samples were then centrifuged (8000g for 10 min), and aliquots were taken for DNA and sGAG quantification. Any material pelleted during centrifugation was resuspended by vortexing, and additional hydrolysis was carried out by transferring the samples to a 100°C oven for 90 min to

solubilize collagen but not elastin [75]. These samples were then centrifuged (8000g for 10 min), and the supernatants were retrieved for collagen quantification. The pellets (containing elastin) were washed with dIH_2O at least four times and stored at -80°C until use.

DNA analysis. Aliquots of the hydrolyzed samples (n = 3–6 per formulation) were neutralized and their DNA content determined using the PicoGreen assay (Invitrogen) [75]. DNA measures were translated to cell number using a conversion factor of 6.6 pg DNA per cell. Calf thymus DNA (Sigma) served as a standard.

Sulfated GAG analysis. sGAG production was measured using a modification of the Blyscan assay (Biocolor). In brief, 80 lL of each sample digest (n = 3–6 per formulation) was neutralized, mixed with 120 μL Blyscan dye reagent, and the absorbance at 525 nm immediately measured relative to chondroitin sulfate B (Sigma).

Collagen analysis. Levels of hydroxyproline were quantified as an indirect measure of total collagen. In brief, supernatants (n = 5–6 per formulation) collected for collagen quantitation were hydrolyzed for 18 h at 110°C in 6M HCl. Hydrolyzed samples were then dried (Centrivap, Labconco) followed by resuspension in dIH_2O and reaction with chloramine T and p-dimethylbenzaldehyde reagents [136]. Sample absorbance was read at 550 nm relative to that of L-4-hydroxyproline (Sigma) [136]. Total collagen content was estimated from measured grams of hydroxyproline by dividing by 0.13.

Elastin analysis Elastin levels were determined according to the procedure detailed in Long and Tranquillo [137]. Briefly, material pelleted following 100 ºC NaOH exposure was further digested in 6M HCl at 110°C for 18 h. Samples (n = 3–8 per formulation) were then dried (Centrivap, Labconco). The resulting free amino acids were boiled in the presence of ninhydrin reagent (Sigma), cooled, and their absorbance read at 570 nm [75]. Hydrolyzed α-elastin (MP Biochemicals) was used as the standard. The

ninhydrin-based elastin readings were verified for a subset of samples (n = 1–6 per formulation) using direct ELISA according to the following protocol. Undigested samples were hydrolyzed with 0.1M NaOH for 24 h at 37°C, neutralized, and further digested with 0.25M oxalic acid at 100 °C overnight. Oxalic acid was then removed and exchanged for PBS using Microcon YM-3 centrifugal filters (Millipore). One hundred microliters of the resulting samples were applied to a high binding EIA 96 well plate (Nunc) for 3 h at room temperature. Adsorbed elastin fragments were detected by applying elastin antibody (clone BA-4, Santa Cruz Biotechnology [SCBT]) followed by donkey anti-mouse HRP secondary antibody (SCBT) and 2,20-azino-bis(3-ethylbenzthiazoline-6-sulphonic acid) (Sigma). Absorbance was read at 410 nm, with bovine aortic elastin (Sigma) serving as a standard.

For the DNA, sGAG, hydroxyproline, and direct ELISA assays, the standards used were subjected to the same association with PEG-DA, hydrolysis, and processing conditions as the samples. Resulting collagen, elastin, and sGAG levels were normalized to cell number.

Histological analyses. Samples harvested for histological analyses were fixed in 10% formalin for 30 min, embedded in Tissue-Tek freezing media, and frozen at -80°C. Sections of 35 μm were cut using a cryomicrotome. All immunostaining steps took place at room temperature unless otherwise noted.

Active RhoA analysis. Active RhoA was detected by a double-staining approach based on the method of Ren et al. [138]. The first immunostaining detected GTP-bound (active) RhoA/B/C, and the second staining detected RhoA (both active and inactive). Overlap between these two stains indicated the presence of active RhoA. In brief, rehydrated sections were treated with cytoskeletal buffer (10 mM HEPES, pH 6.8, 100 mM NaCl, 3 mM $MgCl_2$, 300 mM sucrose, 0.5% triton X-100) for 30 min. GST tagged rhotekin-RBD (Cytoskeleton, Inc.) was applied at 10 μg/mL for 1 h at 4°C in 50 mM Tris-HCl, pH 7.5, 150 mM NaCl, 5 mM $MgCl_2$, 1% NP-40, 1 mM DTT and 5%

glycerol. The sections were then blocked for 10 min with Terminator (Biocare Medical), after which primary antibody for GST (GST-2, Schistosoma japonicum specific, Sigma) diluted in HBS was applied for 2 h. Bound primary antibody was detected by application of donkey anti-mouse AP secondary antibody (Jackson Immunoresearch) followed by chromogen Ferangi Blue (Biocare Medical). The sections were then blocked with peroxidase (Biocare Medical) for 10 min followed by Terminator block for 10 min. Primary antibody for RhoA (C-15, SCBT) diluted in HBS was applied for 2 h. Bound primary antibody was detected by application of bovine antigoat HRP secondary antibody (Jackson Immunoresearch) followed by chromogen DAB (SCBT).

Cell counting was employed to semi-quantitatively evaluate the staining results. For each cell, *i*, in a given section, the intensity of blue stain (GTP-bound RhoA/B/C), denoted bl_i, was recorded on a scale of 0–3, 0 = ‘‘no staining’’ and 3 = ‘‘highest intensity among all treatment groups for the GST antibody.’’ For this same cell, the presence of brown stain (RhoA), denoted Pi, was also recorded, 0 = ‘‘absent’’ and 1 = ‘‘present.’’ The cumulative staining intensity for GTP-bound RhoA, R_{active}, in each section was then calculated according to the following equation: $R_{active} = (\Sigma bl_i * P_i)/(\text{total cell number})$.

To compare the levels of active RhoA to total RhoA, intensity assessments for RhoA staining were separately conducted on the same sections. For each cell, *i*, in a given section, the intensity of brown stain (RhoA), denoted br_i, was recorded on a scale of 0–3, as above. The cumulative staining intensity for RhoA, R_{total}, in a given section was then calculated according to the following equation: $R_{total} = (\Sigma\ br_i)/(\text{total cell number})$. Four sections (1000–2000 cells) per formulation were stained and counted.

ECM and cell phenotype analyses. ECM deposition was analyzed in duplicate sections for each formulation using standard immunohistochemical technique. Rehydrated sections were blocked with peroxidase for 10 min followed by 10 min exposure to Terminator. Primary antibodies for elastin (BA-4, SCBT), collagen type I (Rockland Immunochemicals), or chondroitin sulfate proteoglycan (cs-56, SCBT)

diluted in HBS was then applied for 1 h. Bound primary antibody were detected by using AP-conjugated secondary antibody followed by application of the chromogen Ferangi Blue or by using HRP-conjugated secondary antibody followed by application of the chromogen AEC (Labvision).

Immunohistochemical stainings for calponin h1 (CALP, SCBT) and two regulators of calponin h1 expression, SRF (G-20, SCBT) and myocardin (H-300, SCBT), were similarly conducted to examine SMC phenotype. Prior to Terminator application, SRF and myocardin sections were exposed to cytoskeletal buffer for 10 min. To identify cells undergoing proliferation, separate sections were stained with proliferating cell nuclear antigen (PCNA; PC10, Invitrogen).

For intracellular markers of cell phenotype (SRF, myocardin, calponin h1, and PCNA), cell counts were conducted to semi-quantitatively evaluate immunostaining results. In addition, since deposited ECM remained localized around the parent cells in each hydrogel formulation, the relative ECM production among hydrogel formulations could also be evaluated by cell counts. For each cell, i, a staining intensity, d_i, was recorded on a scale of 0–3, 0 = ‘‘no staining’’ and 3 = ‘‘highest intensity among all treatment groups for that antibody.’’ The cumulative staining intensity, d, for a given antibody in a particular section was calculated using the following equation: $d = (\Sigma d_i)/(\text{total cell number})$. A total of 500–1000 cells were counted per formulation per antibody, and immunostained sections were imaged using an Axiovert 200 microscope (Zeiss).

Cell metabolic state. To evaluate the metabolic state of encapsulated cells, sections were stained for glucose 6-phosphate dehydrogenase (G6PD, Abcam) or for glyceraldehyde 3-phosphate dehydrogenase (GAPDH, SCBT). Both G6PD and GAPDH are key enzymes in cell metabolism, with GAPDH being associated with a catabolic pathway and G6PD being associated with a primarily anabolic pathway essential in the regulation of oxidative stress [139, 140]. Relative G6PD and GAPDH levels among formulations were probed using same intensity- based counting system used to evaluate

collagen type I immunostaining. As cell growth and viability are compromised by oxygen deprivation (hypoxia), immunostaining for hypoxia inducible factor-1α (HIF-1α; C-19, SCBT) was conducted. This staining was performed to ensure that observed differences in G6PD or GAPDH were not due to hypoxia, which could result from the smaller mesh sizes of the 30% 20 kDa and 20% 10 kDa formulations.

5.3.4 Comparative analyses

To gain insight into the potential dependence of ECM production (collagen and elastin), cell phenotype (SRF and myocardin), and cell signaling (G6PD and RhoA) on scaf-fold modulus and mesh size, surface plots were generated using Graphis software (Graphis). In these plots, the measured values for a given ECM component or phenotypic marker were plotted versus initial compressive modulus and mesh size.

5.3.5 Statistical analyses

Data are reported as mean ± standard error of the mean. Comparison of sample means was performed by ANOVA and Tukey's post hoc test (SPSS software), $p < 0.05$.

5.4 Results

The aim of this study was to validate a systematic approach for analyzing, in an uncoupled manner, the effects of initial scaffold mesh size and modulus on cell ECM production and phenotype.

5.4.1 Hydrogel material properties

To identify a set of PEG-DA hydrogels that would permit uncoupled examination of mesh size and modulus, six hydrogel formulations were screened. Hydrogel resistance to the diffusion of dextrans of various M_ws was used as a quantitative indicator of scaffold mesh size. The resulting mesh sizes relative to that of the 10% 10 kDa gels are given in Table 5.1. As expected, initial mesh size increased as PEG-DA concentration decreased or as M_w increased [68, 130].

Furthermore, because cells exert significant contractile forces on their surrounding microenvironment during matrix remodeling, the initial compressive modulus of each hydrogel was characterized to assess the initial mechanical environment experienced by encapsulated SMC. The compressive modulus of each hydrogel ranged from ~30–300 kPa (Table 5.1). In agreement with previous studies, hydrogel compressive modulus decreased as PEG-DA M_w increased or as concentration decreased [75]. To directly compare the mechanical properties of the selected hydrogel formulations to literature values for native arteries, hydrogel incremental tensile modulus was also evaluated. For each gel formulation, the measured incremental tensile modulus matched the corresponding compressive modulus within a multiplicative factor of 1–1.2 (data not shown), as has been observed by other investigators for PEG-DA gels [55]. Four of the six hydrogel compositions, namely the 10% 10 kDa, 20% 10 kDa, 30% 10 kDa, and 30% 20 kDa gels, were within the incremental modulus range of interest (~100–300 kPa, see compressive modulus values in Table 5.1). Of these four formulations, three (10% 10 kDa, 20% 10 kDa, 30% 20 kDa) permitted uncoupled investigation of the impact of modulus and mesh size. Specifically, the 20% 10 kDa and the 30% 20 kDa hydrogels had similar initial mesh sizes but initial compressive moduli which differed by a factor of ~2. Conversely, the 10% 10 kDa and the 30% 20 kDa hydrogels had similar moduli but mesh sizes that differed by a factor of ~1.5. Thus, although the mesh size of a hydrogel prepared from PEG-DA of a single M_w cannot be tailored independently of its compressive modulus, the effects of mesh size and modulus can be explored in an uncoupled manner by appropriately varying both PEG-DA concentration and M_w.

Table 5.1. Modulus and relative mesh size data for six PEG-DA formulations.

Formulation	Compressive Modulus (kPa)	Relative Mesh Size (μ)**
10% 10kDa	110.9 ± 8.4	1.00 ± 0.04
20% 10kDa	221.8 ± 11.0	0.65 ± 0.10
30% 10kDa	311.1 ± 26.6	0.50 ± 0.10
10% 20kDa	29.0 ± 7.5	1.73 ± 0.26
20% 20kDa	54.6 ± 7.7	1.06 ± 0.08
30% 20kDa	109 ± 10.8	0.73 ± 0.04

Highlighted formulations indicated compositions selected for cell studies.
[a]To translate these relative mesh sizes to approximate absolute values, the mesh size of the 30% 10 kDa gel can be estimated as ~ 9 nm, as described in Materials and Methods.

5.4.2 Cell encapsulation studies

SMCs were encapsulated within 10% 10 kDa, 30% 20 kDa, and 20% 10 kDa hydrogels so as to yield a postswelling cell concentration of ~0.5 x 10^6 cells/g. Following equilibrium swelling of the cell-laden gels, samples were collected to characterize the initial (day 3) mechanical properties and mesh size of each formulation. Results are displayed in Figure 5.1. As shown by comparison of Figure 5.1 with Table 5.1, the encapsulated cells had limited impact on hydrogel properties at the selected seeding density. Furthermore, SMCs were intentionally encapsulated at relatively low densities so that the evolution of the modulus of each hydrogel could be assumed to be dominated by scaffold degradation kinetics rather than by cell ECM deposition. Based on the modulus data at day 3 versus day 21, the mean degradation half-life of all hydrogel formulations was ~126 ± 4 days, assuming first-order degradation kinetics per Anseth et al. [73]. Thus, as each hydrogel formulation displayed a similar degradation rate, the rate of change in hydrogel modulus (and, hence, the rate of change in hydrogel mesh size) could be treated as a design ‘‘constant.’’ This allowed variations in SMC phenotype and ECM deposition with scaffold formulation to be evaluated relative to initial scaffold material properties without loss of information. SMC phenotype and ECM production will therefore be discussed referencing initial hydrogel mesh size and compressive modulus.

Cell density, proliferation, and metabolic state. PEG-DA constructs were harvested at day 21 for biochemical and histological analyses. No significant differences in net cell proliferation and loss were observed among hydrogel formulations based on DNA assessments (Figure 5.2(A)). Furthermore, each hydrogel composition showed a similar fraction of cells in a proliferative state (Figure 5.2(B)). In contrast, semi-quantitative analysis of the expression of GAPDH, an enzyme that catalyzes the sixth step of glycolysis, indicated that cell metabolic activity was higher in the 10% 10 kDa hydrogels than in the 20% 10 kDa and 30% 20 kDa gels ($p < 0.001$). Examination of G6PD, a key enzyme in the primarily anabolic pentose phosphate pathway, supported a decrease in average cell metabolic activity from the 10% 10 kDa to the 30% 20 kDa gels ($p = 0.012$). A combined decrease in mesh size and increase in modulus (10% 10 kDa vs. 20% 10 kDa gels) was associated with decreased levels of hypoxia indicator, HIF-1α ($p = 0.017$).

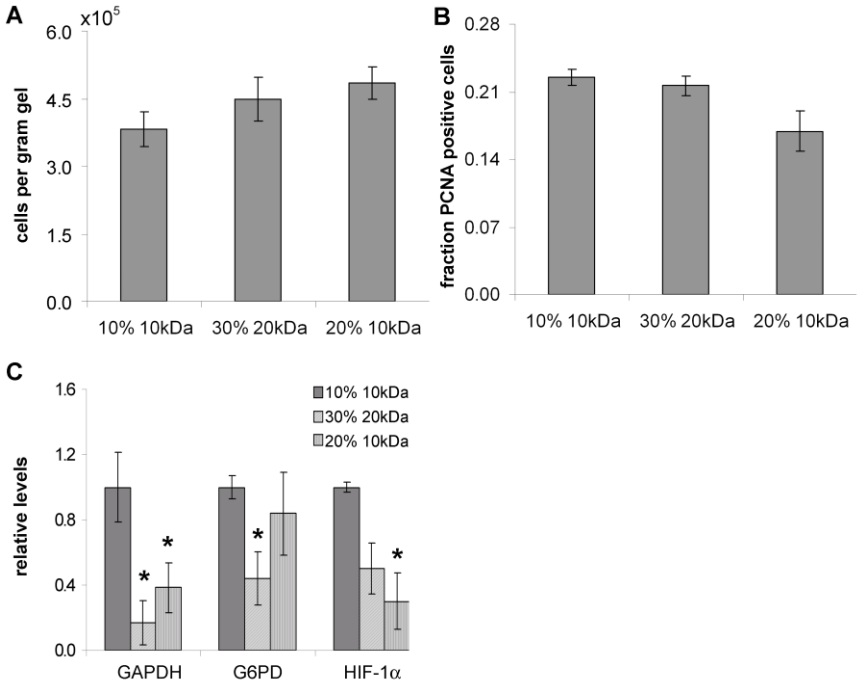

Figure 5.2 Cell density, proliferation, and metabolic activity. (A) SMC density (n = 3–6 per formulation), (B) fraction of cells expressing proliferation marker PCNA, and (C) relative levels of GAPDH, G6PD, and HIF-1α among hydrogel formulations. *, significantly different from 10% 10 kDa hydrogels, $p < 0.05$.

ECM deposition. Measured collagen, sGAG, and elastin levels for each hydrogel formulation are given on a per cell basis in Figure 5.3. Collagen deposition was ~4- and ~2.5-fold higher, respectively, in the 10% 10 kDa and 20% 10 kDa hydrogels than in 30% 20 kDa gels ($p < 0.001$). Total sGAG content was statistically indistinguishable among formulations. Similarly, elastin production in the 10% 10 kDa and the 30% 20 kDa hydrogels did not differ significantly. However, elastin levels were lower in the 20% 10 kDa hydrogels relative to the 10% 10 kDa ($p = 0.004$) and the 30% 20 kDa ($p = 0.038$) gels.

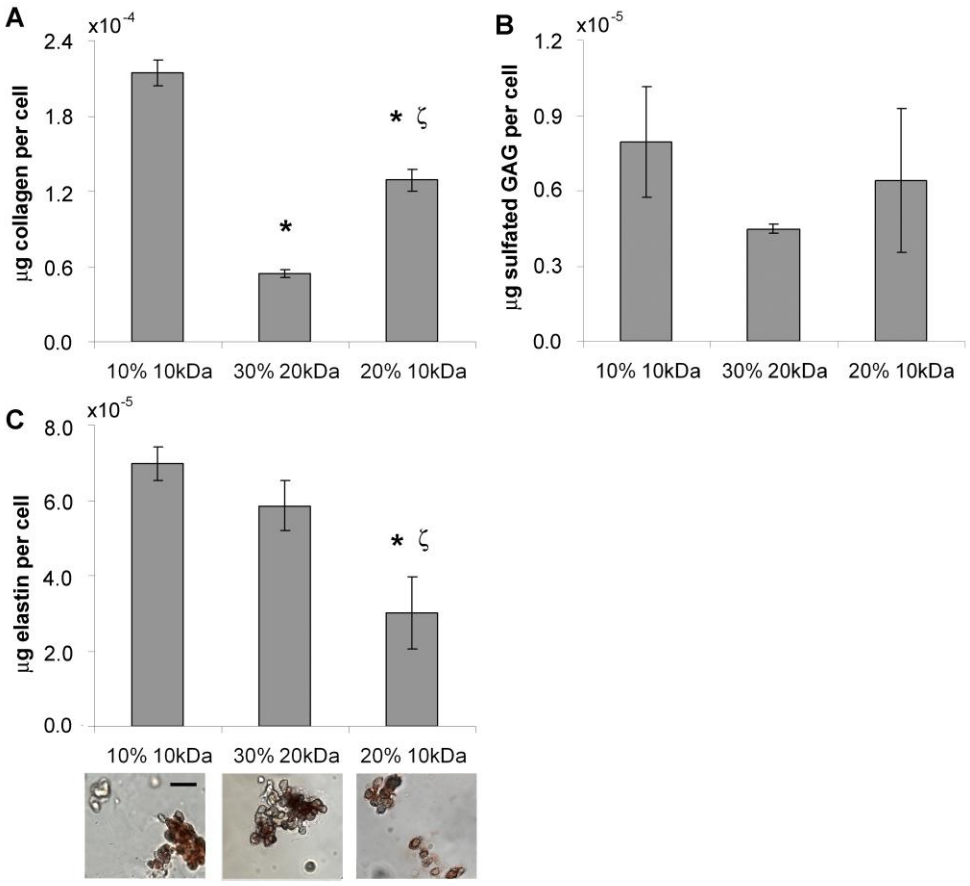

Figure 5.3. SMC ECM deposition. (**A**) Collagen production (n = 5–6 per formulation), (**B**) sGAG content (n = 3–6 per formulation), and (**C**) elastin levels (n 5 4–11 per formulation). Representative images for elastin immunostaining are shown directly below (**C**), scale bar 5 40 lm. *, significantly different from 10% 10 kDa hydrogels, $p < 0.05$. ζ, significantly different from 30% 20 kDa hydrogels, $p < 0.05$.

Semi-quantitative analysis of collagen type I immunostaining supported the total collagen biochemical assessments (Figure 5.4(A)). Although the chondroitin sulfate proteoglycan (CSPG) content of the 10% 10 kDa and 20% 10 kDa gels could not be statistically distinguished, CSPG synthesis was significantly higher in the 10% 10 kDa gels than in the 30% 20 kDa hydrogels ($p = 0.039$, Figure 5.4(A)). As expected for PEG-DA gels, [62] collagen type I, elastin (Figure 5.3(C)), and CSPG staining was confined to the immediate pericellular space in each formulation, although CSPG staining in the 10% 10 kDa gels appeared to be more diffusely present than in the remaining hydrogels.

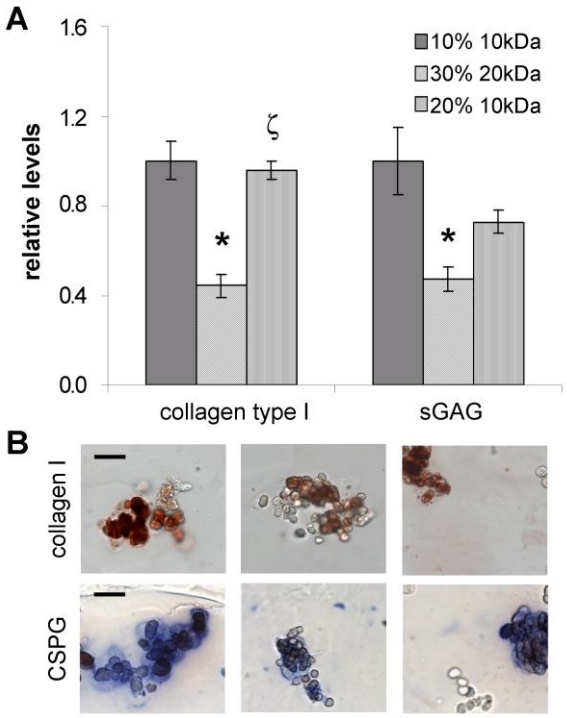

Figure 5.4 Relative intensity of collagen type I and chondroitin sulfate proteoglycan (CSPG) immunostaining (**A**). Representative images for collagen type I and CSPG immunostaining are shown in (**B**). Scale bars 5 40 μm.*, significantly different from 10% 10 kDa hydrogels, $p < 0.05$. ζ, significantly different from 30% 20 kDa hydrogels, $p < 0.05$.

SMC phenotype. Figure 5.5 illustrates results from cell counting of sections immunostained for SRF, myocardin, and calponin h1 toward assessment of SMC phenotype. Expres- sion of transcription factor SRF was significantly higher in the 10%

10 kDa and 20% 10 kDa hydrogels than in 30% 20 kDa hydrogels ($p < 0.001$ and $p = 0.002$, respectively). Calponin h1 levels among formulations could not be statistically distinguished. Myocardin expression, however, was significantly higher in the 10% 10 kDa hydrogels than in the 20% 10 kDa and the 30% 20 kDa gels ($p < 0.001$). Although total RhoA levels were not statistically different among formulations (data not shown), comparison among gels indicated a significant decrease in the fraction of active RhoA (Ractive/Rtotal) from the 10% 10 kDa to the 30% 20 kDa gels ($p = 0.031$, Figure 5.5(D)).

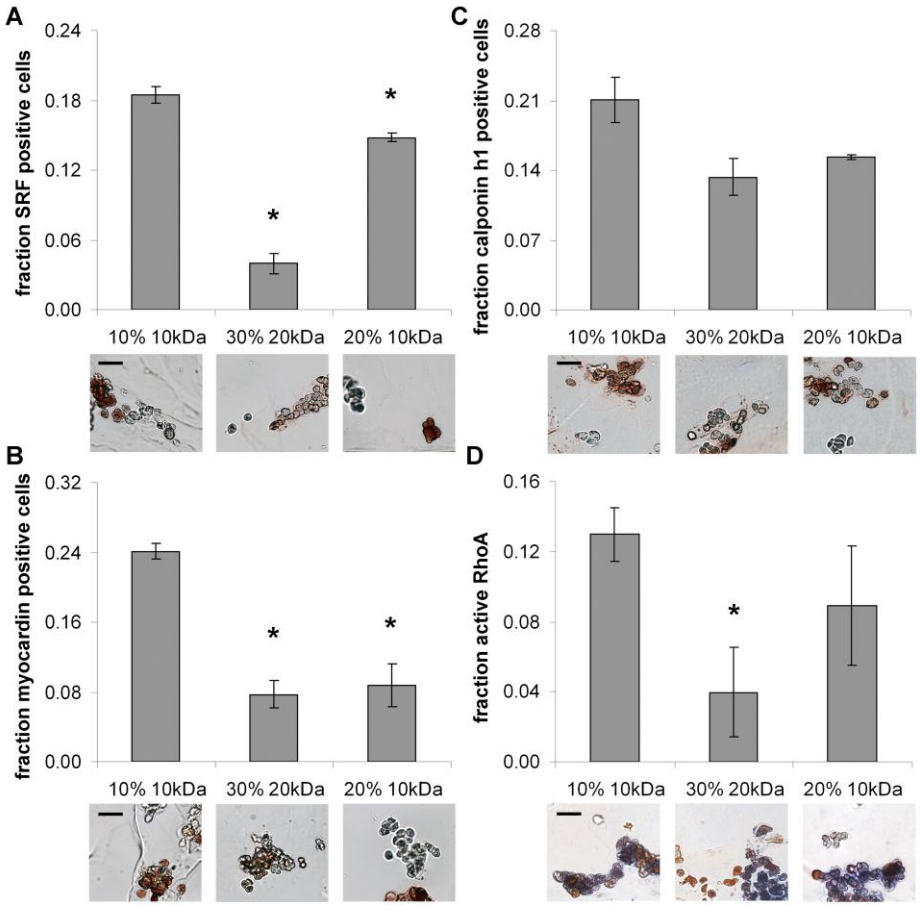

Figure 5.5. Relative expression of (**A**) SRF, (**B**) myocardin, and (**C**) calponin h1. (**D**) Fraction of active RhoA (Ractive/Rtotal) by formulation. Representative images for each immunostaining are shown under the respective bar graphs, scale bars = 40 μm. For the active RhoA images, blue stain indicates rhotekin binding (active RhoA/B/C) and brown stain indicates RhoA. Cells staining for both RhoA and rhotekin indicate the presence of active RhoA. *, significantly different from 10% 10 kDa hydrogels, $p < 0.05$, f significantly different from 30% 20 kDa hydrogels, $p < 0.05$.

Comparative analyses. The above observations regarding the modulation of ECM deposition and SMC phenotype with gel formulation are further underscored in Figure 5.6, which displays surface plots of total collagen and elastin (Figures 5.6(A,B), respectively) as well as SRF and myocar-din (Figures 5.6(C,D), respectively] versus modulus and mesh size. To accurately evaluate the potential impact of mesh size relative to that of modulus, the ECM and cell marker data were plotted such that the modulus and mesh size axes each spanned the same data range, that is, the high and low modulus plotted differed by a factor of 2, and the high and low mesh size plotted also differed by a factor of 2. For each graph, the maximum value of the ECM component or cell marker is shown in red and the minimum in blue.

From these graphs, it is apparent that myocardin expression displayed a strong correlation with mesh size but only a weak correlation with modulus. This can be seen from the fact that the color gradient of the myocardin surface plot is at an ~75° angle to the mesh size axis, that is, at a given mesh size there is minimal change in myocardin levels (color) with a change in modulus. SRF and collagen content increased significantly with an increase in modulus, but increased more markedly with an increase in mesh size. Their greater correlation with mesh size than with modulus is reflected in the ~60° angle of the SRF color gradient and the ~65° angle of the collagen color gradient relative to their respective mesh size axes. Following a similar logic, the angle of the elastin color gradient lines relative to the mesh size axis (~40°) suggests that elastin has a similar degree of correlation with modulus and mesh size. The surface plots for G6PD and active RhoA were similar to that of collagen (data not shown).

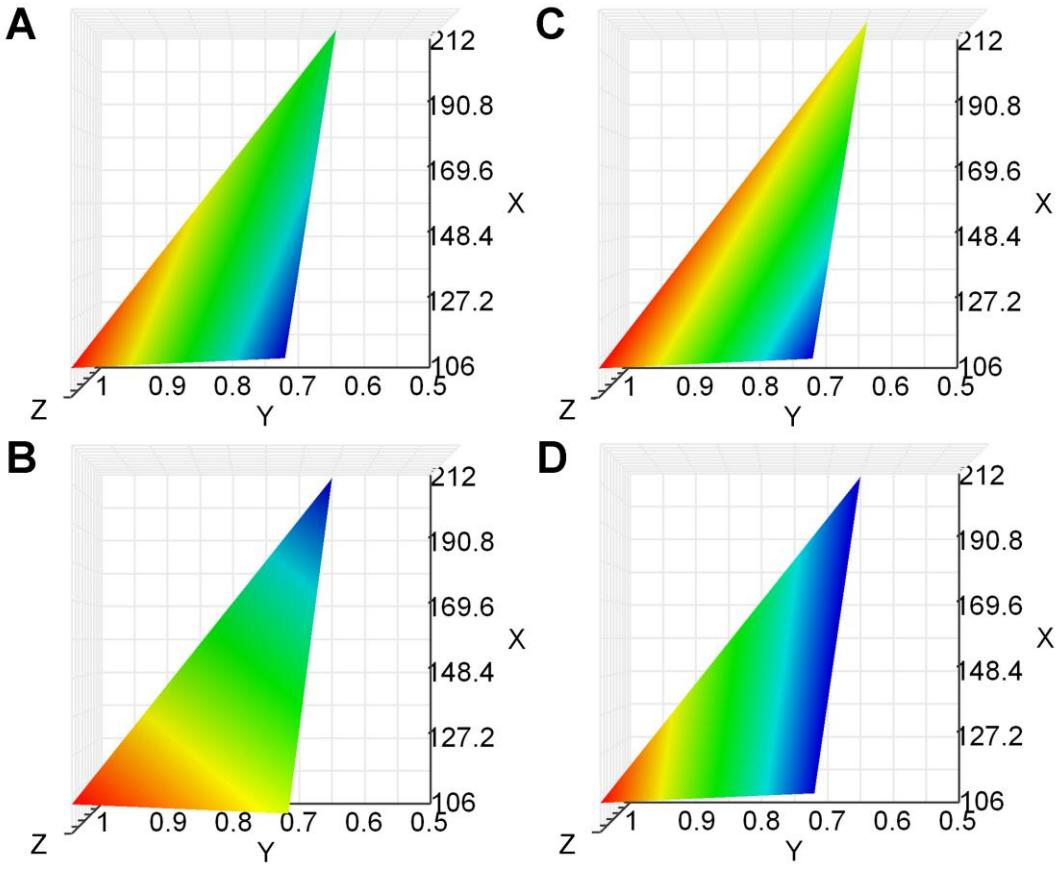

Figure 5.6 Surface plots of (**A**) collagen, (**B**) elastin, (**C**) SRF, and (**D**) myocardin versus mesh size and modulus. For each graph, the maximum value of the ECM component or cell marker is shown in red and the minimum in blue. The axis labeled X represents modulus, whereas the axis labeled Y represents relative mesh size.

5.5 Discussion

Interrogation of the impact of isolated scaffold material properties on cell response has proven problematic due, in part, to the complexity and/or interdependence of scaffold variables. This situation has limited our ability to correlate specific cell responses to particular scaffold properties, hampering the rational selection of scaffold material properties so as to elicit desired cell responses. The aim of this study was to validate an approach for systematically evaluating the dependence of cell phenotype and ECM production on isolated scaffold material properties, with a focus on mesh size and modulus.

For the subset of PEG-DA hydrogels investigated herein, both SMC phenotype and ECM deposition exhibited marked correlations with initial hydrogel mesh size and modulus. For instance, CSPG production increased with increasing scaffold mesh size (30% 20 kDa vs. 10% 10 kDa hydrogels). Previous studies have suggested a dependence of sGAG levels and distribution on scaffold mesh size [62, 117]. However, these works noted a decrease in sGAG content with increasing mesh size, which was attributed to increased diffusional loss of small- to moderately-sized proteoglycans as mesh sizes exceeded ~9 nm.6,8 Although diffusional loss likely modulated CSPG presence to some extent in this work, as suggested by the increased spread of CSPG staining in the 10% 10 kDa hydrogels relative to the lower mesh size formulations, the overall trend in CSPG content (increasing with increasing mesh size) is contrary to that expected if diffusion were the primary regulator of CSPG levels. The discrepancy between the present results and those of Bryant and Anseth [62, 117] may arise from differences in cell type and/or from the fact that hydrogel modulus and mesh size were not uncoupled variables in the latter works (i.e., formulations with lower mesh sizes also had higher moduli).

Although collagen deposition was correlated with modulus (30% 20 kDa vs. 20% 10 kDa), results suggest that mesh size may have a greater absolute impact on SMC collagen production than modulus, at least over the material property range probed (Figure 5.6). Similarly, expression of GAPDH and G6PD displayed a greater correlation with scaffold mesh size than with scaffold modulus. As with collagen and CSPG production, the mechanisms underlying the observed modulation of cell metabolic activity with scaffold formulation are unclear. Specifically, limitations in glucose transport through the hydrogel networks should not be an issue, because glucose, with a hydrodynamic radius ~0.4 nm, should pass rapidly and freely through the PEG-DA gels used herein. In addition, the decrease in G6PD and GAPDH levels with decreasing mesh size is unlikely to be due to hypoxia induced by decreased mesh size. Under hypoxic conditions, HIF-1α expression is increased so as to restore oxygen homeostasis [141]. However, HIF-1α levels decreased, rather than increased, with decreasing mesh size.

As with cell metabolic activity, RhoA activity was highly correlated with hydrogel mesh size, although the mechanisms by which RhoA activity depends on scaffold mesh size remain to be elucidated. Figure 5.5(D) also suggests that RhoA activity may be increased with increasing modulus at constant mesh size (30% 20 kDa vs. 20% 10 kDa), although this link with modulus was not statistically significant. The separate impact of scaffold modulus on RhoA activity therefore requires further confirmation. However, an increase in RhoA activity with increasing PEG-DA hydrogel modulus would be consistent with a number of previous 2D studies [126, 127]. Combined, the current data indicate that the effects of scaffold properties on RhoA activity in 3D may be distinct from those in 2D and underscore the need for controlled and uncoupled examination of the influence of scaffold properties on cell behavior in 3D. Furthermore, these data suggest that RhoA signaling and cell metabolic regulation may be closely linked. This would be consistent with the known influence of RhoA signaling on cell metabolism, in particular on glucose transport and insulin sensitivity [142]. In addition, GAPDH has recently been implicated in several nonmetabolic processes, including transcription activation [143] and initiation of apoptosis [144].

The present results also suggest a correlation between RhoA and cell metabolic activity and the expression of transcription factor SRF, often referred to as the master regulator of SMC phenotype. A link between RhoA activity and SRF would be in agreement with previous studies indicating that RhoA influences SRF through its interactions with SMADs [145-148]. A link between SRF and cell metabolism would also be consistent with the literature. Specifically, a decrease in G6PD levels in rat glial cells has been associated with inhibition of the expression of inducible nitric oxide synthase, [149] an enzyme associated with maintenance of a mature vascular SMC phenotype [150].

Based on the present results, the 10% 10 kDa hydrogels would be the most beneficial of the formulations examined for the fabrication of TEVGs, in which both high rates of ECM production and a mature SMC phenotype are desirable. Data also suggest that at least short-term induction of increased RhoA activity may be desirable in

TEVG development. A limitation of this study is the relatively restricted initial scaffold mesh size/modulus range interrogated. Future experiments will explore a broader range of initial scaffold moduli and mesh sizes as well as probe the impact of degradation rate and bioactivity. An additional limitation of this approach can be seen in examining Figures 5.3, 5.4, and 5.5. Despite the presence of adhesion peptide RGDS, encapsulated SMC took on rounded or stellate morphologies when encapsulated in PEG-DA hydrogels. This particular characteristic of PEG-DA hydrogels, which results from their dense crosslinking and relatively slow degradation rates, [55, 57, 75, 117] is not optimal for cells such as SMC, which natively take on spindleshaped morphologies. However, because of several of their unique properties, PEG-DA hydrogels have been employed as a model scaffold by a number of researchers focusing on smooth muscle- or fibroblast-like cells, in spite of this limitation [75, 113, 151, 152]. In this study, the encapsulated cells showed the ability to display SMC marker, calponin h1, and thus the ability to attain certain key aspects of a native SMC phenotype, lending validity to this model system.

CHAPTER VI
INORGANIC–ORGANIC HYBRID SCAFFOLDS FOR OSTEOCHONDRAL REGENERATION*

6.1 Overview

Ligament graft failure frequently results from poor integration of the replacement tissue with associated bone. Thus, the ability to regenerate the bone-ligament osteochondral interface would be advantageous in ligament reconstruction. At the osteochondral interface, the tissue transitions from a bone-like matrix to fibrocartilage. Therefore, a scaffold which promotes a spatially regulated transition in cell behavior from osteoblast-like to chondrocyte-like would be desirable. Previous research indicates that addition of inorganic components to organic scaffolds can enhance the deposition of bone-like matrix by associated osteoblasts. We therefore reasoned that a gradient in the inorganic content of a hybrid inorganic–organic scaffold may induce an osteochondral-like transition in cell phenotype and matrix production. To test this hypothesis, hydrogels were prepared from poly(ethylene glycol) (PEG) and star poly(dimethylsiloxane) ($PDMS_{star}$). As anticipated, both the matrix deposition and phenotype of encapsulated osteoblasts varied with scaffold inorganic content, although the directionality of this modulation was contrary to expectation. Specifically, osteoblasts appeared to transdifferentiate into chondrocyte-like cells with increasing scaffold inorganic content, as indicated by increased chondroitin sulfate and collagen type II production and by upregulation of sox9, a transcription factor associated with chondrocytic differentiation. Furthermore, the deposition of bone-like matrix (collagen type I, calcium phosphate, and osteocalcin) decreased with increasing $PDMS_{star}$ content.

The resistance of the $PDMS_{star}$-PEG scaffolds to protein adsorption and/or the changes in gel modulus/mesh structure accompanying $PDMS_{star}$ incorporation may underlie the unexpected increase in chondrocytic phenotype with increasing inorganic content. Combined, the present results indicate that $PDMS_{star}$-PEG hybrid gels may prove promising for osteochondral regeneration.

6.2 Introduction

The cruciate ligaments of the human knee withstand a variety of tensile and torsional forces during the course of normal daily routine and athletic activity. Damage can result in pain, joint instability and dysfunction, and eventual degenerative joint disease[153]. As such, ~150,000 surgical procedures are performed to treat injured anterior cruciate ligaments (ACLs) each year in the United States alone [154]. Currently, autologous tissue is the preferred graft material for ACL reconstruction [155]. However, the limited supply of autologous tissue suitable for grafting and the risk of donor site morbidity complicate the use of autologous grafts [156]. Tissue engineering is an alternative approach for ligament repair that may avoid many of limitations associated with autografts.

Although rapid progress has been achieved in ligament tissue engineering over the past decade, engineered ligaments have, thus far, generally failed to achieve mechanical properties sufficiently similar to their native counterparts to serve as viable grafts [157]. In addition, these engineered tissues usually lack the osteochondral interface critical to the appropriate transfer of load between ligament and bone [157]. As graft failure frequently results from poor integration of the replacement tissue with associated bone [158], the ability to regenerate the bone-ligament osteochondral interface would be advantageous in ligament reconstruction.

At the osteochondral interface, the tissue transitions from a bone-like matrix to fibrocartilage-like matrix [159]. Thus, a scaffold which promotes a spatially regulated transition in cell behavior from osteoblastlike to chondrocyte-like would be desirable for osteochondral regeneration [160]. For instance, a recent osteochondral tissue engineering

study employed a scaffold containing a spatial gradient in levels of a retrovirus encoding for Runx2, an osteogenic transcription factor [161]. This design induced a spatiallygraded transdifferentiation of associated dermal fibroblasts into osteoblast-like cells. Similarly, an extensive body of literature indicates that appropriately tailoring scaffold inorganic composition (hydroxyapatite and bioactive glass) can enhance its osteoconductivity [162-165]. Recently, silica-calcium phosphate (CaP) composite scaffolds were shown to induce increasing osteoblast alkaline phosphatase activity [166] and osteocalcin expression [167] with increasing silica (decreasing CaP) content. Another work demonstrated elevated alkaline phosphatase activity in osteoblasts cultured on gelatin scaffolds of increasing siloxane content [168].We therefore reasoned that a gradient in the siloxane content of a hybrid inorganic–organic scaffold may induce an osteochondral-like transition in cell phenotype.

To test this hypothesis, we employed hydrogels composed of varying ratios of poly(ethylene glycol) (PEG) to star poly(dimethylsiloxane) ($PDMS_{star}$). PEG was selected for the organic component since spatial gradients can readily be fabricated in hydrogels prepared from diacrylate-derivatized PEG due to its photoactivity. For instance, PEG hydrogels with a continuous linear material property gradient can be generated by simple adaptation of the equipment normally used to make gradient polyacrylamide gels for electrophoresis [169] More complex spatial gradients or patterns can be fabricated using photolithographic techniques [61, 63, 94]. PDMS was chosen over other polysiloxanes due to its known biocompatibility and its widespread use in biomedical applications [170]. In addition, a star conformation of PDMS was selected over a linear form in order to reduce potential phase separation between the hydrophobic PDMS and hydrophilic PEG prior to hydrogel polymerization [171].

In this study, rat calvarial osteoblasts were encapsulated in PEG gels of varying $PDMS_{star}$ content, and the resulting modulation of cell behavior was examined. In assessing cell response, biochemical and histological analyses were conducted for extracellular matrix (ECM) components associated with mature bone (collagen type I, osteocalcin, and CaP) and fibrocartilage [collagen types I and II as well as chondroitin

sulfate proteoglycan (CSPG)] [159]. To gain insight into the signaling underlying observed cell responses, immunostaining for the chondrogenic transcription factor sox9 [172] was also performed.

6.3 Materials and methods

6.3.1 Polymer synthesis

Synthesis of methacrylate-derivatized PDMSstar (PDMS$_{star}$-MA. Methacrylate-derivatized star PDMS (PDMS$_{star}$-MA) was prepared via a two step synthetic strategy per a modification of the methodology validated in Grunlan et al. [173]. First, silane terminated PDMSstar (PDMS$_{star}$-SiH) was prepared by the acid-catalyzed equilibration of octamethylcyclotetrasiloxane with tetrakis(dimethylsiloxane)silane. The desired PDMS$_{star}$ M_w of ~14 kDa was achieved by appropriately setting the ratio of these two components[173]. Briefly, octamethylcyclotetrasiloxane (30 g, 0.10 mol) and tetrakis(dimethylsiloxane) silane (0.5 g, 1.5 mmol) were combined in a 100 mL round bottom flask and purged with N_2. Triflic acid (15 μL) was then added and the reaction was allowed to stir for 1 h at 90°C. After cooling, the pH was neutralized by combining with $MgCO_3$ (0.5 g) and dichloromethane (DCM, 20 mL) and stirring for 2 h. After filtration through a pad of Celite, the volatiles were removed under reduced pressure. In this way, PDMS$_{star}$-SiH was obtained (26.3 g, 86% yield) as a colorless liquid and subsequently characterized by ^{1}H NMR, ^{13}C NMR, IR, and gel permeation chromatography (GPC). The silane terminal groups of PDMS$_{star}$-SiH were then converted into photosensitive moieties by the hydrosilylation reaction of PDMS$_{star}$-SiH and allyl methacrylate [174]. Briefly, PDMS$_{star}$-SiH (6 g, 0.72 mmol) was combined with 10 mL of dry toluene in a 100 mL round bottom flask and purged with N_2. After Karstedt's catalyst (Pt-divinyltetramethyldisiloxane complex in xylene, 2% Pt; 15 μL) was added, the reaction was heated under constant stirring to 45 °C. Allyl methacrylate (0.39 mL, 2.9 mmol) was added to this solution via an addition funnel over 15 min, after which the reaction was heated to 90°C and stirred overnight. Completion of the reaction was confirmed by the disappearance of the Si—H (~2100 cm^{-1}) absorbance in the IR

spectrum. The reaction mixture was decolorized by refluxing with activated carbon for 12 h. After filtration, the volatile side products were removed under reduced pressure. In this way, methacrylate-derivatized $PDMS_{star}$ ($PDMS_{star}$-MA) was obtained (5.23 g, 82% yield) and subsequently characterized by ^1H NMR.

Preparation of diacrylate-terminated PEG. Photosensitive acrylate groups were introduced to the terminal ends of linear PEG (M_w ~3.4 kDa, Sigma) per established protocols [94]. Briefly, PEG (10 g, 3.3 mmol) and dry DCM (50 mL) were combined in a 100 mL round bottom flask and purged with N_2. Triethylamine (0.96 mL, 6.6 mmol) was added slowly to the solution followed by the dropwise addition of acryloyl chloride (1.08 mL, 13.2 mmol). The reaction mixture was allowed to stir at room temperature overnight. Removal of HCl was accomplished by washing the mixture with 2M K_2CO_3 and separating into aqueous and organic phases. The organic (DCM) phase was then dried with anhydrous $MgSO_4$, and diacrylate- derivatized PEG (PEG-DA) was precipitated in diethyl ether and dried under vacuum. In this way, PEG-DA was obtained and subsequently characterized by ^1H NMR.

Synthesis of acrylate-derivatized cell adhesion ligand. Cell adhesion peptide RGDS (American Peptide) was reacted with acryloyl-PEG-N-hydroxysuccinimide (ACRLPEG-NHS, M_w ~3.4 kDa, Nektar) at a 1:1 molar ratio for 2 h in 50 mM sodium bicarbonate buffer, pH 8.5 [63, 94, 167]. The product (ACRL-PEG-RGDS) was purified by dialysis, lyophilized, and stored at -20°C until use.

6.3.2 Hydrogel fabrication

Three distinct hydrogel precursor solutions were prepared by dissolving desired levels of $PDMS_{star}$-MA and PEG-DA in HEPES buffered saline (HBS; 10 mM HEPES, 150 mM NaCl, pH 7.4). Each solution contained 10 weight percent (wt %) total polymer comprised of one of the following three wt ratios of $PDMS_{star}$-MA to PEG-DA: 0:100, 1:99, and 5:95. Ten microliters of photoinitiator consisting of a 30 wt % solution of 2,2-

dimethyl-2-phenyl-acetophenone in N-vinylpyrrolidone was added per milliliter of precursor solution. The resulting solutions were mixed by vortex and then filtered (0.22 μm PES membrane, Millipore) immediately prior to being pipetted into 0.5-mmthick transparent rectangular molds. In addition to performing a sterilization function, the filtration process served to create a fine and stable dispersion of hydrophobic $PDMS_{star}$-MA within the aqueous PEG-DA solution. The precursor solutions were polymerized by 2 min exposure to longwave UV light (Spectroline, ~6 mW/cm^2, 365 nm).

6.3.3 Hydrogel characterization

The elemental composition, surface hydrophilicity, modulus, mesh size, and equilibrium swelling of prepared hydrogels were characterized using established methods. The hydrogel samples were immersed in media or HBS for at least 24 h before all characterization steps, aside from bulk swelling assessments.

Hydrogel composition. To verify the incorporation of varying levels of $PDMS_{star}$ into the fabricated hydrogels, compositional analysis was performed using a Kratos Axis Ultra X-ray photoelectron spectrometer (XPS) with a monochromatized Mg K_α source. Swollen hydrogels were transferred to dIH_2O for 24 h and then dried under vacuum. The dried gel discs were then placed onto steel gravity mounts and loaded into the XPS. Elemental atomic percent compositions were obtained from survey spectra, which were performed from 0 to 1100 eV. High-resolution analyses with pass energies of 40 eV were performed at a take-off angle of 90°. The binding energies were referenced to C^{1s} peak at 285.0 eV. The raw data was quantified and analyzed using XPS Peak Processing software [175].

Contact angle and protein adsorption. The dependence of gel surface hydrophilicity and protein adsorption on increased $PDMS_{star}$ content was evaluated. Static contact angle measurements were performed on swollen $PDMS_{star}$-PEG hydrogels using a CAM-200 (KSV Instruments) contact angle measurement system equipped with

an autodispenser, video camera, and dropshape analysis software. Briefly, 5 μL of dIH_2O was dispensed onto each hydrogel surface, and the angle of the water droplet relative to the surface was monitored for a period of 2 min. Five separate measurements were performed for each hydrogel formulation.

For protein adsorption analyses, four 6-mm diameter samples were harvested from swollen hydrogels of each formulation. These samples were exposed to a 50 μg/mL solution of AlexaFluor 488-labeled fibronectin in PBS. Fibronectin adsorption was selected for characterization based on previous bone tissue engineering studies [162, 176]. Following 1 h at room temperature, the protein solutions were removed and exchanged with PBS. One hour and12 h after removal of the protein solution, the fluorescence of the hydrogel surfaces was monitored using a Zeiss Axiovert 200 microscope and separately using a microplate reader at ex/em 488/532. Prior to each time point measurement, the PBS was removed and exchanged with fresh PBS. A fibronectin standard curve was used to convert each fluorescence signal to a protein concentration.

Hydrogel swelling. To characterize equilibrium swelling, 8-mm diameter samples were cored from each PEG-DA hydrogel immediately following polymerization and weighed. The samples were then transferred to HBS supplemented with 0.05 wt% sodium azide (HBS-azide). After 24 h, samples were blotted and weighed. The swollen gels were then dried in vacuo and their dry weight recorded. As PEG-DA hydrogels are primarily water, the increase in weight with swelling can be directly related to the increase in gel volume (V) with swelling, i.e., $S = \left(\frac{V_{swollen}}{V_{initial}} \right) \approx \left(\frac{swollenweight}{initialweight} \right)$. S values were found to be 1.10 ± 0.01, 1.07 ± 0.01, and 1.11 ± 0.01 for the 0:100, 1:99, and 5:95 gels, respectively. These ratios were used to calculate the amount of cells and ACRL-PEG-RGDS to be added to each hydrogel precursor solution so as to ensure the desired postswelling cell density and RGDS concentration. The dry weight measures

were used to calculate the swelling ratio for each formulation: R = (swollen weight/dry weight). This ratio served as an indicator of gel crosslink density.

Hydrogel mesh size. PEG-DA hydrogel mesh structure cannot be visualized using techniques such as conventional scanning electron microscopy (SEM) [131]. Thus, a variety of methods to estimate PEG-DA hydrogel mesh size have been developed, including correlations linking measurable quantities, such as equilibrium hydrogel swelling and PEG-DA M_n, to mesh size [68, 130]. Although these correlations yield reasonable mesh size estimates for homopolymer hydrogels, [68, 130] these correlations cannot readily be applied to $PDMS_{star}$-PEG hybrid hydrogels. Thus, in this study, hydrogel mesh size was characterized via dextran diffusion based on an adaptation of the methodology of Watkins et al. [69].

A series of $PDMS_{star}$-PEG hydrogels were prepared, each containing 1 mM ACRL-PEG-RGDS postswelling. These gels were allowed to swell overnight at 37°C in HBS-azide, after which 8 mm discs were cored from each sample. FITC-labeled dextran (70 kDa, Sigma) was dissolved at 0.05 mg/mL in HBS-azide and added at 1 mL per hydrogel disc. Dextran was then allowed to diffuse into the hydrogels for 24 h at 37°C. Each gel disc was gently blotted and transferred to 1 mL fresh HBS-azide.

Dextran that had penetrated into the hydrogels was then permitted to diffuse out into the surrounding solution at 37°C. After 24 h, the fluorescence of the HBS-azide solution surrounding each disc was measured at ex/em 488/532. Dextran standard curves were used to convert each fluorescence signal to microgram dextran. For each gel sample, these dextran readings were divided by gel weight to yield a quantitative indicator of hydrogel permissivity (C). These permissivity measures were used to estimate the relative mesh size (ξ) of each hydrogel (x) as follows: $\xi \approx \left(\frac{C_x}{C_{0:100PDMS-PEG}} \right)$.

Hydrogel mechanical properties. $PDMS_{star}$-PEG hydrogels were prepared containing 1 mM ACRL-PEG-RGDS postswelling. Three 8-mm discs were cored from

each swollen gel and mechanically tested under unconstrained compression at room temperature using an Instron 3342. Following application of a 0.01 N preload, each hydrogel was subjected to 10 μm cyclic compression (~1% cyclic strain) at 1 Hz. The compressive modulus of each hydrogel was extracted from the resulting stress-strain data.

6.3.4 Cell encapsulation studies

Cell expansion. Cryopreserved rat calvarial osteoblasts (Dominion Pharmakine) were thawed and expanded at 37 ºC/5% CO_2 in Dulbecco's Modified Eagles' Media (DMEM, Hyclone) supplemented with 10% fetal bovine serum (FBS), and 100 U/mL penicillin and 100 mg/L streptomycin (Hyclone).

Cell encapsulation. Osteoblasts at passage 6 were harvested and combined. Precursor solutions containing 10 wt % total polymer were prepared by dissolving $PDMS_{star}$-MA and PEG-DA at ratios of 0:100, 1:99, and 5:95 in HBS followed by photoinitiator. These wt ratios will be used to refer to the various hydrogel formulations throughout the remainder of the text. ACRL-PEG-RGDS was added to each precursor solution to achieve 1 mM RGDS post-swelling. Each precursor solution was sterile-filtered, immediately after which osteoblasts were added at a postswelling density of ~$3x10^6$cells/mL. The hydrogel slabs were transferred to Omnitrays (Nunc) fitted with four sterile polycarbonate bars to simultaneously prevent gel flotation and prevent gel contact with the tray bottom. Gels were maintained at 37 °C/ 5% CO_2 in DMEM supplemented with 10% FBS and 100 U/mL penicillin and 100 mg/L streptomycin. Media was changed every 2 days.

Day 3 construct analyses. Following 3 days of culture to allow for complete hydrogel equilibration, 8-mm diameter samples were collected to characterize the initial mechanical properties of the cell-laden gels. These measures were conducted as

described earlier to assess the impact of cells on initial bulk-average hydrogel material properties (since hydrogel modulus, mesh size, and swelling are interdependent) [73].

Day 28 construct biochemical analyses. After 28 days total culture time, a series of 8-mm samples were collected from each hydrogel formulation for biochemical and histological analyses. Samples harvested for biochemical analyses were weighed, flash-frozen in liquid nitrogen, and stored at -80°C.

DNA and total collagen biochemical analyses. Hydrogel samples were digested for 72 h at 37°C in 1 mL of 0.12M NaOH per 0.2 g hydrogel wet weight. Aliquots of the NaOH hydrolyzed samples (n = 5 3–6 per formulation) were neutralized and their DNA content determined using the PicoGreen assay (Invitrogen) [75]. DNA measures were translated to cell number using a conversion factor of 6.6 pg DNA per cell. Calf thymus DNA (Sigma) served as a standard. Levels of hydroxyproline were quantified as an indirect measure of total collagen. NaOH digested hydrogels (n = 5 3–5 per formulation) were further hydrolyzed for 18 h at 110°C in 6M HCl. The samples were then dried (Centrivap, Labconco) followed by resuspension in dIH_2O and reaction with chloramine T and p-dimethylbenzaldehyde reagents [101]. Sample absorbance was read at 550 nm relative to that of l-4-hydroxyproline (Sigma). Total collagen content was estimated from measured hydroxyproline using the collagen type I conversion factor of 0.13 grams hydroxyproline per gram collagen [77]. For each assay, the standards used were subjected to the same association with PEG-DA and $PDMS_{star}$-MA and the same digestion conditions as the samples.

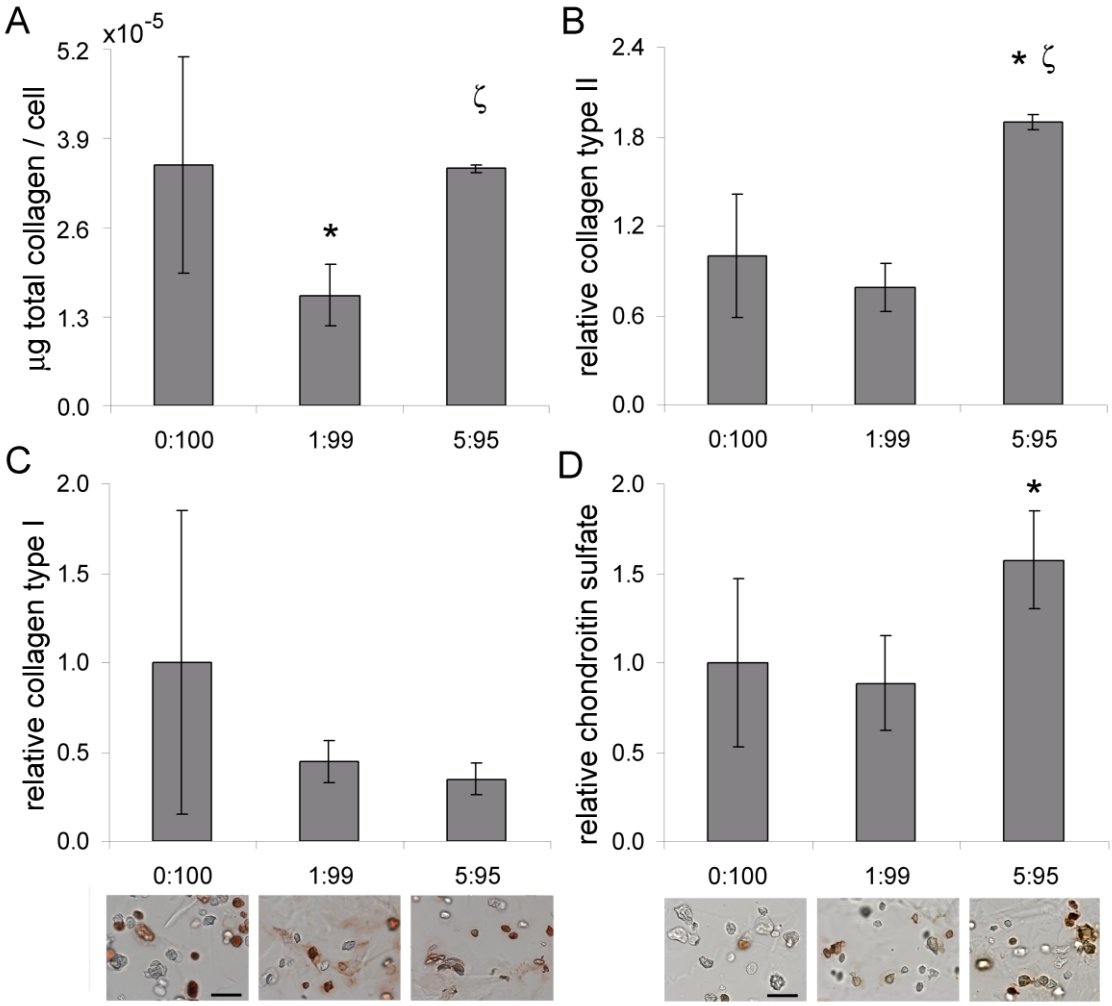

Figure 6.1 Relative expression of (**A**) total collagen, (**B**) collagen type II, (**C**) collagen type I, and (D) chondroitin sulfate across hydrogel formulations. *, significantly different from 0:100 gels; ζ, significantly different from 1:99 gels. Representative images of staining for collagen type I and chondroitin sulfate are shown below the respective graphs. Scale bars apply to each image in the series and equal 50 µm.

Calcium and alkaline phosphatase analyses. Hydrogels (n 5 2 per formulation) were transferred to 2 mL screw-cap microfuge tubes containing 1 mL of lysis buffer from the EnzoLyte FDP Alkaline Phosphatase assay kit and 1 mL of 3.2 mm stainless steel beads. Each sample was homogenized at 4800 rpm in a Bead-Beater homogenizer (Biospec) in 10 s cycles with 1 min intermediate cooling on ice. Two hundred microliter aliquots of each sample homogenate were analyzed for alkaline phosphatase activity

using EnzoLyte kit reagents. Total calcium was assessed from 5 μL aliquots of each sample homogenate using the Calcium CPC liquid color kit (Stanbio).

Day 28 histological analyses. To gain further understanding of the effects of hydrogel composition on the behavior of encapsulated cells, staining was conducted for ECM components associated with mature bone (collagen type I, osteocalcin, and CaP). Similarly, immunostaining for fibrocartilage-associated ECM components (collagen type I, collagen type II, and CSPG) and for chondrogenic transcription factor sox9 was carried out. Samples harvested for histological analyses were fixed with 10% formalin for 30 min, embeddedin freezing media (Tissue-Tek), and cut into 35 μm sections.

Immunostaining. Immunostaining was conducted according to standard protocols. In brief, sections were blocked with peroxidase (Biocare Medical) for 30 min followed by Terminator (Bio-care Medical) for 10 min. Primary antibody for osteocalcin [FL-95, Santa Crux Biotechnology (SCBT)], collagen type I (Rockland Immunochemicals), collagen type II (Rockland), CSPG (cs-56, SCBT), or sox9 (H-90, SCBT) was then applied for 1 h following dilution in HBS. For the sox9 antibody, sections were permeabilized before antibody application with PBS containing 0.05% Triton-100X. For each antibody and hydrogel sample, 2–3 sections were stained. Bound primary antibody was detected by using AP-/HRP-conjugated secondary antibodies (Jackson Immunochemicals) followed by application of chromogen (LabVision).

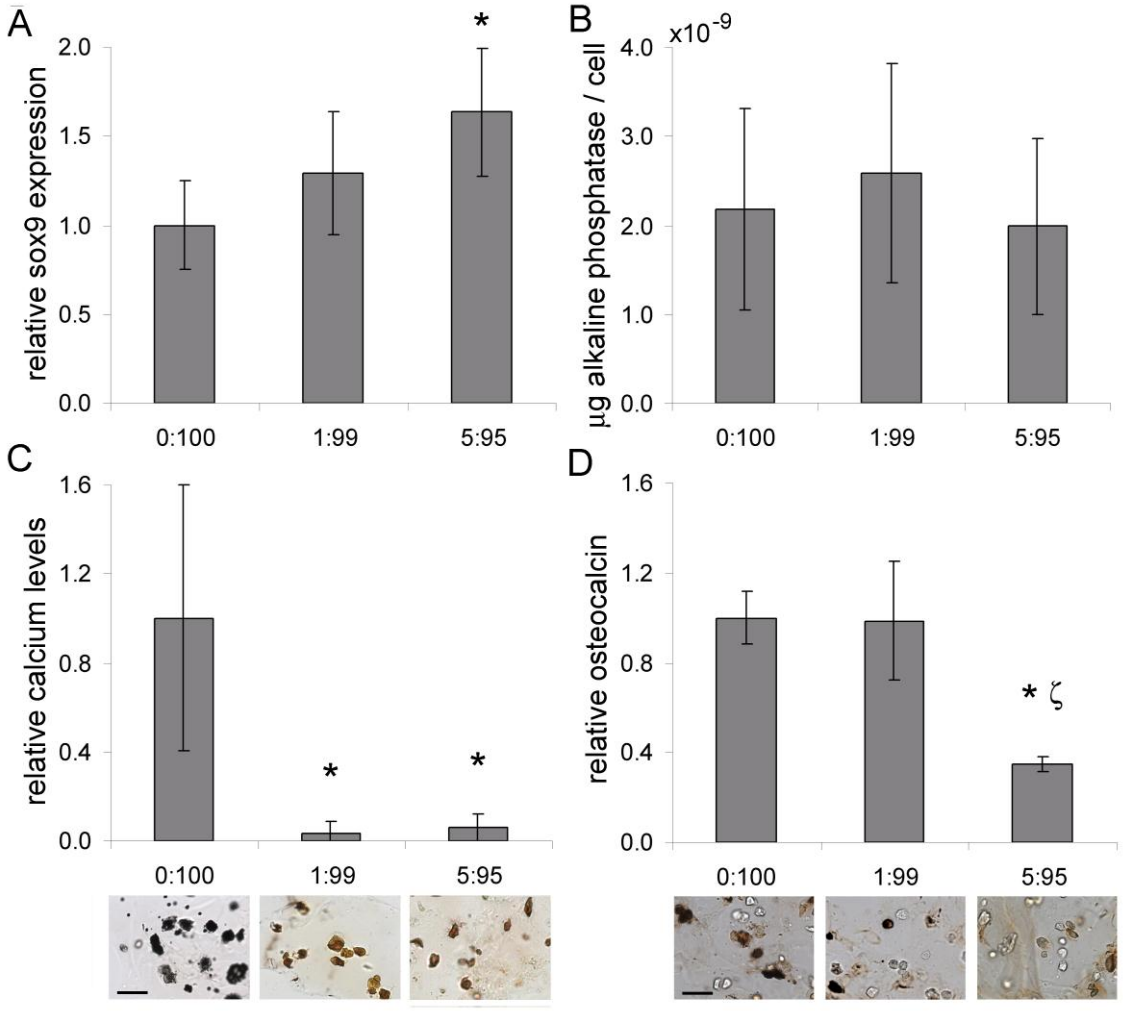

Figure 6.2 Relative expression of (**A**) sox9, (**B**) alkaline phosphatase, (**C**) calcium, and (**D**) osteocalcin levels across hydrogel formulations. *, significantly different from 0:100 gels; ζ, significantly different from 1:99 gels. Representative images of staining for collagen type I and chondroitin sulfate are shown below the respective graphs. Scale bars apply to each image in the series and equal 50 μm.

Van Kossa staining. To detect calcium deposits, sections were stained using a standard van Kossa staining kit (American MasterTech Scientific). In brief, rehydrated sections were rinsed with dIH_2O, after which a 5% silver nitrate solution was applied. Sections were then exposed to full spectrum light in a humidified chamber for 45 min. After rinsing with dIH_2O, sections were exposed to a 5% sodium thiosulfate for 2.5 min, briefly rinsed, and mounted.

Semiquantitative histological assessments. For intracellular transcription factor sox9, cell counts were conducted to semiquantitatively evaluate immunostaining results. In addition, as deposited ECM remained localized around the parent cells in each hydrogel formulation (Figures 6.1 and 6.2), the relative ECM protein production among hydrogel formulations could also be evaluated bycell counts. For each stained section (containing 250 cells), these semiquantitative analyses were conducted perestablished protocol [83, 95, 103, 104]. In brief, staining intensity, d_i, was recorded for each cell, i, on a scale of 0–3, with 0 = ‘‘no staining’’ and 3 = ‘‘highest staining intensity among all sections for that antibody’’. The cumulative staining intensity, d, for a given antibody in a particular section was calculated as: $d = (\Sigma d_i)/(\text{total cell number})$. The d values for all sections of a given hydrogel formulation were averaged to yield an overall sample average for each antibody. Immunostained samples were imaged using an Axiovert 200 microscope (Zeiss).

Table 6.1 Initial material properties of $PDMS_{star}$-PEG Hybrid Hydrogels.

$PDMS_{star}$ to PEG Weight Ratio	Relative Mesh Size (ξ) [a,b]	Modulus (kPa) [b]	Mass Percent Si [c]	
			measured	predicted
0:100	1.0 ± 0.1	167 ± 8	0.0	0.0
1:99	1.1 ± 0.1	142 ± 4[d]	0.6	0.4
5:95	1.3 ± 0.1[d]	142 ± 11[d]	2.3	2.0

[a]To give insight into the absolute mesh sizes represented by these relative mesh size values, the mesh size of the 0:100 $PDMS_{star}$-PEG hydrogel was determined to be ~14 nm per Canal and Peppas [170].
[b]Hydrogels contained 1 mM ACRL-PEG-RGDS postswelling.
[c]The mass percent of Si is given relative to the total mass of Si, C, and O.
[d]Significantly different from 0:100 gels, $P < 0.05$.

6.3.5 Statistical analyses

Data are reported as mean ± standard deviation. Comparison of sample means was performed by ANOVA and Tukey’s post hoc test (SPSS software), $p < 0.05$.

6.4 Results

In the present work, rat calvarial osteoblasts were encapsulated in a series of hybrid hydrogels of increasing inorganic PDMSstar content. Cell ECM production and phenotype were evaluated in all formulations after 28 days of culture.

6.4.1 Hydrogel material properties

Hydrogels with a 0:100, 1:99, or 5:95 wt ratio of $PDMS_{star}$ to PEG were prepared and their initial composition, mesh size, and mechanical properties characterized. Results from these characterization studies are summarized in Table 6.1. For each gel formulation, the mass percent of Si determined by XPS was consistent with the value predicted from the known M_w of both polymers and the wt ratio of $PDMS_{star}$-to-PEG in the precursor solution. These data support the successful incorporation of PDMSstar into the hydrogel networks.

The equilibrium diffusion of dextran was used to evaluate the mesh size of the 1:99 and 5:95 gels relative to the 0:100 gels (i.e., relative to pure PEG hydrogels). Gel mesh size increased directionally with increasing $PDMS_{star}$ content (Table 6.1). In contrast the compressive moduli of the 1:99 ($p = 0.018$) and 5:95 ($p = 0.015$) hydrogels were significantly lower than that of the 0:100 gel (Table 6.1). Cell presence did not significantly impact observed initial bulk modulus assessments (data not shown), as expected given the relatively low initial cell density employed (~3 $x10^6$ cells/mL) [36]. Furthermore, the swelling ratios, R, for the 0:100, 1:99, and 5:95 gels were 8.75 ± 0.03, 8.93 ± 0.06, and 9.73 ± 0.06, respectively. Each of these material property trends was consistent with a reduced hydrogel crosslink density with increasing $PDMS_{star}$ content [32].

As scaffold hydrophilicity [41] and protein adsorption [10, 27] have been demonstrated to significantly impact osteoblast behavior, the surface hydrophilicity of and fibronectin adsorption on each hydrogel was investigated. In agreement with the literature, [26, 42] contact angle measures indicated that $PDMS_{star}$-PEG hybrid scaffolds maintained the hydrophilic character of pure PEG gels (Table 6.2). Similarly, the

equilibrium (12 h) levels of fibronectin adsorption on the PDMSstar-containing gels were statistically indistinguishable from those on pure, ‘‘non-biofouling’’ PEG hydrogels (i.e., the 0:100PDMS$_{star}$-PEG gels, Table 6.2) [43]. Furthermore, the swelling ratios, R, for the 0:100, 1:99, and 5:95 gels were 8.75 ± 0.03, 8.93 ± 0.06, and 9.73 ± 0.06, respectively. Each of these material property trends was consistent with a reduced hydrogel crosslink density with increasing PDMS$_{star}$ content [32].

6.4.2 Cell ECM production and phenotype

Net cell density and ECM synthesis were evaluated in each hydrogel formulation to probe the influence of PDMS$_{star}$ levels on osteoblast behavior. Based on DNA measures, the cell densities in the 0:100, 1:99, and 5:95 hydrogels at day 28 were 1.93 ± 0.11, 1.93 ± 0.25, and 2.15 ± 0.19 million cells per gram, respectively. These data indicate that the net cell proliferation and loss over the time course of the study was similar across hydrogels and consistent with previous tissue engineering studies using ‘‘nondegradable’’ PEG-DA gels [44]. In contrast, osteoblast total collagen production showed marked variations with hydrogel composition. Specifically, the total collagen levels in the 0:100 ($p = 0.049$) and 5:95 ($p = 0.006$) gels were ~2 times greater than in the 1:99 hydrogels (Figure 6.1(A)).

Table 6.2 PDMS$_{star}$-PEG hydrogel surface hydrophilicity and protein adsorption.

PDMS$_{star}$ to PEG Weight Ratio	Contact Angle (°)		Fibronectin Adsorption (ng/cm^2)	
	1 min	2 min	1 h	12 h
0:100	38.8 ± 3.9	35.3 ± 4.9	48.9 ± 1.1	13.3 ± 2.3
1:99	34.2 ± 3.4	32.0 ± 2.9	36.6 ± 3.0	14.5 ± 3.1
5:95	37.0 ± 9.1	34.6 ± 8.5	33.0 ± 14.7	14.5 ± 3.1

To gain further insight into the observed total collagen results, immunostaining was conducted for collagen type I (associated with mature bone and, to a lesser extent, with fibrocartilage) and for collagen type II (associated with fibrocartilage) [7]. These histological analyses revealed a modulation of collagen types I and II with gel formulation. Collagen type II production was significantly higher in the 5:95 hydrogels

relative to the 0:100 ($p = 0.032$) and 1:99 ($p = 0.019$) gels (Figure 6.1(B)). In contrast, collagen type I expression appeared to decrease directionally with increasing hydrogel inorganic content, although this trend was not statistically significant (Figure 6.1(C)).

CSPG and sox9 (associated with fibrocartilage) as well as alkaline phosphatase, calcium deposits, and osteocalcin (mid-to-late term markers of bone tissue formation) were also assessed. CSPG levels were significantly higher in the 5:95 gels relative to the 0:100 hydrogels ($p=0.037$, Figure 6.1(D)). In addition, sox9 expression increased with an increase in hydrogel inorganic content from 0:100 to 5:95 ($p = 0.011$, Figure 6.2(A)). Although no significant differences in alkaline phosphatase expression were noted among formulations (Figure 6.2(B)), van Kossa staining results revealed the levels of deposited calcium to be markedly higher in the 0:100 $PDMS_{star}$-PEG gels than in the 1:99 ($p < 0.001$) and 5:95 ($p < 0.001$) gels (Figure 6.2(C)). This decrease in calcium deposition with increasing hydrogel inorganic content was further reflected in the results from the CPC assay, which yielded 0.54 ± 0.13, 0.20 ± 0.14, and 0.18 ± 0.05 ng calcium per cell for the 0:100, 1:99, and 5:95 gels, respectively. Similarly, osteocalcin levels were reduced in the 5:95 gels relative to both the 0:100 ($p = 0.008$) and 1:99 ($p = 0.027$) hydrogels (Figure 6.2(D)).

6.5 Discussion

This study was designed to test the hypothesis that a gradient in the siloxane content of a hybrid inorganic–organic scaffold would induce a transition in cell behavior from osteoblast-like to chondrocytelike. Both the matrix deposition and phenotype of encapsulated osteoblasts were indeed modulated by varying scaffold inorganic content. In terms of cell ECM production, increasing hydrogel $PDMS_{star}$ content was associated with increased production of collagen type II and CSPG. This increase in the synthesis of fibrocartilage-like ECM components was accompanied by a decrease in cell production of bone-like ECM. Specifically, both osteocalcin and calcium deposition decreased with increasing inorganic content. To further evaluate the modulation of cell phenotype with scaffold composition, the relative expression of sox9, a transcription

factor associated with chondrocytic differentiation, was examined. Consistent with the trends in fibrocartilage-like matrix production, sox9 levels increased with increasing $PDMS_{star}$ levels. Combined, the present results suggest that encapsulated osteoblasts were transdifferentiating into chondrocyte-like cells in the higher inorganic content hydrogels.

These trends in osteoblast response are contrary to those expected based on the literature, which collectively supports the idea of heightened osteoinductivity with increasing scaffold silica/siloxane content [14, 15, 45, 46]. It is possible that the observed discrepancies with previous literature arise from the absence of calcium or phosphate in the initial $PDMS_{star}$-PEG hydrogels. For instance, Song et al. [16] observed a significant increase in the alkaline phosphatase levels produced by MC3T3-E1 cells cultured on gelatin-siloxane scaffolds relative to pure gelatin controls only when the gelatin-siloxane hybrids were prepared in the presence of $CaCl_2$. However, Ning et al. [14] observed increased osteoblast alkaline phosphatase activity with an increase in the silica levels of silica-CaP composite scaffolds despite an associated decrease in scaffold CaP content. Similarly, the highest silica (lowest CaP) content scaffold examined by Gupta et al. [15] stimulated greater cell collagen type I and osteocalcin expression than hydroxyapatite ($Ca_{10}(PO_4)_6(OH)_2$). Thus, the impact of the absence of CaP in the initial $PDMS_{star}$-PEG gels is unclear.

Another potential source of the observed discrepancies between the current results and previous literature is differences in the levels, identities, and orientations of scaffold absorbed proteins. It is now well established that cell responses to a particular scaffold depend not only on the initial scaffold composition but also on the scaffold pretreatment, hydrophilicity, and resultant protein adsorption [10, 12, 41, 47]. Both the contact angle and fibronectin adsorption profiles for the $PDMS_{star}$-PEG scaffolds suggest that these hybrid scaffolds maintain the ‘‘biological blank slate’’ character of pure PEG gels, in agreement with the literature [26, 42, 43]. The term ‘‘biological blank slate’’ refers that the fact that the adsorption of cell adhesive proteins on pure PEG gels is sufficiently low that cells cannot significantly attach and spread onto these hydrogels

without the specific addition of cell adhesion ligands [43]. This is in contrast to most silica-containing scaffolds, pure PDMS substrates, and native polymer scaffolds (e.g., gelatin) which generally adsorb significant levels bioactive proteins from serum [12, 42, 48]. Thus, although the adhesion ligand RGDS was incorporated into the present $PDMS_{star}$-PEG formulations, the adsorption of serum proteins conducive to bone formation was likely limited.

A limitation of this study is that the observed modulation of osteoblast responses cannot be defini-tively attributed to the inorganic composition of the scaffolds alone. Specifically, alterations in the inorganic content of the $PDMS_{star}$-PEG gels resulted in concomitant alterations in scaffold modulus and mesh size, both of which can influence cell behavior [34, 36, 49]. Indeed, just as calcium deposition is negatively correlated with gel $PDMS_{star}$ levels, it is also negatively correlated with mesh size and positively correlated with modulus. Similarly, collagen type II and CSPG are positively correlated with hydrogel $PDMS_{star}$ content and scaffold mesh size, and negatively correlated with modulus. Thus, it is possible that scaffold modulus and/or mesh size could be the primary compositional variables underlying observed cell behaviors. This limitation results from the M_w of the $PDMS_{star}$ (~14 kDa) employed in this study relative to that of PEG (~3.4 kDa). That being said, the present results indicate that gradient $PDMS_{star}$-PEG hydrogels may be promising for osteochondral tissue engineering. Future studies will probe the impact of a broader range of siloxane levels on osteoblast responses while employing a $PDMS_{star}$ M_w that minimally alters base hydrogel mesh size and modulus.

CHAPTER VII
INFLUENCE OF INORGANIC-ORGANIC HYBRID HYDROGELS ON MULTIPOTENT STEM CELL DIFFERENTIATION

7.1 Overview

The cellular microenvironment appears to modulate stem cell lineage specification. In particular, matrix stiffness and the identity and concentration of biochemical stimuli have been demonstrated to influence stem cell differentiation. The aim of the present study was to evaluate the influence of two additional matrix parameters, hydrophobicity and inorganic content, on the lineage progression and extracellular matrix (ECM) production of 10T½ mouse mesenchymal stem cells. To execute these studies, novel hybrid hydrogels formed from the photocure of hydrophilic poly(ethyleneglycol) diacrylate (PEG-DA) and methacrylated star polydimethylsiloxane ($PDMS_{star}$-MA) were developed so as to extend the material property range attainable by single component PEG hydrogels. Naive 10T½ cells were shown to commit to phenotypes with fine sensitivity to tissue-level hydrophobicity. Increasing scaffold hydrophobicity was associated with an increased percent of osteoblast-like cells. In contrast, levels of adipocyte-like myocoyte-like and chondrocyte-like seem to be unaffected across the selected formulations. This modulation of cell lineage specification toward osteoblast differentiation was reflected on the observed ECM deposition of collagen type I as well as the differentiation marker osteocalcin.

7.2 Introduction

Mesenchymal stem cells (MSCs) are naturally found in tissue and are considered to play an important role in cell renewal and tissue regeneration. MSCs are multipotent cells, capable of differentiating into different cell types including adipocytes, chondrocytes, myocytes and osteoblasts. Even though the plasticity potential of MSCs has motivated its study for tissue engineering applications, the achievement of the

optimal control and guidance of this exceptional ability constitutes a major challenge. Several works in this research area have provided insight about the effect of soluble factors in cell fate; however, the influence of scaffold biochemical stimuli on MSC differentiation still remains unclear, which in turn brings about the necessity to enhance the understanding of the chemical functionality of the material scaffold and its impact on stem cell behavior, initial protein adsorption and ultimately, cell differentiation.

For example, some studies have already started elucidating the influence of the chemical character of tethered functional groups. For instance, 2D studies have revealed that the introduction of hydrophobic groups guides adipogenic differentiation, and that inorganic content through silicon or phosphate groups promotes stem cell differentiation into osteoblast-like cells [103, 177].

The main goal of this manuscript is to explore the effects of inorganic content of 3D environments on stem cell response. In order to achieve this, we have chosen to use a novel organic-inorganic hydrogel system, which was previously described by Hou et al. [178]. This hydrogel scaffold is based on the crosslink between hydrophilic poly(ethylene glycol) diacrylated (PEG-DA) and hydrophobic inorganic star poly(dimethyl siloxane) metacrylated ($PDMS_{star}MA$).

PEG-DA was selected because of its photoactivity, low cytotoxicity, high controllability and wide conjugation potential to several substrates through vinyl bone conjugation. On the other hand, PDMS was chosen given the fact that it is highly biocompatible and widely used in biomedical applications.

The aims of the present study were: (1) to characterize the material properties of a set of $PDMS_{star}$-PEG hydrogel formulations which allow the study of the effect of inorganic content on cell behavior as well as the modulation of the hydrophilicity/hydrophobicity interactions, and (2) to examine the impact of these material property variations on the lineage specification of 10T½ mouse mesenchymal stem cells. 10T½ cells have been demonstrated to differentiate into a variety of cell types, including myocytes, smooth muscle cells (SMC), adipocytes, osteoblasts and chondrocytes. In analyzing 10T½ cell lineage commitment, immunostaining for various

mid-to-late term differentiation markers was conducted. Specifically, smooth muscle alpha actin (SM22α), adipocyte fatty acid binding protein (A-FABP), collagen type II, and osteocalcin were examined as indicators of 10T½ progression down SMC, adipocyte, chondrocyte, or osteoblast lineages, respectively.

7.3 Material and methods

7.3.1 Preparation of diacrylate-terminated PEG (PEG-DA)

Photo-sensitive acrylate groups were introduced to the terminal ends of linear PEG in accordance to known methods [75]. Briefly, in a 250 mL round bottom (rb) flask equipped with a Teflon-covered stir bar, PEG (Sigma M_n = 3.4 kDa) was dissolved in dry DCM (20 mL/mmol PEG) and purged with Ar. Triethylamine (Sigma, 2:1 molar ratio) was added slowly to the solution, followed by the dropwise addition of acryloyl chloride (Sigma, 4:1 molar ratio) via a syringe. The reaction mixture was allowed to stir at room temperature (RT) overnight. Removal of HCl was accomplished by washing the mixture 2X with 2M K_2CO_3 and separating into aqueous and organic phases. The organic (DCM) phase was then dried with anhydrous $MgSO_4$ and the volatiles removed under reduced pressure. The resulting crude oil was precipitated in diethyl ether in an ice bath, filtered and dried under vacuum at RT overnight. Extent of acrylation was confirmed by ^{1}H NMR.

7.3.2 Synthesis of methacrylate-terminated $PDMS_{star}$ ($PDMS_{star}$-MA)

$PDMS_{star}$-MA (M_n = 2 kDa) was prepared via a two-step synthetic strategy per a modification of the methodology validated in Grunlan et al. [173]. In brief, silane (SiH)-terminated star PDMS ($PDMS_{star}$-SiH) was prepared by the acid-catalyzed equilibration of D_4 (octamethylcyclotetrasiloxane) with tetrakis(dimethylsiloxane)silane (tetra-SiH) [173]. Briefly, D_4 and tetra-SiH were combined in a 100 mL rb flask equipped with a Teflon-covered stir bar under N_2 at a 4:1 molar ratio, with the ratio of D_4 and tetra-SiH selected to yield a product of the desired M_n.. Triflic acid (0.060 μL/mmol D_4) was then added and the reaction was allowed to stir for 1 h at 90 ºC. After cooling, the mixture

was neutralized by combining with $MgCO_3$ and DCM (0.020 mL/mmol D_4) and stirring for 2 h. After filtration through a pad of Celite, the volatiles were removed under reduced pressure. The chemical structure and M_n of the resulting colorless product ($PDMS_{star}$-SiH) were confirmed by ^1H NMR, ^{13}C NMR, IR, and gel permeation chromatography (GPC).

The SiH terminal groups of the $PDMS_{star}$-SiH were converted into photo-sensitive methacrylate moieties by the subsequent hydrosilylation reaction with allyl methacrylate [174]. Briefly, $PDMS_{star}$-SiH was dissolved in dry toluene using a 100 mL rb flask equipped with a Teflon-covered stir bar and purged with N_2. Karstedt's catalyst (Pt-divinyltetramethyldisiloxane complex in xylene, 2% Pt) was added at 33 μL/mmol, and the reaction mixture was heated to 45 ºC. Allyl methacrylate was then added via an addition funnel over 15 min in a 4:1 molar ratio, after which the reaction was heated to 90 ºC and stirred overnight. Completion of the reaction was confirmed by the disappearance of the Si-H (~2100 cm^{-1}) absorbance in the IR spectrum. The reaction mixture was decolorized by refluxing with activated carbon for 12 h. After filtration, the volatiles were removed under reduced pressure. The resulting product ($PDMS_{star}$-MA) was confirmed by ^1H-NMR.

7.3.3 Synthesis of acrylate-derivatized cell adhesion ligand

Cell adhesion peptide RGDS (American Peptide) was reacted with acryloyl-PEG-N-hydroxysuccinimide (ACRL-PEG-NHS, 3.4 kDa, Nektar) at a 1:1 molar ratio for 2 h in 50 mM sodium bicarbonate buffer, pH 8.5 [63, 94]. The product (ACRL-PEG-RGDS) was purified by dialysis, lyophilized, and stored at -20 ºC until use.

7.3.4 Cell culture

Cyropreserved 10T½ mouse mesenchymal stem cells (ATCC) were thawed and expanded in monolayer culture. Prior to encapsulation, cells were maintained at 37 ºC 5% CO2 in Dulbecco`s Modified Eagle's Media (DMEM, Hyclone) supplemented with 10% heat-inactivated fetal bovine serum (FBS, Hyclone).

7.3.5 Hydrogel preparation

PEG-PDMS$_{star}$ hydrogels were prepared by the photopolymerization of aqueous mixtures of PEG-DA and PDMS$_{star}$-MA. A series of precursor solutions were prepared, each with 10 weight % (wt%) total polymer but with varying weight ratios of PEG-DA to PDMS$_{star}$-MA. Three weight ratios were investigated: 100:0, 95:5, and 80:20. ACRL-PEG-RGDS was added to each solution so as to yield 1 mM RGDS in the swollen gels. Photoinitiator consisting of a 30 wt% solution of 2,2-dimethyl-2-phenyl-acetophenone in N-vinylpyrrolidone was added at 10 μL/mL of precursor solution. The resulting mixtures were passed through 0.22 μm PET filters, which served both to sterilize the solutions as well as to create a fine dispersion of hydrophobic PDMS in the aqueous PEG solutions. Thee dispersions, although used immediately in the present studies, were stable (displayed no visible phase separation) for at least several hours. The filtered precursor solutions were vortexed, immediately poured into 0.75 mm thick transparent rectangular molds, and polymerized by 6 min exposure to longwave UV light (Spectroline, ~6 mW/cm^2, 365 nm). The time between vortexing and the onset of polymerization was held constant at ~ 1 min to ensure consistency in sample preparation.

7.3.6 Initial construct evaluation

Hydrogel mechanical properties. Following 24 h immersion in PBS, four 8-mm discs were cored from each hydrogel formulation for mechanical tested under unconstrained compression at RT using an Instron 3342. Following application of a 0.05 N preload, each hydrogel was subjected to 10 μm cyclic compression (~1% cyclic strain) at 1 Hz. The compressive modulus of each hydrogel was extracted from the resulting stress-strain data over a 10-20% strain range.

Hydrogel mesh size. PEG-based hydrogel mesh structure cannot be readily visualized using techniques such as conventional scanning electronmicroscopy (SEM). Thus, a variety of methods to estimate PEG-DA hydrogel mesh size have been developed, including correlations linking measurable quantities, such as equilibrium

hydrogel swelling and PEG-DA M_n, to mesh size [66, 68]. Although these correlations yield reasonable average mesh size estimates for homopolymer hydrogels, [66, 68] they cannot readily be applied to PEG-$PDMS_{star}$ hybrid hydrogels. Thus, in this study, average hydrogel mesh size was characterized via dextran diffusion based on an adaptation of the methodology of Watkins et al. [69]. Briefly, four 8 mm discs were cored from each hydrogel formulation following 24 h swelling and immersed in 0.5 mL HBS-azide (HEPES-buffered saline plus 0.05 wt% azide) containing 50 μg/mL FITC-labeled dextran (10 kDa, Sigma). Dextran was then allowed to diffuse into the hydrogels for 24 h at 37 ºC, after which each disc was gently blotted and transferred to 0.5 mL fresh HBS-azide. After 24 h at 37 ºC, the fluorescence of the HBS-azide solution surrounding each disc was measured at ex/em 488/532. Each fluorescence measure was converted to micrograms dextran using dextran standard curves and then divided by gel weight to yield a quantitative indicator of hydrogel permissivity (C). These permissivity measures were used to estimate the mesh size (ξ) of each hydrogel (x) relative to pure PEG-DA (A-control) as follows: $\xi_x = \left(\frac{C_x}{C_{A,control}} \right)$

Serum protein adsorption. Following 24 h of swelling, twelve 21 mm discs were harvested from hydrogels of each formulation to evaluate the dependence of hydrogel serum protein adsorption on increasing $PDMS_{star}$ content. Each disc samples was exposed to 10% FBS in PBS for 24 h at 37 °C. Non-adsorbed proteins were then removed by immersing he specimens in dIH_2O at 37 °C for 60 min, with dIH_2O changes every 20 min. Adsorbed proteins were then stripped from the hydrogels by progressive extraction with 10%, 30%, 50%, and 70% aqueous isopropanol solutions (I10, I30, I50, I70) at 37 °C. For each hydrogel sample, the resulting isopropanol fractions were combined, evaporated under vacuum, and resuspended in 500 μL of PBS. The total amount of protein in each fraction was quantified using the CBQCA total protein quantitation kit (Invitrogen). For the purpose of comparison, the resulting protein

measures for each hydrogel compositiom were normalized to that of the 100:0 PEG-$PDMS_{star}$ formulation.

Relative bulk hydrophilicity/hydrophobicity. Contact angle measurements are widely used to analyze differences in the hydrophilic/hydrophobic character of material surfaces. However, this method is limited to assessment of surface interactions, and associated results cannot generally be readily extended to bulk behavior. An alternative method that can be used to assess differences in the bulk hydrophilicity/hydrophobicity of PEG-$PDMS_{star}$ hydrogels involves the comparison of hydrogel swelling in solvents of varying polarity. Specifically, solvents of higher polarity interact preferentially with hydrophilic domains of the bulk material while solvents of lower polarity show more affinity for hydrophobic segments of the material. Thus, differences in the relative uptake of solvents of distinct polarities by a given hydrogel formulation can serve as an indicator of its bulk hydrophilicity/hydrophobicity.

The bulk hydrophilicity of each PEG-$PDMS_{star}$ hydrogel formulation was therefore evaluated by conducting swelling assays using two solvents with different polarity indices (P): deionized water (dIH_2O; P =12.1) and 70% isopropanol in dIH_2O (I70; P = 10.0) [179]. In brief, four discs from each hydrogel formulation were submerged in dIH_2O or I70 for 24 h at RT, after which the swollen weight (W_s) of each disc was recorded. The samples were then dried under vacuum for 48 h and their corresponding dry weights (W_d) measured. The equilibrium mass swelling ratio (q) of each formulation in each solvent (x) was calculated as $q_x = \left(\frac{W_s}{W_d}\right)$. The relative bulk hydrophilicity of each hydrogel formulation was estimated as follows: $H = \left(\frac{q_{water}}{q_{I70}}\right)$.

7.3.7 Fabrication and culture of cell-laden constructs

Mixtures containing 10 wt% total polymer at PEG-DA:$PDMS_{star}$-MA ratios of 100:0, 95:5, and 80:20 were prepared in HBS. Following addition of ACRL-PEG-RGDS

(to yield a bulk RGDS concentration of 1 mM in each swollen hydrogel) and photoinitiator, the mixtures were sterilized by filtration. 10T½ cells were harvested and resuspended in each precursor solution such that the post-swelling cell density would be ~$3x10^6$ cells/g. The resulting suspensions were polymerized into hydrogel networks by 6 min exposure to longwave UV light (~6 mW/cm^2), a process which has been demonstrated to be cytocompatible in a number of tissue engineering studies [62, 64, 65]. Gels were immersed in DMEM supplemented with 10% heat-inactivated FBS, 100 U/mL penicillin and 100 mg/L streptomycin and maintained at 37 ºC and 5% CO_2. Media was changed every two days.

7.3.8 Endpoint construct analyses

After 21 days of culture, a series of samples were collected from each hydrogel formulation for biochemical and histological analyses.

Biochemical analyses. Proteins were extracted from samples harvested for biochemical analyses either via homogenization in Trizol followed by protein isolation as detailed in Bulick et al.[180] or by base hydrolysis per Liao et al. [101] Isolated sample proteins were analyzed as detailed below.

Competitive ELISA for differentiation markers. Sample proteins isolated by homogenization were evaluated via competitive ELISA using antibodies for various mid-to-late term markers of osteogenesis (osteocalcin), chondrogenesis (collagen II), smooth muscle progression (SM22α), and adipogenesis (A-FABP) as well as housekeeping protein GAPDH. In brief, primary antibodies and their corresponding peptide antigens were purchased from Santa Cruz Biotechnology (SCBT). High binding EIA 96 well plates (Costar) were coated overnight at 4 °C with 2 ng per well of peptide for A-FABP (FABP4, C-15), SM22α (Transgelin, P-15), osteocalcin (M-15), or collagen II (Col2A1, N-19) and 1 ng per well of peptide for GAPDH (V-18). The coated wells were then blocked with bovine serum albumin (BSA). Peptide standards and aliquots of

isolated sample proteins were diluted in PBS containing 3% BSA and 0.05% Tween 20 and incubated with primary antibody for 1 h at RT prior to transfer to the coated wells. Well plates were then incubated for 1 h at RT with continuous gentle mixing. For both samples and standards, primary antibody which had bound to the coated well surface was detected using an appropriate HRP-conjugated secondary antibody (Jackson ImmunoResearch Laboratories, JIRL), followed by application of 2,2'-azino-bis(3-ethylbenzthiazoline-6-sulphonic acid) (ABTS, Sigma) and monitoring of absorbance at 410 nm. Each target protein was as analyzed in duplicate/triplicate for each sample (n = 3 – 4 per hydrogel formulation) and normalized to GAPDH. For the purposes of comparison, the resulting protein concentrations for each formulation were further normalized to the 100:0 $PDMS_{star}$-PEG hydrogels.

Indirect ELISA analyses. Proteins isolated by hydrolysis were also used for elastin and collagen III quantification (n = 3 per formulation per assay). collagen III samples and standards were applied to a high binding 96 well EIA plate for 3 h at RT, after which the plate was blocked with 3 wt% BSA. Following application of primary antibody for collagen III (Calbiochem, San Diego, CA) donkey anti-rabbit HRP secondary antibody (JIRL) and ABTS were applied. Absorbance was read at 410 nm, with human collagen III (Sigma) serving as a standard. To quantify elastin, the above produced was followed except that isolated sample proteins were first exposed to 0.25 M oxalic acid at 100 ºC overnight to convert elastin to α-elastin. Oxalic acid was then removed and exchanged for PBS using Microcon YM-3 centrifugal filters (Millipore). Resulting samples were then applied to a high binding EIA 96 well plate (Nunc) for 3 h at RT. Adsorbed elastin fragments were detected by applying elastin antibody (BA-4, SCBT), with bovine aortic elastin (Sigma) serving as a standard. Measured elasitn and collagen III levels were normalized to cell number as assessed by the PicoGreen assay (Invitrogen). For the purposes of comparison, the resulting protein concentrations for each formulation were further normalized to the 100:0 $PDMS_{star}$-PEG hydrogels.

Hydroxyproline and Blyscan assays. Sample proteins isolated by hydrolysis were evaluated using standard assays for sulfated glycosaminoglycans (sGAG) and total collagen. sGAG production was measured using a modification of the Blyscan assay (Biocolor). In brief, 40 μL of sample protein (n = 4 per formulation) was neutralized, mixed with 60 μL Blyscan dye reagent, and the absorbance at 525 nm immediately measured relative to chondroitin sulfate B (Sigma). Similarly, levels of hydroxyproline were quantified as an indirect measure of total collagen. Sample proteins (n = 4 per formulation) were first further hydrolyzed for 18 h at 110 ºC in 6 M HCl. The samples were then dried under vacuum followed by resuspension in dIH_2O and reaction with chloramine T and p-dimethylbenzaldehyde reagents [31]. Sample absorbance was read at 550 nm relative to that of L-4-hydroxyproline (Sigma). Total collagen content was estimated from measured grams of hydroxyproline by dividing by 0.13. For both the total collagen and sGAG assays, standards used were subjected to the same association with PEG-DA and $PDMS_{star}$-MA and the same digestion conditions as the samples. Measured total collagen and sGAG levels were normalized to cell number as assessed by the PicoGreen assay (Invitrogen). For the purposes of comparison, the resulting protein concentrations for each formulation were further normalized to the 100:0 $PDMS_{star}$-PEG hydrogels.

Histological analyses. Samples harvested for histological analyses were fixed with 10% formalin for 30 min, embedded in Tissue-Tek media, and cut into 35 μm sections. To gain insight into cell differentiation, immunohistochemical staining was conducted using the same A-FABP, SM22α, osteocalcin, and collagen II primary antibodies used for competitive ELISA analyses. After 10 min treatment with peroxidase (Biocare Medical), sections for were blocked with Terminator (Biocare Medical) for 30 min followed by exposure for 1 h to primary antibody diluted in HBS. Bound primary antibody (SCBT) was detected by using either AP- or HRP-conjugated secondary antibodies (JIRL) followed by application of an appropriate chromogen (LabVision).Immunostained sections were imaged under brightfield using an Axiovert microscope (Zeiss).

7.3.9 Statistical analyses

All data are reported as mean ± standard error of the mean. Comparison of sample means was performed by ANOVA and Tukey`s post-hoc test (SPSS software), $p < 0.05$.

7.4 Results

In the present work, mouse 10T½ cells were encapsulated in a series of PEG-$PDMS_{star}$ hydrogels. Cell phenotype was assessed in all formulations after 21 days of culture, a time point selected based on previous studies examining stem cell lineage progression in 3D materials [181].

7.4.1 Hydrogel material properties

In order to assess the initial microenvironment experienced by encapsulated cells, we characterized modulus, mesh size, hydrophilicity/hydrophobicity interactions as well as the protein adsorption profile of each selected hydrogel formulation. Analysis of mechanical properties and mesh size reveals that while the modulus of the 80:20 hydrogels was significantly lower than the 95:5 formulation ($p < 0.001$), its mesh size increased around 37%. In addition, there were no statistic differences between the moduli and mesh size of the 100:0 and 95:5 formulations (Figures 7.1A and 7.1B).

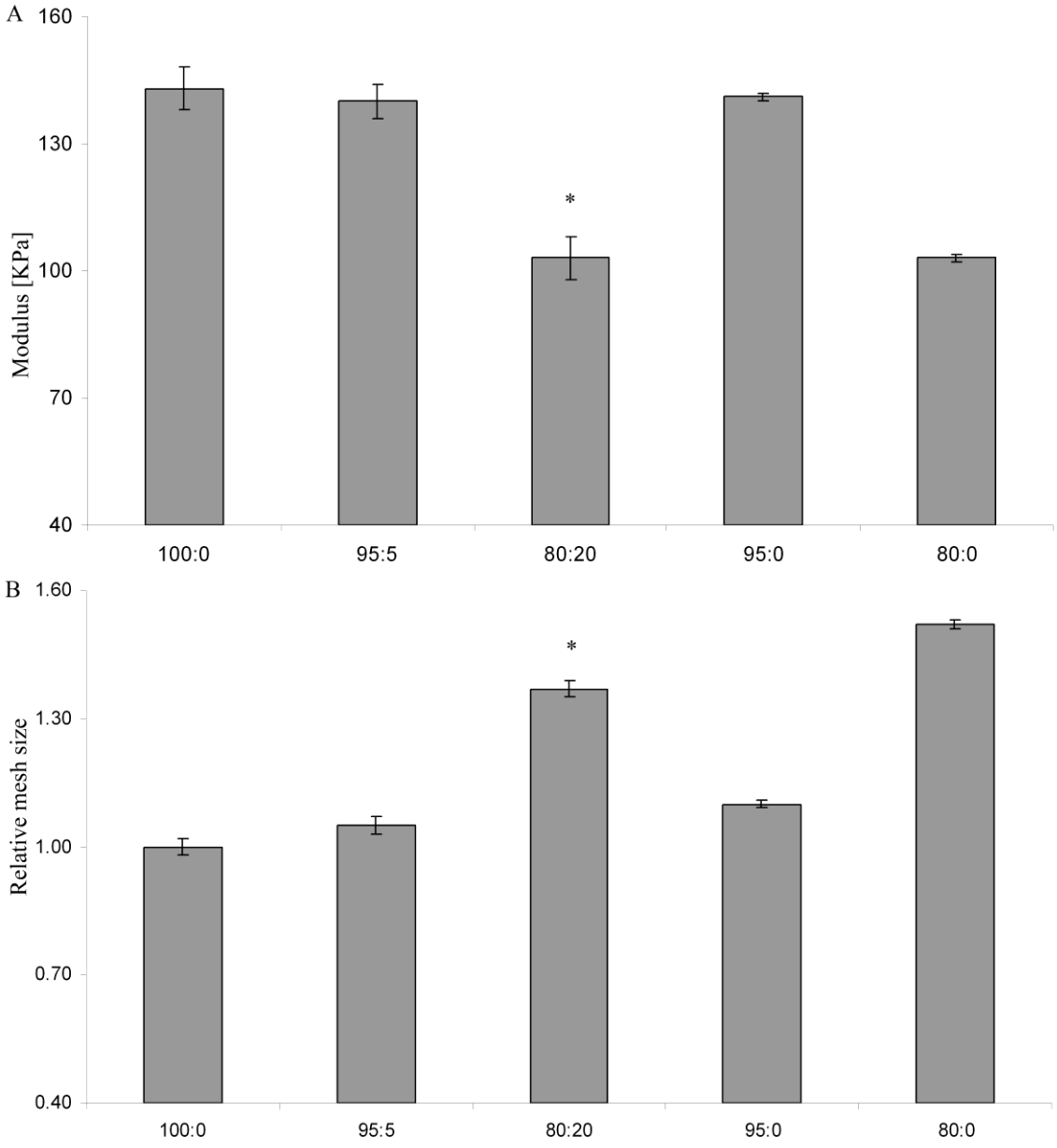

Figure 7.1 Elastic modulus and relative mesh size. (A) Modulus. (B) Relative mesh size.
* Significantly different from 0:100 gels, $P < 0.001$.

Increasing levels of $PDMS_{star}$-MA induced significant alterations in hydrophilic/hydrophobic interactions (Table 7.1), with a monotonic decrease from 100:0 to 80:20 hydrogels (100:0 vs 95:5, $p = 0.017$; 100:0 vs 80:20, $p = 0.001$; 95:5 vs 80:20, $p = 0.022$). Changes in $PDMS_{star}MA$ levels seem to primarily control changes in hydrophilicity/hydrophobicity interactions as well as the enhancement of the protein retention profiles when compared to similar formulations in the absence of $PDMS_{star}MA$. Furthermore, 5% $PDMS_{star}MA$ content showed a 2 fold increase while the 20% $PDMS_{star}MA$ formulation revealed an average 5 fold increase in the total retained protein relative to pure PEG-DA. Hydrogels lacking $PDMS_{star}MA$ content but with similar levels of PEG-DA showed an unchanged profile in hydrophilicity/hydrophobicity interactions. $PDMS_{star}MA$ content appears to modulate protein adsorption through changes in the hydrophilicity/hydrophobicity interaction by enhancing protein retention, while PEG-DA content primarily modulates modulus (Table 7.1); mesh size was impacted by both the reduction of PEG-DA content and the increase in $PDMS_{star}MA$ levels**.**

Table 7.1 Hydrophilicity/Hydrophobicity interaction and protein retention.

Formulation	Water uptake	I70 uptake	H q_{water}/q_{I70}	Relative adsorbed protein
100:0	8.0 ± 0.0	8.3 ± 0.1	0.96 ± 0.01	1.00 ± 0.18
95:5	7.6 ± 0.0	8.4 ± 0.1	0.91 ± 0.01[a]	1.97 ± 0.17
80:20	8.8 ± 0.1	10.2 ± 0.2	0.85 ± 0.02[a,b]	5.06 ± 0.27
95:0	8.4 ± 0.1	8.7 ± 0.1	0.96 ± 0.01	1.12 ± 0.25
80:0	10.0 ± 0.1	10.2 ± 0.1	0.97 ± 0.01	2.76 ± 0.68

7.4.2 Cell differentiation

Biochemical analysis of mid-to-late term cell differentiation into smooth muscle cells (SMC) (SM22α), osteoblasts (osteocalcin), adipocytes (A-FABP), and chondrocytes (collagen type II) indicated that encapsulated cells phenotype appeared to be modulated by hydrogel formulation. ELISA analysis exposed a modulation of osteocalcin production with $PDMS_{star}$-MA levels. Specifically, osteocalcin expression

seemed to increase from the 100:0 to the 80:20 hydrogels ($p = 0.013$ and $p = 0.02$, respectively, Figure 7.2). On the other hand, increasing $PDMS_{star}$-MA levels across formulations did not appear to have an effect on collagen type II, AFABP and SM22α production.

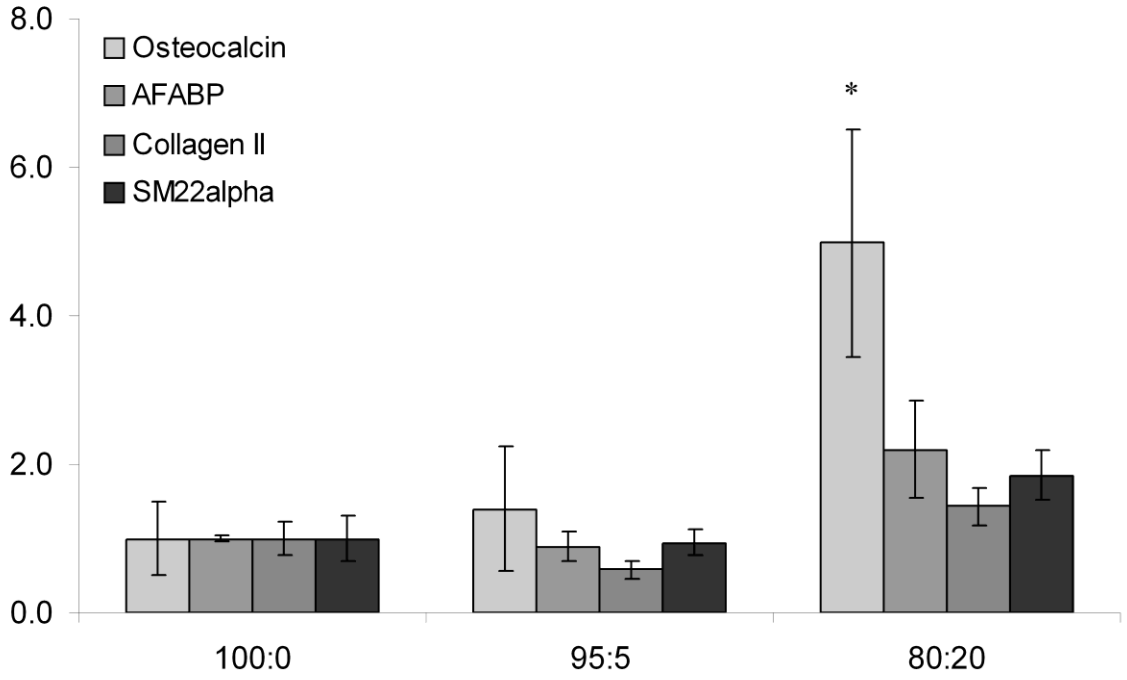

Figure 7.2 Relative expression of osteocalcin, AFABP, Collagen II and SM22alpha.

Additional biochemical analysis (Figure 7.3) by hydroxyproline analysis, collagen III ELISA, GAG quantitation and elastin levels, showed significant expression of total collagen production. Since collagen type II and III were maintained consistent across formulations, the increase in total collagen production can be attributed to an increase in collagen type I production (another osteoblast marker) given the fact that collagen production is mostly composed of collagen type I, II and III in connective tissues.

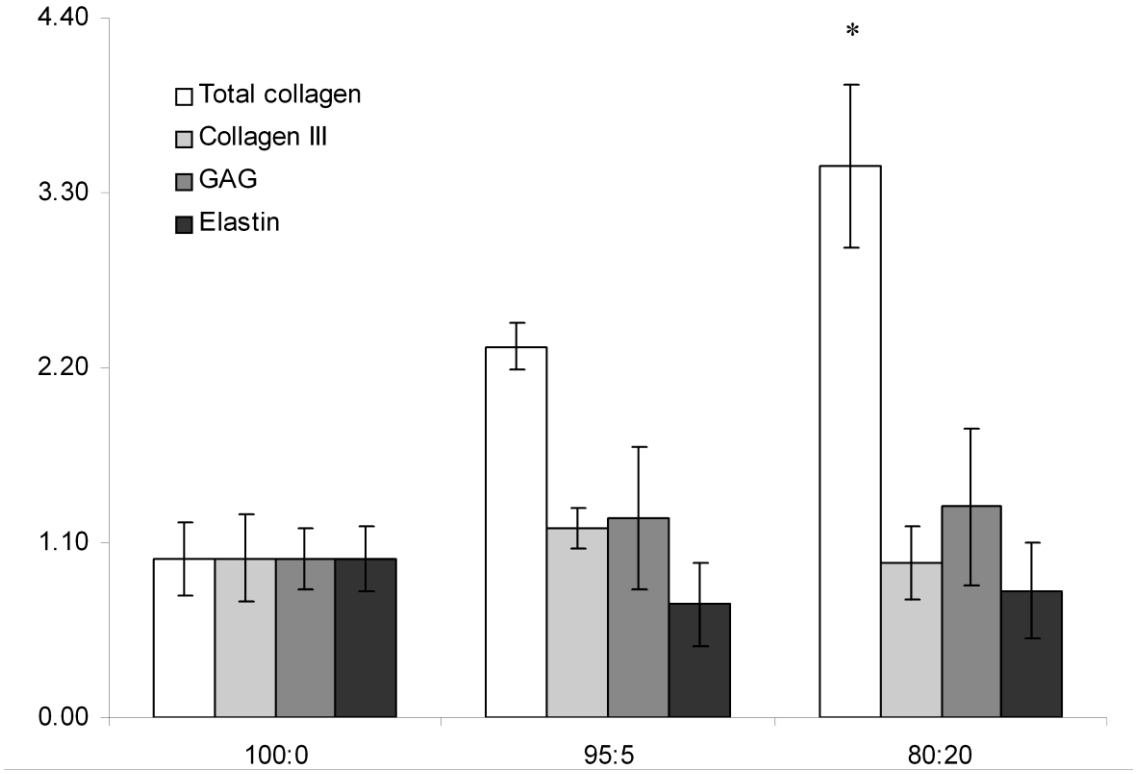

Figure 7.3 Total collagen, collagen III, GAG and elastin relative production.

In addition to the ELISA analysis, qualitative assessments by immunostaining were conducted for the selected differentiation markers. The results obtained supported the substantial differences in cell lineage progression with gel formulation. Specifically, osteocalcin levels were highest in the 80:20 hydrogels compared to the other formulations. In addition, collagen II and SM22α expression tended to be relatively consistent across formulations (Figure7.4).

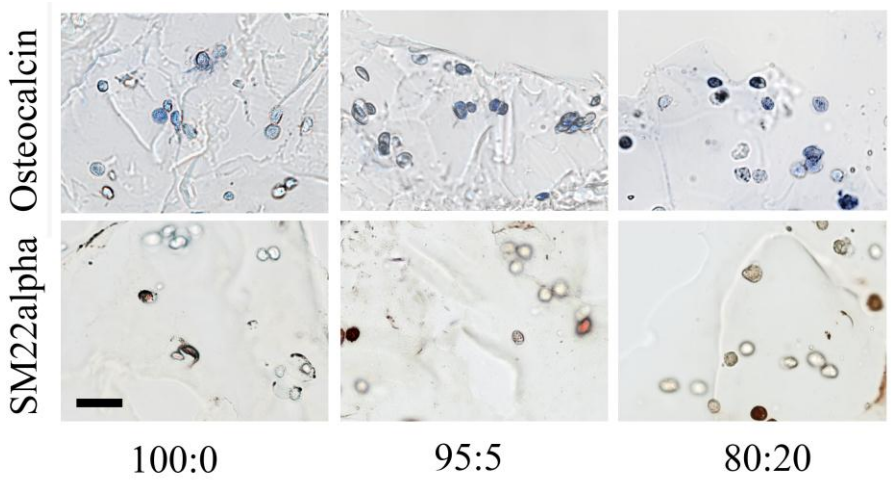

Figure 7.4 Representative inmunostaining for osteocalcin and SM22alpha.

7.5 Discussion

We have developed a novel hydrogel system formed by the photocrosslinking of hydrophilic PEG-DA and hydrophobic $PDMS_{star}$-MA in order to enable the study of the impact of scaffold inorganic content and hydrophilicity/hydrophobicity interactions on cell lineage progression. In the present study, hydrogel composition was formulated such that the levels of ACRL-PEG-RGDS in each formulation were 1 mM after full swelling was achieved. Thus, in examining the modulation of cell response by PEG-$PDMS_{star}$ hydrogel systems, we were able to consider bulk concentration and identify the biochemical stimulus initially presented to the cells as a design constant. Aqueous precursor solutions containing $PDMS_{star}$-MA were stable but slightly cloudy (hazy) compared to aqueous solutions containing pure PEG-DA, which indicated phase separation. Therefore, it is likely that PEG-$PDMS_{star}$ bead-like "islands" of less than 0.22 μm size (two order of magnitude of encapsulated cells) after filtration were formed. Previous studies reported by Hou, Y., et al. [178] revealed that unfiltered PEG-$PDMS_{star}$ hydrogels showed regions of crosslinked $PDMS_{star}$-MA surrounded by crosslinked PEG-DA resulting from the phase separation of hydrophilic PEG-DA and hydrophobic $PDMS_{star}$-MA prior to gelation. Since the incorporated cell adhesion ligand RGDS was conjugated to PEG (ACRL-PEG-RGDS), the phase separation between PEG-DA and

$PDMS_{star}$-MA implies that the RGDS was localized primarily in the PEG regions surrounding the PEG-$PDMS_{star}$ bead-like particles.

In contrast, increasing incorporation of $PDMS_{star}$-MA into PEG-DA based hydrogels induced significant variations in scaffold hydrophilic/hydrophobic interactions and total protein retention. Increased hydrophobicity levels were observed with increased $PDMS_{star}$-MA content by comparison of the swelling behavior of the hydrogels in the two different solvent systems. The ratio between the more polar (water) to the less polar (I70) solvent was decreased by the increase in $PDMS_{star}$-MA content, while this ratio in gels with same levels of PEG-DA but in the absence of $PDMS_{star}$-MA appeared to remain constant. The observed increase in hydrophobicity with increasing levels of $PDMS_{star}$-MA seemed to modulate protein retention.

It has been shown that adsorption of protein as well as protein configuration is affected by the hydrophilic/hydrophobic interactions of material scaffolds [182] having direct impact on cell behavior. Studies in 2D have demonstrated that high cell attachment and cell spreading are observed at intermedia levels of hydrophobicity due the appropriated amount of adsorbed protein as well as their configuration.

The modulation of scaffold hydrophilicity/hydrophobicity interaction and protein retention appeared to contribute significantly to the lineage progression of 10T½ progenitor cells. In hydrogels of relatively high hydrophobicity (80-20 gels), cells displayed a significant preference for an osteocyte phenotype relative to the remaining formulations. Cells expressing higher levels of osteocalcin in 80-20 formulations were exposed to higher level of siloxane levels, increase in hydrophobicity as well as high protein retention profile. Although modulus and mesh size also may be impacting cell fate, the decrease in modulus should be resulting in a decrease in osteoblast cell phenotype, since stiffer materials are considered more appropriate for osteogenic scaffold [92]. Therefore, we hypothesized that a synergy effect between increase and mesh size, siloxane content, modulation of hydrophobicity and retention protein from serum, overcome the effect in reduction in modulus. Furthermore, inorganic content (phosphate or silane) has been reported to contribute to osteogenesis of human

mesenchymal stem cells (hMSC). Particularly, in 2D studies by Curran at al [177], silane content was reported to promote and maintain osteogenesis in the presence or absence of biological stimuli. Interestedly, osteoblast differentiation also seems to show high dependence on the initial cell state; when mature rat osteoblast were cultured in a similar system, Munoz-Pinto et al. [183] reported that decreasing levels in siloxane content promoted a more osteoblast-like cell phenotype. In addition, Liao et al. [184] show in 2D systems that increased hydrophilicity on flat surface as well as patterned surfaces promoted and maintained osteoblast phenotype of rat calvarian osteoblasts.

On the other hand, adipogenic, chondrogenic and myogenic differentiation seem to be unaffected by changes in material properties at least in the range explored. Unexpectedly, the increasing levels of hydrophobicity of the scaffold did not lead adipogenic differentiation as it has been suggested by Benoit at al. [103]. This could be explained by the fact that increased levels of hydrophobicity were achieved by the increase in levels of inorganic siloxane content.

CHAPTER VIII
CONCLUSIONS

8.1 Summary

The accomplished work has shown that scaffold properties impact mature cell phenotype. Specifically, the results indicated that VFFs were induced into an undesirable myofibroblast-like phenotype. Increasing levels of SM-α-actin collagen production were coupled with decreasing initial mesh size/increasing initial modulus. Similarly, slight alterations in the biochemical stimuli presented to VFF cells (HA_{IMW} versus HA_{HMW}) impacted VFF behavior, which suggests that, among the examined formulations, the HA_{HMW} gels would be the most suitable system for VF regeneration. Particularly, the elastin and collagen composition of the HA_{HMW} gel most closely resembled normal superficial LP, which contains ~40% collagen type III and a relatively low elastin to collagen ratio. Furthermore, for prolonged culture times, the lower induction of a myofibroblastic phenotype observed in the HA_{HMW} gels relative to the HA_{IMW} gels is desirable for the inhibition of LP scar formation.

In addition, this work has validated a systematic approach for uncoupled evaluation of the impact of initial scaffold modulus and mesh size on SMC responses toward rational TEVG scaffold design. Collagen deposition and SMC phenotype were strongly correlated with initial hydrogel mesh size. Modulation of RhoA and metabolic activity may underlie these observed correlations, although further studies are required to establish causation. Even though the current study has focused on the influence of initial scaffold modulus and mesh size on SMC behavior, the described approach can be expanded to include the systematic interrogation of cell responses to scaffold degradation rate and bioactivity and can be employed in a variety of tissue engineering contexts.

Moreover, the effect of inorganic siloxane content was examined for bone and osteochondral tissue engineering applications. Rat calvarial osteoblasts were encapsulated in a series of organic PEG hydrogels of increasing inorganic $PDMS_{star}$

content. Osteoblasts appeared to transdifferentiate into chondrocyte-like cells with increasing scaffold inorganic content, as indicated by the increased chondroitin sulfate and collagen type II production and the upregulation of sox9. Furthermore, the deposition of bone-like matrix (collagen type I, calcium phosphate, and osteocalcin) decreased with increasing $PDMS_{star}$ content. In contrast, increasing levels of inorganic content seemed to have a different effect on undifferentiated cells, driving mesenchymal stem cells toward bone-like cells. Relative production of osteocalcin and total collagen in 10T ½ cells seemed to be upregulated by the increase in siloxane content while levels of collagen type II, AFABP, SM22α specific markers for chondrocytes, adipocyte and myocytes respectably appears be unperturbed across selected formulations.

8.2 Recommendations

PEG-DA hydrogels have been shown to be a useful tool in the study of the impact of scaffold properties on cell behavior. The explored range of mesh size and modulus of PEG-DA hydrogels could be expanded by the introduction of non-linear PEG conformations. Specifically, four-arm PEG tetraacrylated (PEG-TA) may be able to retain the biochemical inert character of liner PEG while offering a higher degree of control over mechanical properties and mesh structure. The present study also tested the relevance of two different HA M_w on VFF ECM production and cell phenotype. It has also shown the effect of inorganic content on rat osteoblast and mouse mesenchymal stem cell behavior.

These results evidenced the potential of PEG-DA hydrogels as platforms for the study of physical and biochemical stimuli on cell behavior, which opens the window for more comprehensive studies that could include the incorporation of human mesenchymal stem cells (hMSC), given their high potential for regenerative medicine.

REFERENCES

1. Yang, S., Leong, K.-F., Du, Z., and Chua, C.-K., The design of scaffolds for use in tissue engineering. Part I. Traditional factors. Tissue Engineering. **7**(6), 679-689, 2001.

2. Lanza, R., Langer, R., and Vacanti, J., ed. Principles of tissue engineering. Third ed. San Diego, California: Elsevier Academic Press, 1997.

3. Zhu, J., Bioactive modification of poly(ethylene glycol) hydrogels for tissue engineering. Biomaterials. **31**(17), 4639-4656, 2010.

4. Benoit, D.S., Schwartz, M.P., Durney, A.R., and Anseth, K.S., Small functional groups for controlled differentiation of hydrogel-encapsulated human mesenchymal stem cells. Nat Mater. **7**(10), 816-823, 2008.

5. Engler, A.J., Sweeney, H.L., Discher, D.E., and Schwarzbauer, J.E., Extracellular matrix elasticity directs stem cell differentiation. J Musculoskelet Neuronal Interact. **7**(4), 335, 2007.

6. Shastri, V.P., Non-degradable biocompatible polymers in medicine: Past, present and future. Current Pharmaceutical Biotechnology. **4**, 331-337, 2003.

7. Schmedlen, R.H., Elbjeirami, W.M., Gobin, A.S., and West, J.L., Tissue engineered small-diameter vascular grafts. Clinics in Plastic Surgery. **30**(4), 507-517, 2003.

8. Johnna, S.T., Kyriacos, A.A., Richard, G.L., and Antonios, G.M., Effect of poly(ethylene glycol) molecular weight on tensile and swelling properties of oligo(poly(ethylene glycol) fumarate) hydrogels for cartilage tissue engineering. Journal of Biomedical Materials Research. **59**(3), 429-437, 2002.

9. Kalakkunnath, S., Kalika, D.S., Lin, H., Raharjo, R.D., and Freeman, B.D., Molecular relaxation in cross-linked poly(ethylene glycol) and poly(propylene glycol) diacrylate networks by dielectric spectroscopy. Polymer. **48**(2), 579-589, 2007.

10. Benoit, D.S.W., Durney, A.R., and Anseth, K.S., The effect of heparin-functionalized peg hydrogels on three-dimensional human mesenchymal stem cell osteogenic differentiation. Biomaterials. **28**(1), 66-77, 2007.

11. Lipke, E.A. and West, J.L., Localized delivery of nitric oxide from hydrogels inhibits neointima formation in a rat carotid balloon injury model. Acta Biomaterialia. **1**(6), 597-606, 2005.

12. Bohl Masters, K.S., Lipke, E.A., Rice, E.E.H., Liel, M.S., Myler, H.A., Zygourakis, C., Tulis, D.A., et al., Nitric oxide-generating hydrogels inhibit neointima formation. Journal of Biomaterials Science, Polymer Edition. **16**, 659-672, 2005.

13. Benoit, D.S.W. and Anseth, K.S., Heparin functionalized peg gels that modulate protein adsorption for hmsc adhesion and differentiation. Acta Biomaterialia. **1**(4), 461-470, 2005.

14. Sawhney, A.S., Pathak, C.P., and Hubbell, J.A., Bioerodible hydrogels based on photopolymerized poly(ethylene glycol)-co-poly(alpha-hydroxy acid) diacrylate macromers. Macromolecules. **26**(4), 581-587, 1993.

15. Elbert, D.L. and Hubbell, J.A., Conjugate addition reactions combined with free-radical cross-linking for the design of materials for tissue engineering. Biomacromolecules. **2**(2), 430-441, 2001.

16. West, J.L. and Hubbell, J.A., Polymeric biomaterials with degradation sites for proteases involved in cell migration. Macromolecules. **32**(1), 241-244, 1998.

17. McGowan, K.B., Kurtis, M.S., Lottman, L.M., Watson, D., and Sah, R.L., Biochemical quantification of DNA in human articular and septal cartilage using Picogreen and Hoechst 33258. Osteoarthritis and Cartilage. **10**(7), 580-587, 2002.

18. Catten, M., Gray, S.D., Hammond, T.H., Zhou, R., and Hammond, E., Analysis of cellular location and concentration in vocal fold lamina propria. Otolaryngol Head Neck Surg. **118**(5), 663-667, 1998.

19. Culav, E.M., Clark, C.H., and Merrilees, M.J., Connective tissues: Matrix composition and its relevance to physical therapy. Physical Therapy. **79**(3), 308-319, 1999.

20. Myllyharju, J. and Kivirikko, K.I., Collagens, modifying enzymes and their mutations in humans, flies and worms. Trends in Genetics. **20**(1), 33-43, 2004.

21. Lodish, H.F., Molecular cell biology. 4th ed. New York: W.H. Freeman, 2000.

22. Tateya T, T.I., Bless DM, Immuno-scanning electron microscopy of collagen types I and III in human vocal fold lamina propria. Ann Otol Rhinol Laryngol. **116**(2), 156-159, 2207.

23. Tateya T, T.I., Bless DM, Collagen subtypes in human vocal folds. Ann Otol Rhinol Laryngol. **115**(6), 469-476, 2006.

24. Madruga de Melo, E.C., Lemos, M., Aragão Ximenes Filho, J., Sennes, L.U., Nascimento Saldiva, P.H., and Tsuji, D.H., Distribution of collagen in the lamina propria of the human vocal fold. The Laryngoscope. **113**(12), 2187-2191, 2003.

25. Hahn MS, K.J., Zeitels SM, Langer R, Quantitative and comparative studies of the vocal fold extracellular matrix II: Collagen. Ann Otol Rhinol Laryngol. **115**(3), 225-232, 2006.

26. T.R, G., Nucleotypic effects without nuclei: Genome size and erythrocyte size in mammals. Genome. **43**(5), 895-901, 2000.

27. Light, N.D., Estimation of types I and III collagens in whole tissue by quantitation of cnbr peptides on sds-polyacrilamide gels. Biochimica et Biophysica Acta Protein Structure and Molecular Enzymology. **702**(1), 30-36, 1982.

28. Reiser, K.M. and Last, J.A., Quantitation of specific collagen types from lungs of small mammals. Analytical Biochemistry. **104**(1), 87-98, 1980.

29. Van Kuppevelt, T.H., Veerkamp, J.H., and Timmermans, J.A.H., Immunoquantification of type i, iii, iv and v collagen in small samples of human lung parenchyma. The International Journal of Biochemistry & Cell Biology. **27**(8), 775-782, 1995.

30. Miller EJ, G.S., Collagen: An overview. Methods Enzymol. **82**, 3-32, 1982.

31. Hahn, M.S., Teply, B.A., Stevens, M.M., Zeitels, S.M., and Langer, R., Collagen composite hydrogels for vocal fold lamina propria restoration. Biomaterials. **27**(7), 1104-1109, 2006.

32. Gray S, H.M., Sato K, eds, Molecular and cellular structure of vocal fold tissue. San Diego, California: Singular Publishing Group, 1993.

33. Kurita S, N.K., Hirano M, A comparative study of the layer structure of the vocal fold. San Diego, California: College-Hill Press, 1993.

34. Catten M, G.S., Hammond TH, Zhou R, Hammond E, Analysis of cellular location and concentration in vocal fold lamina propria. Otolaryngol Head Neck Surg. **118**(5), 663-667, 1998.

35. Randolph RK, S.M., Dermal fibroblasts actively metabolize retinoic acid but not retinol. J Invest Dermatol. **111**(3), 478-484, 1998.

36. Epstein, E.H. and Munderloh, N.H., Human skin collagen. Presence of type i and type iii at all levels of the dermis. Journal of Biological Chemistry. **253**(5), 1336-1337, 1978.

37. Ramig, L.O. and Verdolini, K., Treatment efficacy: Voice disorders. J Speech Lang Hear Res. **41**(1), S101-S116, 1998.

38. Gray, S.D., Cellular physiology of the vocal folds. Otolaryngologic Clinics of North America. **33**(4), 679-697, 2000.

39. Dailey, S.H. and Ford, C.N., Surgical management of sulcus vocalis and vocal fold scarring. Otolaryngologic Clinics of North America. **39**(1), 23-42, 2006.

40. Hirano M. and Kakita.Y., Daniloft R., ed. Cover-body theory of vocal fold vibration. San Diego, California: College-Hill Press, 1-46, 1985.

41. Kurita S, Nagata K. and Hirano M, A comparative study of the layer structure of the vocal fold. San Diego, California: College-Hill Press, 3-21, 1983.

42. Benninger MS, A.D., Archer S, Bastian R, Ford C, Koufman J, Sataloff RT, Spiegel JR, Woo P, Vocal fold scarring: Current concepts and management. Otolaryngol Head Neck Surg. **115**(5), 474-482, 1996.

43. Hansen, J.K. and Thibeault, S.L., Current understanding and review of the literature: Vocal fold scarring. Journal of voice. **20**(1), 110-120, 2006.

44. Rosen, C.A., Vocal fold scar: Evaluation and treatment. Otolaryngol Clin North Am. **33**(5), 1081-1086, 2000.

45. Rosen, C.A., Phonosurgical vocal fold injection: Procedures and materials. Otolaryngol Clin North Am. **33**(5), 1087-1096, 2000.

46. Chan, R.W. and Titze, I.R., Viscosities of implantable biomaterials in vocal fold augmentation surgery. The Laryngoscope. **108**(5), 725-731, 1998.

47. Chan, R.W. and Titze, I.R., Hyaluronic acid (with fibronectin) as a bioimplant for the vocal fold mucosa. Laryngoscope. **109**(7 Pt 1), 1142-1149, 1999.

48. Jia, X., Burdick, J.A., Kobler, J., Clifton, R.J., Rosowski, J.J., Zeitels, S.M., and Langer, R., Synthesis and characterization of in situ cross-linkable hyaluronic acid-based hydrogels with potential application for vocal fold regeneration. Macromolecules. **37**(9), 3239-3248, 2004.

49. Titze, I.R., Hitchcock, R.W., Broadhead, K., Webb, K., Li, W., Gray, S.D., and Tresco, P.A., Design and validation of a bioreactor for engineering vocal fold tissues under combined tensile and vibrational stresses. Journal of Biomechanics. **37**(10), 1521-1529, 2004.

50. Hallen, L., Johansson, C., and Laurent, C., Cross-linked hyaluronan (hylan b gel): A new injectable remedy for treatment of vocal fold insufficiency--an animal study. Acta Otolaryngol. **119**(1), 107-111, 1999.

51. Hallen, L., Testad, P., Sederholm, E., Dahlqvist, Å., and Laurent, C., DiHA (dextranomers in hyaluronan) injections for treatment of insufficient closure of the vocal folds: Early clinical experiences. The Laryngoscope. **111**(6), 1063-1067, 2001.

52. Bryant, S.J., Arthur, J.A., and Anseth, K.S., Incorporation of tissue-specific molecules alters chondrocyte metabolism and gene expression in photocrosslinked hydrogels. Acta Biomaterialia. **1**(2), 243-252, 2005.

53. Bryant, S.J., Chowdhury, T.T., Lee, D.A., Bader, D.L., and Anseth, K.S., Crosslinking density influences chondrocyte metabolism in dynamically loaded photocrosslinked poly(ethylene glycol) hydrogels. Annals of Biomedical Engineering. **32**(3), 407-417, 2004.

54. Gray, D.S., Tien, J., and Chen, C.S., Repositioning of cells by mechanotaxis on surfaces with micropatterned Young's modulus. Journal of Biomedical Materials Research Part A. **66A**(3), 605-614, 2003.

55. Peyton, S.R., Raub, C.B., Keschrumrus, V.P., and Putnam, A.J., The use of poly(ethylene glycol) hydrogels to investigate the impact of ECM chemistry and mechanics on smooth muscle cells. Biomaterials. **27**(28), 4881-4893, 2006.

56. Stegemann, J.P., Hong, H., and Nerem, R.M., Mechanical, biochemical, and extracellular matrix effects on vascular smooth muscle cell phenotype. Journal of Applied Physiology. **98**(6), 2321-2327, 2005.

57. Bryant, S.J., Durand, K.L., and Anseth, K.S., Manipulations in hydrogel chemistry control photoencapsulated chondrocyte behavior and their extracellular

matrix production. Journal of Biomedical Materials Research Part A. **67A**(4), 1430-1436, 2003.

58. Gombotz, W.R., Wang, G.H., Horbett, T.A., and Hoffman, A.S., Protein adsorption to poly(ethylene oxide) surfaces. J Biomed Mater Res. **25**(12), 1547-1562, 1991.

59. Kim, B.S., Nikolovski, J., Bonadio, J., Smiley, E., and Mooney, D.J., Engineered smooth muscle tissues: Regulating cell phenotype with the scaffold. Exp Cell Res. **251**(2), 318-328, 1999.

60. Chastain, S.R., Kundu, A.K., Dhar, S., Calvert, J.W., and Putnam, A.J., Adhesion of mesenchymal stem cells to polymer scaffolds occurs via distinct ECM ligands and controls their osteogenic differentiation. Journal of Biomedical Materials Research Part A. **78A**(1), 73-85, 2006.

61. Hahn, M.S., Miller, J.S., and West, J.L., Three-dimensional biochemical and biomechanical patterning of hydrogels for guiding cell behavior. Advanced Materials. **18**(20), 2679-2684, 2006.

62. Bryant, S.J. and Anseth, K.S., Hydrogel properties influence ECM production by chondrocytes photoencapsulated in poly(ethylene glycol) hydrogels. Journal of Biomedical Materials Research. **59**(1), 63-72, 2002.

63. Hahn, M.S., Taite, L.J., Moon, J.J., Rowland, M.C., Ruffino, K.A., and West, J.L., Photolithographic patterning of polyethylene glycol hydrogels. Biomaterials. **27**(12), 2519-2524, 2006.

64. Bryant, S.J., Nuttelman, C.R., and Anseth, K.S., Cytocompatibility of UV and visible light photoinitiating systems on cultured NIH/3T3 fibroblasts in vitro. J Biomater Sci Polym Ed. **11**(5), 439-457, 2000.

65. Williams, C.G., Malik, A.N., Kim, T.K., Manson, P.N., and Elisseeff, J.H., Variable cytocompatibility of six cell lines with photoinitiators used for polymerizing hydrogels and cell encapsulation. Biomaterials. **26**(11), 1211-1218, 2005.

66. Canal, T. and Peppas, N.A., Correlation between mesh size and equilibrium degree of swelling of polymeric networks. Journal of Biomedical Materials Research. **23**(10), 1183-1193, 1989.

67. Ford, M.C., Bertram, J.P., Hynes, S.R., Michaud, M., Li, Q., Young, M., Segal, S.S., et al., A macroporous hydrogel for the coculture of neural progenitor and

endothelial cells to form functional vascular networks in vivo. Proc Natl Acad Sci U S A. **103**(8), 2512-2517, 2006.

68. Mellott, M.B., Searcy, K., and Pishko, M.V., Release of protein from highly cross-linked hydrogels of poly(ethylene glycol) diacrylate fabricated by UV polymerization. Biomaterials. **22**(9), 929-941, 2001.

69. Watkins, A.W. and Anseth, K.S., Investigation of molecular transport and distributions in poly(ethylene glycol) hydrogels with confocal laser scanning microscopy. Macromolecules. **38**(4), 1326-1334, 2005.

70. Armstrong, J.K., Wenby, R.B., Meiselman, H.J., and Fisher, T.C., The hydrodynamic radii of macromolecules and their effect on red blood cell aggregation. Biophysical journal. **87**(6), 4259-4270, 2004.

71. Chan, R.W. and Titze, I.R., Viscoelastic shear properties of human vocal fold mucosa: Measurement methodology and empirical results. J Acoust Soc Am. **106**(4 Pt 1), 2008-2021, 1999.

72. Anseth, K.S., Bowman, C.N., and Brannon-Peppas, L., Mechanical properties of hydrogels and their experimental determination. Biomaterials. **17**(17), 1647-1657, 1996.

73. Anseth, K.S., Metters, A.T., Bryant, S.J., Martens, P.J., Elisseeff, J.H., and Bowman, C.N., In situ forming degradable networks and their application in tissue engineering and drug delivery. Journal of Controlled Release. **78**(1-3), 199-209, 2002.

74. Garrett, C.G., Coleman, J.R., and Reinisch, L., Comparative histology and vibration of the vocal folds: Implications for experimental studies in microlaryngeal surgery. The Laryngoscope. **110**(5), 814-824, 2000.

75. Hahn, M., McHale, M., Wang, E., Schmedlen, R., and West, J., Physiologic pulsatile flow bioreactor conditioning of poly(ethylene glycol)-based tissue engineered vascular grafts. Annals of Biomedical Engineering. **35**(2), 190-200, 2007.

76. Gregory, T.R., Nucleotypic effects without nuclei: Genome size and erythrocyte size in mammals. Genome. **43**(5), 895-901, 2000.

77. Miller, E.J. and Gay, S., Collagen: An overview. Methods Enzymol. **82**, 3-32, 1982.

78. Luo, Y., Kobler, J.B., Zeitels, S.M., and Langer, R., Effects of growth factors on extracellular matrix production by vocal fold fibroblasts in 3-dimensional culture. Tissue Engineering. **12**(12), 3365-3374, 2006.

79. Long, J.L. and Tranquillo, R.T., Elastic fiber production in cardiovascular tissue-equivalents. Matrix Biology. **22**(4), 339-350, 2003.

80. Nguyen, K.T. and West, J.L., Photopolymerizable hydrogels for tissue engineering applications. Biomaterials. **23**(22), 4307-4314, 2002.

81. Rishikof, D., Lucey, E., Kuang, P.-P., Snider, G., and Goldstein, R., Induction of the myofibroblast phenotype following elastolytic injury to mouse lung. Histochemistry and Cell Biology. **125**(5), 527-534, 2006.

82. Shi, Y., Niculescu, R., Wang, D., Ormont, M., Magno, M., San Antonio, J.D., Williams, K.J., et al., Myofibroblast involvement in glycosaminoglycan synthesis and lipid retention during coronary repair. J Vasc Res. **37**(5), 399-407, 2000.

83. Burdick, J.A. and Anseth, K.S., Photoencapsulation of osteoblasts in injectable RGD-modified peg hydrogels for bone tissue engineering. Biomaterials. **23**(22), 4315-4323, 2002.

84. Gray, S.D., Titze, I.R., Alipour, F., and Hammond, T.H., Biomechanical and histologic observations of vocal fold fibrous proteins. Ann Otol Rhinol Laryngol. **109**(1), 77-85, 2000.

85. Finck, C. and Lefebvre, P., Implantation of esterified hyaluronic acid in microdissected Reinke's space after vocal fold microsurgery: First clinical experiences. The Laryngoscope. **115**(10), 1841-1847, 2005.

86. Hansen, J.K., Thibeault, S.L., Walsh, J.F., Shu, X.Z., and Prestwich, G.D., In vivo engineering of the vocal fold extracellular matrix with injectable hyaluronic acid hydrogels: Early effects on tissue repair and biomechanics in a rabbit model. Ann Otol Rhinol Laryngol. **114**(9), 662-670, 2005.

87. David-Raoudi, M., Tranchepain, F., Deschrevel, B., Vincent, J.-C., Bogdanowicz, P., Boumediene, K., and Pujol, J.-P., Differential effects of hyaluronan and its fragments on fibroblasts: Relation to wound healing. Wound Repair and Regeneration. **16**(2), 274-287, 2008.

88. Joddar, B. and Ramamurthi, A., Elastogenic effects of exogenous hyaluronan oligosaccharides on vascular smooth muscle cells. Biomaterials. **27**(33), 5698-5707, 2006.

89. Joddar, B. and Ramamurthi, A., Fragment size and dose-specific effects of hyaluronan on matrix synthesis by vascular smooth muscle cells. Biomaterials. **27**(15), 2994-3004, 2006.

90. Meran, S., Thomas, D., Stephens, P., Martin, J., Bowen, T., Phillips, A., and Steadman, R., Involvement of hyaluronan in regulation of fibroblast phenotype. Journal of Biological Chemistry. **282**(35), 25687-25697, 2007.

91. Hui, T.Y., Cheung, K.M.C., Cheung, W.L., Chan, D., and Chan, B.P., In vitro chondrogenic differentiation of human mesenchymal stem cells in collagen microspheres: Influence of cell seeding density and collagen concentration. Biomaterials. **29**(22), 3201-3212, 2008.

92. Engler, A.J., Sen, S., Sweeney, H.L., and Discher, D.E., Matrix elasticity directs stem cell lineage specification. Cell. **126**(4), 677-689, 2006.

93. Mann, B.K., Tsai, A.T., Scott-Burden, T., and West, J.L., Modification of surfaces with cell adhesion peptides alters extracellular matrix deposition. Biomaterials. **20**(23-24), 2281-2286, 1999.

94. Hahn, M.S., Miller, J.S., and West, J.L., Laser scanning lithography for surface micropatterning on hydrogels. Advanced Materials. **17**(24), 2939-2942, 2005.

95. Munoz-Pinto, D.J., Bulick, A.S., and Hahn, M.S., Uncoupled investigation of scaffold modulus and mesh size on smooth muscle cell behavior. Journal of Biomedical Materials Research Part A. **90A**(1), 303-316, 2009.

96. Elisseeff, J., Anseth, K., Sims, D., McIntosh, W., Randolph, M., Yaremchuk, M., and Langer, R., Transdermal photopolymerization of poly(ethylene oxide)-based injectable hydrogels for tissue-engineered cartilage. Plast Reconstr Surg. **104**(4), 1014-1022, 1999.

97. Humphries, J.D., Byron, A., and Humphries, M.J., Integrin ligands at a glance. J Cell Sci. **119**(19), 3901-3903, 2006.

98. Slevin, M., Krupinski, J., Gaffney, J., Matou, S., West, D., Delisser, H., Savani, R.C., et al., Hyaluronan-mediated angiogenesis in vascular disease: Uncovering RHAMM and CD44 receptor signaling pathways. Matrix Biology. **26**(1), 58-68, 2007.

99. Slevin, M., Kumar, S., and Gaffney, J., Angiogenic oligosaccharides of hyaluronan induce multiple signaling pathways affecting vascular endothelial cell mitogenic and wound healing responses. Journal of Biological Chemistry. **277**(43), 41046-41059, 2002.

100. Turley, E.A., Noble, P.W., and Bourguignon, L.Y.W., Signaling properties of hyaluronan receptors. Journal of Biological Chemistry. **277**(7), 4589-4592, 2002.

101. Liao, H., Munoz-Pinto, D., Qu, X., Hou, Y., Grunlan, M.A., and Hahn, M.S., Influence of hydrogel mechanical properties and mesh size on vocal fold fibroblast extracellular matrix production and phenotype. Acta Biomaterialia. **4**(5), 1161-1171, 2008.

102. Buxton, A.N., Zhu, J., Marchant, R., West, J.L., Yoo, J.U., and Johnstone, B., Design and characterization of poly(ethylene glycol) photopolymerizable semi-interpenetrating networks for chondrogenesis of human mesenchymal stem cells. Tissue Engineering. **13**(10), 2549-2560, 2007.

103. Benoit, D.S.W., Schwartz, M.P., Durney, A.R., and Anseth, K.S., Small functional groups for controlled differentiation of hydrogel-encapsulated human mesenchymal stem cells. Nat Mater. **7**(10), 816-823, 2008.

104. Salinas, C.N. and Anseth, K.S., The enhancement of chondrogenic differentiation of human mesenchymal stem cells by enzymatically regulated RGD functionalities. Biomaterials. **29**(15), 2370-2377, 2008.

105. Munoz-Pinto, D.J, Whittaker, P, and Hahn,S.M., Lamina propria cellularity and collagen composition : An integrated assessment of structure in humans. Ann Otol Rhinol Laryngol. **118**(4), 299-306, 2009.

106. Masters, K.S., Shah, D.N., Leinwand, L.A., and Anseth, K.S., Crosslinked hyaluronan scaffolds as a biologically active carrier for valvular interstitial cells. Biomaterials. **26**(15), 2517-2525, 2005.

107. Bogatkevich, G.S., Tourkina, E., Silver, R.M., and Ludwicka-Bradley, A., Thrombin differentiates normal lung fibroblasts to a myofibroblast phenotype via the proteolytically activated receptor-1 and a protein kinase c-dependent pathway. Journal of Biological Chemistry. **276**(48), 45184-45192, 2001.

108. Broadley, C., Gonzalez, D.A., Nair, R., Koriwchak, M.J., Ossoff, R.H., and Davidson, J.M., A tissue-culture model for the study of canine vocal fold fibroblasts. The Laryngoscope. **105**(1), 23-27, 1995.

109. Chailley-Heu, B., Boucherat, O., Barlier-Mur, A.M., and Bourbon, J.R., Fgf-18 is upregulated in the postnatal rat lung and enhances elastogenesis in myofibroblasts. Am J Physiol Lung Cell Mol Physiol. **288**(1), L43-L51, 2005.

110. Hoff, C.R., Perkins, D.R., and Davidson, J.M., Elastin gene expression is upregulated during pulmonary fibrosis. Connect Tissue Res. **40**(2), 145-153, 1999.

111. Mariani, T.J., Crouch, E., Roby, J.D., Starcher, B., and Pierce, R.A., Increased elastin production in experimental granulomatous lung disease. Am J Pathol. **147**(4), 988-1000, 1995.

112. Koh, W.G., Itle, L.J., and Pishko, M.V., Molding of hydrogel microstructures to create multiphenotype cell microarrays. Anal Chem. **75**(21), 5783-5789, 2003.

113. Liu, V.A. and Bhatia, S.N., Three-dimensional photopatterning of hydrogels containing living cells. Biomedical Microdevices. **4**(4), 257-266, 2002.

114. Shah, D.N., Recktenwall-Work, S.M., and Anseth, K.S., The effect of bioactive hydrogels on the secretion of extracellular matrix molecules by valvular interstitial cells. Biomaterials. **29**(13), 2060-2072, 2008.

115. Gray, D.S., Tien, J., and Chen, C.S., Repositioning of cells by mechanotaxis on surfaces with micropatterned Young's modulus. J Biomed Mater Res A. **66**(3), 605-614, 2003.

116. Stegemann, J.P., Hong, H., and Nerem, R.M., Mechanical, biochemical, and extracellular matrix effects on vascular smooth muscle cell phenotype. J Appl Physiol. **98**(6), 2321-2327, 2005.

117. Bryant, S.J. and Anseth, K.S., Controlling the spatial distribution of ECM components in degradable PEG hydrogels for tissue engineering cartilage. J Biomed Mater Res A. **64**(1), 70-79, 2003.

118. Kempezinski, R., ed. Vascular surgery. Philadelphia, Pensilvania: WB Saunders, 2000.

119. Schmedlen, R.H., Elbjeirami, W.M., Gobin, A.S., and West, J.L., Tissue engineered small-diameter vascular grafts. Clin Plast Surg. **30**(4), 507-517, 2003.

120. Burkel, W.E., The challenge of small diameter vascular grafts. Med Prog Technol. **14**(3-4), 165-175, 1988.

121. Tranquillo, R.T., Girton, T.S., Bromberek, B.A., Triebes, T.G., and Mooradian, D.L., Magnetically orientated tissue-equivalent tubes: Application to a circumferentially orientated media-equivalent. Biomaterials. **17**(3), 349-357, 1996.

122. Isenberg, B.C. and Tranquillo, R.T., Long-term cyclic distention enhances the mechanical properties of collagen-based media-equivalents. Annals of Biomedical Engineering. **31**(8), 937-949, 2003.

123. Miano, J.M., Long, X., and Fujiwara, K., Serum response factor: Master regulator of the actin cytoskeleton and contractile apparatus. American Journal of Physiology - Cell Physiology. **292**(1), C70-C81, 2007.

124. Wang, Z., Wang, D.Z., Hockemeyer, D., McAnally, J., Nordheim, A., and Olson, E.N., Myocardin and ternary complex factors compete for SRF to control smooth muscle gene expression. Nature. **428**(6979), 185-189, 2004.

125. Miano, J.M., Carlson, M.J., Spencer, J.A., and Misra, R.P., Serum response factor-dependent regulation of the smooth muscle calponin gene. J Biol Chem. **275**(13), 9814-9822, 2000.

126. Kim, T.J., Seong, J., Ouyang, M., Sun, J., Lu, S., Hong, J.P., Wang, N., et al., Substrate rigidity regulates Ca^{2+} oscillation via RhoA pathway in stem cells. J Cell Physiol. **218**(2), 285-293, 2009.

127. Jacot, J.G., McCulloch, A.D., and Omens, J.H., Substrate stiffness affects the functional maturation of neonatal rat ventricular myocytes. Biophysical journal. **95**(7), 3479-3487, 2008.

128. Hahn, M.S., Taite, L.J., Moon, J.J., Rowland, M.C., Ruffino, K.A., and West, J.L., Photolithographic patterning of polyethylene glycol hydrogels. Biomaterials. **27**(12), 2519-2524, 2006.

129. Lu, X., Pandit, A., and Kassab, G.S., Biaxial incremental homeostatic elastic moduli of coronary artery: Two-layer model. Am J Physiol Heart Circ Physiol. **287**(4), H1663-H1669, 2004.

130. Canal, T. and Peppas, N.A., Correlation between mesh size and equilibrium degree of swelling of polymeric networks. J Biomed Mater Res. **23**(10), 1183-1193, 1989.

131. Ford, M.C., Bertram, J.P., Hynes, S.R., Michaud, M., Li, Q., Young, M., Segal, S.S., et al., A macroporous hydrogel for the coculture of neural progenitor and endothelial cells to form functional vascular networks in vivo. Proceedings of the National Academy of Sciences of the United States of America. **103**(8), 2512-2517, 2006.

132. Armstrong, J.K., Wenby, R.B., Meiselman, H.J., and Fisher, T.C., The hydrodynamic radii of macromolecules and their effect on red blood cell aggregation. Biophys J. **87**(6), 4259-4270, 2004.

133. Weirich, J., Seiler, L., Hug, M.J., and Fleckenstein-Grun, G., Ca(2+) entry into primary cultured pig coronary smooth muscle cells after previous store depletion by repetitive P2Y purinoceptor stimulation. Cell Calcium. **29**(5), 359-367, 2001.

134. Gockerman, A. and Clemmons, D.R., Porcine aortic smooth muscle cells secrete a serine protease for insulin-like growth factor binding protein-2. Circ Res. **76**(4), 514-521, 1995.

135. Metters, A.T., Bowman, C.N., and Anseth, K.S., A statistical kinetic model for the bulk degradation of pla-b-peg-b-pla hydrogel networks. The Journal of Physical Chemistry B. **104**(30), 7043-7049, 2000.

136. Hahn, M.S., Teply, B.A., Stevens, M.M., Zeitels, S.M., and Langer, R., Collagen composite hydrogels for vocal fold lamina propria restoration. Biomaterials. **27**(7), 1104-1109, 2006.

137. Long, J.L. and Tranquillo, R.T., Elastic fiber production in cardiovascular tissue-equivalents. Matrix Biol. **22**(4), 339-350, 2003.

138. Ren, X.D. and Schwartz, M.A., Determination of GTP loading on Rho. Methods Enzymol. **325**, 264-472, 2000.

139. Zhang, Z., Apse, K., Pang, J., and Stanton, R.C., High glucose inhibits glucose-6-phosphate dehydrogenase via cAMP in aortic endothelial cells. J Biol Chem. **275**(51), 40042-40047, 2000.

140. Goodrich, R.P., Sowemimo-Coker, S.O., Zerez, C.R., and Tanaka, K.R., Preservation of metabolic activity in lyophilized human erythrocytes. Proceedings of the National Academy of Sciences of the United States of America. **89**(3), 967-971, 1992.

141. Wang, G.L., Jiang, B.H., Rue, E.A., and Semenza, G.L., Hypoxia-inducible factor 1 is a basic-helix-loop-helix-pas heterodimer regulated by cellular o2 tension. Proceedings of the National Academy of Sciences of the United States of America. **92**(12), 5510-5514, 1995.

142. Calo, L.A. and Pessina, A.C., Rhoa/Rho-kinase pathway: Much more than just a modulation of vascular tone. Evidence from studies in humans. J Hypertens. **25**(2), 259-64, 2007.

143. Zheng, L., Roeder, R.G., and Luo, Y., S phase activation of the histone H2B promoter by OCA-S, a coactivator complex that contains GAPDH as a key component. Cell. **114**(2), 255-266, 2003.

144. Tarze, A., Deniaud, A., Le Bras, M., Maillier, E., Molle, D., Larochette, N., Zamzami, N., et al., GAPDH, a novel regulator of the pro-apoptotic mitochondrial membrane permeabilization. Oncogene. **26**(18), 2606-2620, 2007.

145. Lee, H.J., Yun, C.H., Lim, S.H., Kim, B.C., Baik, K.G., Kim, J.M., Kim, W.H., et al., SRF is a nuclear repressor of Smad3-mediated TGF-beta signaling. Oncogene. **26**(2), 173-185, 2007.

146. Carson, J.A., Culberson, D.E., Thompson, R.W., Fillmore, R.A., and Zimmer, W., Smooth muscle [gamma]-actin promoter regulation by Rhoa and serum response factor signaling. Biochimica et Biophysica Acta (BBA) - Gene Structure and Expression. **1628**(2), 133-139, 2003.

147. Chen, S., Crawford, M., Day, R.M., Briones, V.R., Leader, J.E., Jose, P.A., and Lechleider, R.J., RhoA modulates Smad signaling during transforming growth factor-beta-induced smooth muscle differentiation. J Biol Chem. **281**(3), 1765-1770, 2006.

148. Wei, L., Zhou, W., Croissant, J.D., Johansen, F.E., Prywes, R., Balasubramanyam, A., and Schwartz, R.J., RhoA signaling via serum response factor plays an obligatory role in myogenic differentiation. J Biol Chem. **273**(46), 30287-30294, 1998.

149. Won, J.-S., Im, Y.-B., Key, L., Singh, I., and Singh, A.K., The involvement of glucose metabolism in the regulation of inducible nitric oxide synthase gene expression in glial cells: Possible role of glucose-6-phosphate dehydrogenase and ccaat/enhancing binding protein. J. Neurosci. **23**(20), 7470-7478, 2003.

150. Kibbe, M.R., Li, J., Nie, S., Watkins, S.C., Lizonova, A., Kovesdi, I., Simmons, R.L., et al., Inducible nitric oxide synthase (inos) expression upregulates p21 and inhibits vascular smooth muscle cell proliferation through p42/44 mitogen-activated protein kinase activation and independent of p53 and cyclic guanosine monophosphate. Journal of vascular surgery. **31**(6), 1214-1228, 2000.

151. Masters, K.S., Shah, D.N., Leinwand, L.A., and Anseth, K.S., Crosslinked hyaluronan scaffolds as a biologically active carrier for valvular interstitial cells. Biomaterials. **26**(15), 2517-25125, 2005.

152. Koh, W.-G., Itle, L.J., and Pishko, M.V., Molding of hydrogel microstructures to create multiphenotype cell microarrays. Analytical Chemistry. **75**(21), 5783-5789, 2003.

153. Woo, S.L.-Y., Hildebrand, K., Watanabe, N., Fenwick, J.A., Papageorgiou, C.D., and Wang, J.H.-C., Tissue engineering of ligament and tendon healing. Clinical Orthopaedics and Related Research. **367**, S312-S323, 1999.

154. Cooper, J.A., Lu, H.H., Ko, F.K., Freeman, J.W., and Laurencin, C.T., Fiber-based tissue-engineered scaffold for ligament replacement: Design considerations and in vitro evaluation. Biomaterials. **26**(13), 1523-1532, 2005.

155. Fu, F.H., Bennett, C.H., Ma, C.B., Menetrey, J., and Lattermann, C., Current trends in anterior cruciate ligament reconstruction. The American Journal of Sports Medicine. **28**(1), 124-130, 2000.

156. Weitzel, P.P., Richmond, J.C., Altman, G.H., Calabro, T., and Kaplan, D.L., Future direction of the treatment of acl ruptures. Orthop Clin North Am. **33**(4), 653-661, 2002.

157. Vunjak-Novakovic, G., Altman, G., Horan, R., and Kaplan, D.L., Tissue engineering of ligaments. Annu Rev Biomed Eng. **6**, 131-156, 2004.

158. Deehan, D.J. and Cawston, T.E., The biology of integration of the anterior cruciate ligament. J Bone Joint Surg Br. **87**(7), 889-895, 2005.

159. Thomopoulos, S., Williams, G.R., Gimbel, J.A., Favata, M., and Soslowsky, L.J., Variation of biomechanical, structural, and compositional properties along the tendon to bone insertion site. Journal of Orthopaedic Research. **21**(3), 413-419, 2003.

160. Yang, P.J. and Temenoff, J.S., Engineering orthopedic tissue interfaces. Tissue Eng Part B Rev. **15**(2), 127-141, 2009.

161. Phillips, J.E., Burns, K.L., Le Doux, J.M., Guldberg, R.E., and García, A.J., Engineering graded tissue interfaces. Proceedings of the National Academy of Sciences of the United States of America. **105**(34), 12170-12175, 2008.

162. Ducheyne, P. and Qiu, Q., Bioactive ceramics: The effect of surface reactivity on bone formation and bone cell function. Biomaterials. **20**(23-24), 2287-2303, 1999.

163. Kretlow, J.D. and Mikos, A.G., Review: Mineralization of synthetic polymer scaffolds for bone tissue engineering. Tissue Eng. **13**(5), 927-938, 2007.

164. García, A.J., Ducheyne, P., and Boettiger, D., Effect of surface reaction stage on fibronectin-mediated adhesion of osteoblast-like cells to bioactive glass. Journal of Biomedical Materials Research. **40**(1), 48-56, 1998.

165. Khan, Y., Yaszemski, M.J., Mikos, A.G., and Laurencin, C.T., Tissue engineering of bone: Material and matrix considerations. J Bone Joint Surg Am. **90**(Supplement_1), 36-42, 2008.

166. Ning, C.Q., Mehta, J., and El-Ghannam, A., Effects of silica on the bioactivity of calcium phosphate composites. Journal of Materials Science: Materials in Medicine. **16**(4), 355-360, 2005.

167. Gautam, G., Ahmed, E.-G., Sreenatha, K., Marwan, K., and Hussein, Z., Enhancement of osteoblast gene expression by mechanically compatible porous si-rich nanocomposite. Journal of Biomedical Materials Research Part B: Applied Biomaterials. **81B**(2), 387-396, 2007.

168. Song, J.H., Yoon, B.H., Kim, H.E., and Kim, H.W., Bioactive and degradable hybridized nanofibers of gelatin-siloxane for bone regeneration. J Biomed Mater Res A. **84**(4), 875-884, 2008.

169. DeLong, S.A., Moon, J.J., and West, J.L., Covalently immobilized gradients of bfgf on hydrogel scaffolds for directed cell migration. Biomaterials. **26**(16), 3227-3234, 2005.

170. McDonald, J.C. and Whitesides, G.M., Poly(dimethylsiloxane) as a material for fabricating microfluidic devices. Accounts of Chemical Research. **35**(7), 491-499, 2002.

171. Gong, C. and Fréchet, J.M.J., End functionalization of hyperbranched poly(siloxysilane): Novel crosslinking agents and hyperbranched–linear star block copolymers. Journal of Polymer Science Part A: Polymer Chemistry. **38**(16), 2970-2978, 2000.

172. Panda, D.K., Miao, D., Lefebvre, V., Hendy, G.N., and Goltzman, D., The transcription factor SOX9 regulates cell cycle and differentiation genes in chondrocytic CFK2 cells. Journal of Biological Chemistry. **276**(44), 41229-41236, 2001.

173. Grunlan, M.A., Lee, N.S., Mansfeld, F., Kus, E., Finlay, J.A., Callow, J.A., Callow, M.E., et al., Minimally adhesive polymer surfaces prepared from star oligosiloxanes and star oligofluorosiloxanes. Journal of Polymer Science Part A: Polymer Chemistry. **44**(8), 2551-2566, 2006.

174. Boutevin, B., Guida-Pietrasanta, F., and Ratsimihety, A., Synthesis of photocrosslinkable fluorinated polydimethylsiloxanes: Direct introduction of acrylic pendant groups via hydrosilylation. Journal of Polymer Science Part A: Polymer Chemistry. **38**(20), 3722-3728, 2000.

175. Murthy, R., Shell, C.E., and Grunlan, M.A., The influence of poly(ethylene oxide) grafting via siloxane tethers on protein adsorption. Biomaterials. **30**(13), 2433-2439, 2009.

176. El-Ghannam, A.R., Advanced bioceramic composite for bone tissue engineering: Design principles and structure-bioactivity relationship. J Biomed Mater Res A. **69**(3), 490-501, 2004.

177. Curran, J.M., Chen, R., and Hunt, J.A., The guidance of human mesenchymal stem cell differentiation in vitro by controlled modifications to the cell substrate. Biomaterials. **27**(27), 4783-4793, 2006.

178. Hou, Y., Schoener, C.A., Regan, K.R., Munoz-Pinto, D., Hahn, M.S., and Grunlan, M.A., Photo-cross-linked PDMSstar-PEG hydrogels: Synthesis, characterization, and potential application for tissue engineering scaffolds. Biomacromolecules. **11**(3), 648-656, 2010.

179. Freed, B.K., Biesecker, J., and Middleton, W.J., Spectral polarity index: A new method for determining the relative polarity of solvents. Journal of Fluorine Chemistry. **48**(1), 63-75, 1990.

180. Bulick, A.S., Munoz-Pinto, D.J., Qu, X., Mani, M., Cristancho, D., Urban, M., and Hahn, M.S., Impact of endothelial cells and mechanical conditioning on smooth muscle cell extracellular matrix production and differentiation. Tissue Engineering Part A. **15**(4), 815-825, 2009.

181. Levenberg, S., Huang, N.F., Lavik, E., Rogers, A.B., Itskovitz-Eldor, J., and Langer, R., Differentiation of human embryonic stem cells on three-dimensional polymer scaffolds. Proceedings of the National Academy of Sciences of the United States of America. **100**(22), 12741-12746, 2003.

182. Absolom, D.R., Zingg, W., and Neumann, A.W., Protein adsorption to polymer particles: Role of surface properties. Journal of Biomedical Materials Research. **21**(2), 161-171, 1987.

183. Munoz-Pinto, D.J., McMahon, R.E., Kanzelberger, M.A., Jimenez-Vergara, A.C., Grunlan, M.A., and Hahn, M.S., Inorganic–organic hybrid scaffolds for

osteochondral regeneration. Journal of Biomedical Materials Research Part A. **94A**(1), 112-121, 2010.

184. Liao, H., Andersson, A.-S., Sutherland, D., Petronis, S., Kasemo, B., and Thomsen, P., Response of rat osteoblast-like cells to microstructured model surfaces in vitro. Biomaterials. **24**(4), 649-654, 2003.

VITA

Dany Jair Munoz Pinto received his B.S in chemical engineering from The Universidad Industrial de Santander, Colombia, in 2005. He entered the chemical engineering graduate program at Texas A&M University in Spring 2006 and received his Doctor of Philosophy degree in May 2011. During his research studies, in 2009, he received the Paul and Ellen Deiser Fellowship in chemical engineering and the Texas Experimental Station (TEES) Fellowship for Spanish Speakers. His research interests include the study of cell material interactions for tissue engineering applications. He plans to continue his research in a postdoctoral position at Texas A&M University, in the area of mesenchymal stem cell research.

Dr. Munoz Pinto may be reached at: 200 Jack E. Brown Enginering Building, Chemical Enginering Department, Texas A&M University, College Station TX 77843-3122. His email address is: danyjair@neo.tamu.edu.